Technische Universität München

Department für Biowissenschaftliche Grundlagen

Method development and application for the analysis of hydro- and lipophilic hormones and neurotransmitters in murine tissues

Joachim Nagler

Vollständiger Abdruck der von der Fakultät Wissenschaftszentrum Weihenstephan für Ernährung, Landnutzung und Umwelt der Technischen Universität München zur Erlangung des akademischen Grades eines

Doktors der Naturwissenschaften

genehmigten Dissertation.

Vorsitzender: **Prof. Dr. Jürgen Geist**

Prüfer der Dissertation:

1. **apl. Prof. Dr. Dr. Karl-Werner Schramm**

2. **Prof. Dr. Ilona Grunwald Kadow**

Die Dissertation wurde am 07.11.2019 bei der Technischen Universität München eingereicht und durch die Fakultät Wissenschaftszentrum Weihenstephan für Ernährung, Landnutzung und Umwelt am 21.01.2020 angenommen.

Danksagung

Ich möchte an dieser Stelle die Möglichkeit nutzen und Allen danken, die zum Erfolg dieser Arbeit beigetragen haben.

Zuallererst danke ich meinem Doktorvater Prof. Schramm sehr herzlich für die Möglichkeit die vorliegende Promotionsarbeit in seiner Arbeitsgruppe anfertigen zu können. Sein Führungsstil erlaubte das unabhängige Arbeiten und Einbringen eigener Ideen in die Forschungsarbeit. Gleichzeitig stand seine Tür dennoch zu jeder Zeit offen und er war mit guten Ratschlägen aus seiner langjährigen analytischen Erfahrung zur Stelle. Er ermöglichte ebenso die Teilnahme an Konferenzen sowie Kursen, die neben wissenschaftlicher Erfahrung auch für persönliche Weiterentwicklung sorgten.

Ich danke auch Dr. Daniela Vogt-Weisenhorn für ihre regelmäßige Mitwirkung als externe Expertin in meinem Thesis Committee, wo sie den Fortschritt der Arbeit mitverfolgte und förderte und stets gute Ratschläge einbrachte.

Dr. Meri De Angelis möchte ich ebenso für ihre Teilnahme an meinem Thesis Committee als weiterer Supervisor danken. Sie verfolgte den Fortschritt der Arbeit immer aufmerksam und gab hilfreiche Hinweise für das Publizieren der Ergebnisse. Des Weiteren danke ich ihr für ihre Einweisung in das Massenspektrometer und für ihre Unterstützung meiner Arbeiten zur Identifizierung von unbekannten Peaks an diesem Gerät.

Ein besonderer Dank gilt Bernhard Henkelmann, der immer mit IT Unterstützung zur Seite stand und mit seiner Expertise für die Rettung wichtiger Daten aus alten Computersystemen sorgte.

Danke auch an Silke Bernhöft und Felix Antritter für ihre Hilfe in den Abläufen der Laborорganisation, für viele tolle Gespräche und für das Beitragen zu einer sehr angenehmen Arbeitsatmosphäre. Dazu haben natürlich ebenso Dr. Marchela Pandelova, Dr. Cedrique Temoka, Claudia Korsten, Norbert Fischer und Zhong-Min Li als weitere Mitglieder der Arbeitsgruppe beigetragen.

Ich danke Dr. Sonja Schriever, Dr. Katrin Fischer, Prof. Paul Pfluger und Dr. Timo Müller für ihre Mitwirkung bei meinen Projekten durch das Bereitstellen von Probematerialien, die angenehmen Kooperationen und ihre Hilfe bei der Interpretation der Ergebnisse. Ich danke auch Dr. Artem Romanov für seinen Hinweis auf den interessanten Metaboliten Norlaudanosolin.

Natürlich dürfen in dieser Liste auch die zahlreichen Kollegen der Arbeitsgruppe CMA nicht fehlen. Besonders danke ich Dr. Janos Varga, Dr. Sebastian Wohlfahrt, Dr. Micheal Fischer, Dr. George Dragan, Dr. Vesta Kohlmeier, Matthias Fuchs und Josie Kunze für eine gute Zeit in den Pausen und sozialen Aktivitäten außerhalb der Arbeit. Dasselbe gilt auch für Christoph Kurz, Julia Walter und Bogi Szentes vom IGM.

Danke auch an meine Praktikanten Fadi Shanan, Muhammad Rammadan, Raimond Scheirich, und Michael Zorzi für ihre Unterstützung bei den praktischen Laborarbeiten.

Ich möchte auch meinen Eltern und meiner Familie für ihre Unterstützung bei der Verwirklichung dieser Arbeit danken. Das letzte Dankeschön geht an meine Freundin Simone, die mich während der Promotionszeit stets unterstützt hat. Ohne sie wäre das Durchhalten in anstrengenden Zeiten wesentlich schwieriger gewesen.

List of publications

Parts of this work have already been published in peer reviewed journals or are in preparation for submission.

Nagler, J, Schriever, SC, De Angelis, M, Pfluger, PT, Schramm, K-W. Comprehensive analysis of nine monoamines and metabolites in small amounts of peripheral murine (C57Bl/6 J) tissues. Biomedical Chromatography. 2018; 32:e4151.
doi:10.1002/bmc.4151

Fischer K, Ruiz HH, Jhun K, Finan B, Oberlin DJ, van der Heide V, Kalinovich AV, Petrovic N, Wolf Y, Clemmensen C, Shin AC, Divanovic S, Brombacher F, Glasmacher E, Keipert S, Jastroch M, Nagler J, Schramm KW, Medrikova D, Collden G, Woods SC, Herzig S, Homann D, Jung S, Nedergaard J, Cannon B, Tschöp MH, Müller TD, Buettner C. Alternatively activated macrophages do not synthesize catecholamines or contribute to adipose tissue adaptive thermogenesis. Nature Medicine. 2017 (5):623-630.
doi: 10.1038/nm.4316.

Nagler, J, Schriever SC, Romanov, A, Vogt-Weisenhorn, D, Wurst, W, Pfluger PT, Schramm, KW, Simultaneous extraction and detection of morphine and norlaudanosoline from murine brain regions with dispersive liquid liquid microextraction,
in preparation

Schriever, SC, Kabra DG, Pfuhlmann, K, Johar, H, Nagler, J, Harrison, L, Baumann P, Yi CX, IrmLer, M, Castel, J, Wu, M, Jain, R, Schug, H, Kullmann, S, Häring, HU, Beckers, J, Müller, T, Stemmer, K, Rozman, J, Nogueiras R, Schramm, KW, Gieger, C, Grallert, H, Schmidt, M, Luquet, S, Ladwig, KH, Heni, M, Tschöp, MH, and Pfluger, PT, Type 2 diabetes risk gene Dusp8 is a gatekeeper for hypothalamic Jnk signaling and insulin sensitivity,
in preparation

Kurzfassung

Neurotransmitter sind ein essentieller Teil des Nervensystems und verantwortlich für die Signalweiterleitung und –modifikation zwischen Neuronen. Die Untergruppe der Monoamine, wie z. Bsp. Dopamin, Noradrenalin, Adrenalin und Serotonin, können durch elektrochemische Detektion mit hoher Selektivität und Sensitivität analysiert werden. Aufgrund ihrer integralen Rolle in der Funktion des Organismus, sind sie oft in Krankheiten und psychischen Störungen involviert. In der Erforschung dieser Krankheiten werden Mäuse als der Hauptmodellorganismus vor Humanstudien eingesetzt. Deshalb ist es wichtig die Möglichkeit zu haben Monoamine in Mausgewebe zu analysieren, um die mechanistischen Auswirkungen von Neurotransmittern und Metaboliten zu ermitteln. Bisherige analytische Methoden haben sich hauptsächlich auf die Anwendung im Gehirngewebe konzentriert. Neuronale Netzwerke sind jedoch über den ganzen Körper verteilt, wo ebenfalls Effekte auftreten können.

In der vorliegenden Arbeit wurde eine Methode zur Analyse von aktiven Monoaminen sowie Metaboliten in peripheren Mausgeweben (Leber, Pankreas, Muskeln, sowie braunes und weißes Fett) und Zellkulturen mithilfe von HPLC, gekoppelt mit einem elektrochemischen Detektor, entwickelt. Aufgrund der hohen Selektivität des Detektors konnte eine einfache Extraktionsmethode, bestehend aus Gewebehomogenisierung und direkter Injektion nach Zentrifugation, angewendet werden. Spezifische Modifikationen waren jedoch für jede Geweberegion notwendig, um die volle Extraktion der Analyten zu gewährleisten. Eine Säule mit halb porösen Partikeln wurde angewandt und die chromatographischen Bedingungen angepasst, um eine kurze Laufzeit im HPLC Instrument und einen hohen Durchsatz an Proben zu erreichen. Die Methode wurde validiert und zeigte eine hohe Präzision, Genauigkeit und Sensitivität bis in den einstelligen Pikogrammbereich. Die aktiven Neurotransmitter Dopamin, Noradrenalin, Adrenalin und Serotonin, sowie ihre Metaboliten 3,4-Dihydroxyphenylglycol, 3,4-Dihydroxyphenylessigsäure, 3-Methoxytyramin, Homovanillinsäure und 5-Hydroxyindolylessigsäure konnten mit der Methode analysiert werden. Weiterhin wurde die Stabilität von Standardlösungen unter verschiedenen Bedingungen getestet, um eine zuverlässige Qualitätskontrolle während der täglichen Kalibrierungen zu erreichen. Die Stabilität von extrahierten Proben wurde dabei ebenso über ein Jahr beobachtet, um die Möglichkeit einer erneuten Analyse zu kontrollieren. Die Methode wurde anschließend in zwei verschieden Projekten angewandt. Dort konnte sie zeigen, dass, im Gegensatz zu vorherigen Berichten, alternativ aktivierte Makrophagen nach Stimulation mit Interleukin keine Katecholamine produzieren und kein Mechanismus für die adaptive Thermogenese von Fettgewebe sind. Sie konnte auch die sympathische Innervierung in Geweben von *dual-specifity-phosphatase* defizienten Mäusen bestimmen und dabei dazu beitragen den Mechanismus eines Risikofaktors für Diabetes in genomweiten Assoziationsstudien zu erklären.

Ebenso wurde eine Methode zur Identifizierung von unbekannten Peaks aus den elektrochemischen Chromatogrammen untersucht. Ein Arbeitsablauf für die Extraktion von Unbekannten nach der HPLC Trennung und anschließende massenspektrometrische Analyse nach dem chemischen Anhängen eines Benzoylchlorid Labels zur Erhöhung der Sensitivität wurde dafür entwickelt. Das zur Verfügung stehende Instrument wies jedoch Limitationen im Bereich der Sensitivität auf, so dass die Anwendung nicht möglich war.

Zusätzlich beschäftigt sich die vorliegende Arbeit mit Morphium. Dieses wird normalerweise als Schmerzmedikament eingesetzt, kann aber auch im Körper von Säugetieren ausgehend vom Neurotransmitter Dopamin über die Zwischenstufe Norlaudanosolin produziert werden. Die genaue Funktion dieses Pfades ist unbekannt, jedoch besteht möglicherweise ein Zusammenhang zu Parkinson, da im Urin von Patienten, die mit L-DOPA behandelt wurden, erhöhte Werte gefunden wurden. Deshalb wurde eine sensitive Methode zur Untersuchung von beiden Substanzen in einzelnen Mausgehirnregionen entwickelt. Die Methode beinhaltet eine dispersive flüssig flüssig Mikroextraktion der Analyten. Eine neue Variante, in der Methanol erstmals als Extraktant eingesetzt wird, wurde entwickelt und mit Hilfe von statistischer Versuchsplanung optimiert. Die Methode wurde validiert und zeigte eine hohe Präzision, Genauigkeit und Sensitivität. Sie wurde in einzelnen Gehirnregionen von Mäusen angewandt, wo beide Analyten im Thalamus, Striatum und Hippocampus gefunden wurden, was die Möglichkeit zur Anwendung in zukünftigen Studien zur Untersuchung des Morphinpfades im Zusammenhang mit Parkinson zeigt.

Abstract

Neurotransmitters are an essential part of the nervous system and responsible for the signal transduction and modulation across neurons. A subgroup called monoamines, including dopamine, norepinephrine, epinephrine, and serotonin, can be analyzed through electrochemical detection with high selectivity and sensitivity. Due to their integral role in the functioning of the organism, they are often involved in diseases and psychological disorders. In the research of these, mice are the main model organism to precede human studies. Therefore, it is important to have the means for the analysis of monoamines in murine tissues, to help elucidate the mechanistic involvements of neurotransmitters and metabolites. Previous analytical methods focused mostly on the application in brain tissues. However, neuronal networks spread throughout the body where effects might also develop.

In the presented work, a method for the analysis of active monoamines and metabolites in peripheral murine tissues (liver, pancreas, muscle, and brown and white adipose tissues) as well as cell cultures with HPLC coupled to an electrochemical detector was developed. According to the high selectivity of the detector, a simple method of tissue homogenization and injection of the supernatant after centrifugation could be used. However, specific modifications for each tissue region had to be established to ensure proper extraction of analytes. A solid core particle column was employed and suitable chromatographic conditions established, to lower measurement time on the HPLC instrument and enable high throughput of samples. The method was validated and showed high precision, accuracy, and sensitivity into single digit picogram range. The active neurotransmitters dopamine, norepinephrine, epinephrine, and serotonin, as well as their metabolites 3,4-dihydroxyphenylglycol, 3,4-dihydroxyphenylacetic acid, 3-methoxytyramine, homovanillic acid, and 5-hydroxyindoleacetic acid could be assayed with the method. Further, stability of analyte standards were tested under different storage conditions to ensure reliable quality control during daily calibrations. The stability of extracted samples was also observed over a year to check the possibility of reanalysis. The method was also employed in two different research projects. There it helped to show that, in contrast to recent reports, alternatively activated macrophages do not synthesize catecholamines upon interleukin administration and that they are not a mechanism for adipose tissue adaptive thermogenesis. It also helped in the analysis of sympathetic innervation in tissues of dual specifity phosphatase deficient mice, further explaining the mechanistic pathway of a diabetes risk factor in genome wide association studies.

Additionally, a method for the identification of unknown peaks in the electrochemical chromatograms was tested in this work. A workflow was designed for the extraction of unknowns after HPLC and mass spectrometry analysis after a preceding tagging reaction with benzoyl chloride

to raise sensitivity. However sensitivity limitations of the available instrumentation prevented application in analytes tissue regions.

Further, the presented work deals with Morphine. Usually employed as an analgesic, it is also endogenously produced in mammals via the intermediate norlaudanosoline starting from the neurotransmitter dopamine. Exact functions of this pathway remain unknown, however, a link to Parkinson's disease is possible as higher levels were found in urine of patients treated with L-DOPA. Here, a sensitive method for the analysis of both compounds in single murine brain regions was developed. The method employed dispersive liquid liquid microextraction to achieve a pre-concentration of the analytes before analysis. A novel variant, where methanol was used as an extractant for the first time, was developed and optimized with statistical experimental design. The method was validated and showed high precision, accuracy, and sensitivity. It was applied in single brain regions of mice, where both analytes could be found in the thalamus, striatum, and hippocampus, showing the possibility of future applications in the research of the endogenous morphine pathway concerning Parkinson's disease.

Table of Content

List of Abbreviations

3-MT	3-methoxytyramine
5-HIAA	5-Hydroxyindoleacetic acid
5-HT	Serotonin
AADC	Aromatic L-amino acid decarboxylase
ACN	Acetonitrile
ADH	Aldehyde dehydrogenase
ALDH	Alcohol dehydrogenase
AR	Aldehyde reductase
BAT	Brown adipose tissue
C18	Octadecyl
CA	Catecholamine
CCD	Central composite design
CNS	Central nervous system
COMT	Catechol-o-methyl transferase
Conc.	Concentration
DA	Dopamine
DBH	Dopamine β-hydroxylase
DC	Direct current
DCM	Dichlormethane
DHBA	3,4-Dihydroxybenzylamine
DLLME	Dispersive liquid liquid microextraction
DoE	Design of Experiment
DOPAC	3,4-Dihydroxyphenylacetic acid
Dusp	Dual-specifity phosphatase
E	Epinephrine
ECD	Electrochemical detector
EDL	Extensor digitorum longus
ELISA	Enzyme-linked immunosorbent assay

ESI	Electrospray ionization
FFA	Free fatty acids
GABA	γ-Aminobutyric acid
GI	Gastrointestinal
HETP	Height equivalent to theoretical plate
HG	Higenamine
HPLC	High Performance Liquid Chromatography
HVA	Homovanillic acid
IL	Interleukin
IS	Internal standard
JNK	c-Jun N-terminal kinase
L-DOPA	3,4-Dihydroxyphenylalanine
L-DOPAL	3,4-Dihydroxyphenylacetaldehyde
LLE	Liquid liquid extaction
LOD	Limit of detection
LOQ	Limit of quantification
MA	Monoamine
MAO	Monoamine oxidase
MAPK	Mitogen-activated protein kinase
MeOH	Methanol
MHPG	3-Methoxy-4-hydroxyphenylglycol
min	minute
MO	Morphine
MRM	Multiple reaction monitoring
MS	Mass spectrometry
n.d.	non-detectable
NE	Norepinephrine
NL	Norlaudanosoline
NP	Nalorphine
NS	Nervous system

OFAT	One-factor-at-the-time
PD	Parkinson’s disease
PH	Phenylalanine hydroxylase
PNMT	Phenyl ethanolamine N-methyltransferase
PNS	Peripheral nervous system
PTFE	Polytetrafluorethylene
Q-TOF	Tandem quadrupole and time of flight
R^2	Coefficient of determination
Resp.	Response
RF	Radiofrequency
RP	Reversed phase
RSD	Relative standard deviation
RSP	Response surface plot
RT	Room temperature
SHE	Standard hydrogen electrode
SIM	Single ion monitoring
SPE	Solid phase extraction
SRM	Selected reaction monitoring
TBP	Tributyl phosphate
TCE	Tetrachloroethylen
TH	Tyrosine hydroxylase
THF	Tetrahydrofuran
TIC	Total ion count
TOF	Time of flight
TPH	Tryptophan hydroxylase
TRP	Tryptophan
UPLC	Ultra Performance Liquid Chromatography
Vol.	Volume
WAT	White adipose tissue
α-MPT	α -methyl-p-tyrosine

I. Introduction

The nervous system (NS) is what allows animals to process information and to operate in the world. The first versions possibly evolved around 600 million years ago, which provided a significant advantage in survival and propagation of the organisms. [1] Subsequently, it evolved into the complex system that governs the body of all animals. Key components of the NS are small molecules called neurotransmitters and hormones that relay information and cause specific effects on their receptor cites. As the NS is an integral part of the body, it is also often involved in diseases, such as Parkinson's disease, and psychiatric disorders, such as addiction. In research on these afflictions, laboratory animals, especially mice, are often used. [2] Even though there are many differences, mice and humans are sufficiently similar to allow the use of mice in the research of human conditions. [3]

1.1. Nervous system

In the animal kingdom, the simplest multicellular organisms, such as sponges, do not have a full NS, but already contain precursors, which functions are not fully understood. More advanced radially symmetric organism, such as jellyfish and anemones, don't have a central control structure but neural nets with clusters, called ganglia. Bilateral symmetric organisms represent the majority of the animals with a separate mouth and anus as well as a left and right side. The basic NS structure is conserved in higher mammals, where it can be divided into several subsystems. These subsystems work together in receiving signals and controlling the body, but are responsible for specific tasks. The central nervous system (CNS) consists of the brain as the central command structure at the top together with a relegation ganglia system in the spinal cord, while the peripheral nervous system (PNS) spreads out through the remaining body as a connection from the CNS to muscles and organs. Both contain afferent and efferent pathways, which receive and spread out information, respectively. The PNS can be further divided into two subsystems. The somatic nervous system is responsible for voluntary control of muscles. It is also responsible for involuntary reflex arcs, such as the knee jerk reflex, which bypass the brain and allow for a much faster response. The autonomic nervous system can be further divided in two antagonistic but complementary sides, which are not under voluntary control. The sympathetic nervous system activates the neuronal and hormonal fight-and-flight stress response to external threats. It thereby raises the heart rate and prepares the body for physical exertion. It also controls internal organs and slows down digestion and repair functions. The parasympathetic nervous system on the other side activates the rest and digestion state. It also controls internal organs, slows down the heart rate, and is connected to facial muscles. The enteric nervous system is contained within the lining of the gastrointestinal (GI) tract and is responsible for digestion. It is influenced by and communicates with the para- and sympathetic nervous system, but is also capable of independent, autonomous function.

1.2. Brain

The brain of mice consists of around 70 million neurons while the one of humans contains around 90 billion neurons. [4] Even though this difference in complexity is large, the basic structure between the two organisms is similar. [5] Three major parts can be identified, in turn consisting of smaller regions, responsible for separate tasks (Figure 1).

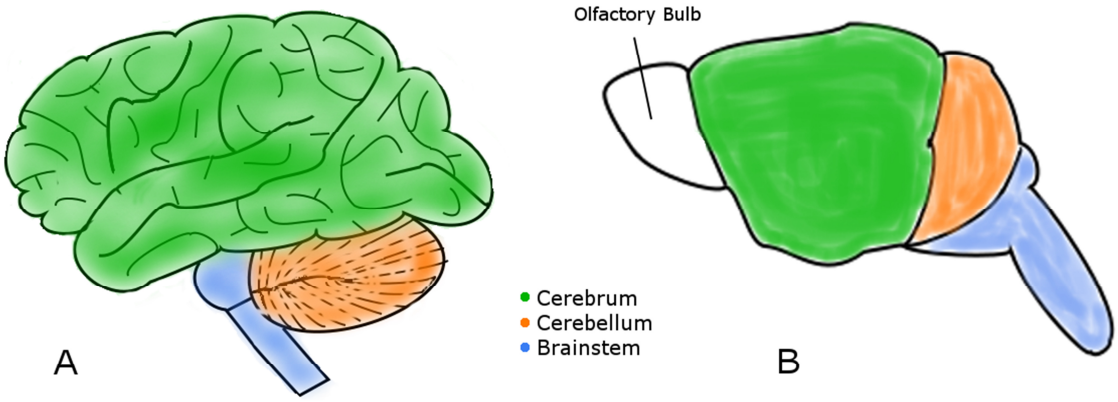

Figure 1: Human (A) and mouse brain (B) with three major regions cerebellum, cerebrum and brainstem; olfactory bulb in humans is in the same position as in mice, however comparatively much smaller.

The lowest compartment is called the brain stem. It consists of the medulla oblongata at the bottom, the pons, and the midbrain at the top. It serves as an important relay station between higher parts of the brain and the spinal cord. It also relays information between the cerebrum and the cerebellum. It is involved in many basic body functions, such as sleep, eating, digestion, heart rate, and blood pressure. [6]

The cerebellum lies behind and above the brainstem. It is involved in motor control of the muscles. However, it does not initiate movement, but integrates information from the spinal cord and the cerebrum to aid in coordination, accuracy, and timing of the movement. Newer research also suggests that it is involved in non-motor functions as well. [7]

The Cerebrum can be divided into the cerebral cortex and subcortical structures. The cerebral cortex is divided into two hemispheres and made up of outer grey and inner white matter. [8] In humans, the outer layer is structured into folds to increase surface area, which gives this structure the typical look of a brain. The hemisphere can be separated into four different lobes with varying functions. The frontal lobe is involved in voluntary motor control, planning, control of emotions, and memory formation. [9] The parietal lobe processes sensory information from the body. It is involved in spatial perception, but also, reading, writing, and mathematics. [10] The occipital lobe is predominantly involved in the formation of vision. [11] The temporal lobe's major functions are hearing and language recognition, vision, and memory formation. [12]

Below the cortices lie several small, important structures that control many functions of the body. The olfactory bulb is below the frontal part of the cortices and is responsible for the sense of smell. [13] Compared to total brain volume, mice have a 200 times larger olfactory bulb, even though no conclusion to an improved sense of smell can be drawn. [14] The thalamus acts as a relay station between the cortices and subcortical regions, is involved in the regulation of sleep cycles, but might also be connected to cognitive functions. [15] The hypothalamus controls the pituitary gland via releasing hormones, which cause secretion of further hormones. Thereby it controls many autonomic functions such as body temperature, sleep and circadian rhythm, hunger, thirst, sexual behavior, and is also involved in stress management. [16] The hippocampus plays an important role in memory formation and spatial navigation. [17] The amygdala is responsible for emotional response such as anger or fear, as well as memory formation. [18] The basal ganglia including the striatum are involved in motor control and executive functions. [19]

These structures are highly interlinked and communicate with and control each other. Oftentimes specific functions cannot be connected to a single part of the brain, but are a result of many structures working together. These regions could also be further divided into smaller neuronal clusters that are each involved in certain functional aspects. For the present work, this overview offers enough resolution, to understand the importance of the NS anatomy and the involvement in diseases and neurological conditions.

1.3. Nervous system and neurotransmitters

The basic components of the NS are called neurons. These cells are responsible for the transmission of signals and consist of a cell body which contains the nucleus and functional compartment of cells. Before the cell body are cell extensions called dendrites that typically receive signals from other neurons and are divided into numerous smaller branches, which can form many connections to other neurons. On the other side of the cell body a single extension, called axon, is present. These are responsible for the transmission of signals and transfer the signal to dendrites of other neurons or to muscles and organs. A cell has only one axon, which differs from the dendrites, in that the radius is constant and does not taper off. The length of these axons varies from a few millimeters up to one meter. The axons also have braches at their end, which form connections to dendrites of other neurons. These connections are called terminal synapses. Several axons bundle together and form nerve tracts in the CNS or nerves in the PNS. [20]

The transmission of signals through neurons functions through an electric potential caused by ions. Neurons have embedded ion pumps that actively transport certain ions across the membrane, creating a chemical potential gradient called resting potential. A signal is transported through an action potential, which is a rapid depolarization of the membrane potential that is propagated along

the axon due to opening of ion channels. This action potential cannot be modulated, but is an all-or-nothing response. Therefore, the strength of a signal is not a degree of the action potential, but rather of an increased firing rate. The signal transmission can be vastly accelerated by myelination of the axons, which is a fat sheath, supplied by so called glia cells. These myelinated axons form the white matter inside the brain, where the axons bundle together in the nerve tracts. The grey matter contains the cell bodies of the neurons. [20]

The transfer of a signal from the axon to another neuron happens at the synapses. When the action potential reaches the axon terminal, voltage gated calcium channels open and calcium ions flood the cell. Inside the terminal are synaptic vesicles, that contain small organic molecules, called neurotransmitters. The concentration increase of calcium ions causes synaptic vesicles to merge with the membrane of the presynaptic neuron and release the neurotransmitters into the synaptic cleft between the two neurons. Once the neurotransmitters pass the presynaptic cleft, they bind to their specific receptors which are linked to ion channels on the membrane of the post synaptic dendrite. Depending on the neurotransmitter and receptor, this can have various effects. It can be excitatory or inhibitory, meaning that the initiation of an action potential at the postsynaptic neuron becomes more or less likely, respectively. These effects arriving at the dendrites of a neuron superimpose onto each other and either trigger a new action potential along the axon or not. Other neurotransmitters also bind not to ion channels, but to receptors that cause a signal cascade within the cell, which can make for example opening of ion channels more or less likely. Altogether, this allows for a modulated response to a signal, instead of the all-or-nothing principle of the action potential. In order to prevent a permanent effect of the neurotransmitters at the receiving neuron, they are released from their receptors and are either taken up by the presynaptic neuron and stored again for further use or metabolized by enzymes in the synaptic cleft. Altogether, neurotransmitters are an essential part of the transmission and modulation of signals along neurons and of the functioning of the NS. [20]

Next to gaseous neurotransmitter such as nitric oxide, regulating synaptic plasticity, [21] and peptides such as oxytocin, relevant in social bonding behavior, [22] another important subclass is made up of single amino acids. Glutamate is the most abundant one in vertebrates and acts excitatory on postsynaptic neurons. [23] It is therefore involved in almost all functions of the nervous system, but can also have an effect on neuroplasticity, meaning it can modulate neuronal connections. Glutamate can be decarboxylated into γ-aminobutyric acid (GABA), which is mainly an inhibitory transmitter of the CNS. [24] Acetylcholine is used for the signal transmission in all preganglionic neurons of the autonomic nervous system. In the parasympathetic nervous system it also used for the signal transfer from the neurons to organs and at the neuromuscular junction, where the neurons meet and activate the according muscles. [25] These compounds play an

important role, yet, they are not part of the method development in this work, as they are not accessible by the applied electrochemical detector.

However, due to their molecule properties, explained in section 2.2.1., monoamines (MA), which comprise multiple important neurotransmitters, can be detected with this instrumentation. Norepinephrine (NE) is one of the major agents involved in the fight-or-flight response. In the brain it is mostly produced in the locus coeruleus, a small nucleus residing in the pons of the brainstem. Even though this region comparatively small, it has wide reaching projections to all major brain regions. The effects of NE in the brain promote wakefulness, alertness, and improve its sensory processing capacity. It also appears to have an effect on memory consolidation. In the body it is the chief neurotransmitter of the ganglia of the sympathetic nervous system. These ganglia project to all major organs and prepare the body for action. A small amount of NE is also released into the blood stream by the adrenal gland, from where it also affects tissues not innervated by the sympathetic nervous system. [26, 27]

Epinephrine (E) is mostly produced by the adrenal gland and also released during the fight and flight stress response. It raises blood flow, heart rate, respiration, and blood glucose levels, thereby also preparing the body for action. Some neurons in the brain also produce E, mostly located in the hypothalamus, where it might be involved in the regulation of arousal. [26, 28]

Dopamine (DA) is produced in the midbrain, specifically the substantia nigra and the ventral tegmental area, from where projections range throughout the whole brain. Depending on the receptor at the postsynaptic neuron it can have both excitatory and inhibitory effects. It has a great effect on motor functions and control, but is also part of the reward and motivation system. Outside the brain, it is present in the blood stream where it increases blood flow and inhibits NE effects. It is also present in several organs such as the pancreas, where it reduces the amount of secreted insulin. [29]

About 90 % of serotonin in the body (5-HT) is produced and stored in the enterochromaffin cells of the gut. Secreted from there, it controls gut peristaltic. It can, however, also play a role in the sensory function of the gut. Also here, depending on the binding receptor, the effects can be either excitatory or inhibitory. Therefore, released into the blood stream, 5-HT can have both vasoconstricting and vasodilating effects and is also involved in blood clotting. It might also be a factor in energy homeostasis. In the brain, it is produced by serotonergic neurons in the raphe nuclei of the brainstem. From there, wide ranging projections reach the whole brain. It influences the sleep-wakefulness cycle, pain perception, and, most well-known, mood. [30]

MAs generally cannot pass the blood-brain barrier and must be produced and stored separately in the body and the brain. [31] Figure 2 shows their metabolization pathways. The active compounds

DA, NE, and E, belong to a class called catecholamines (CAs), which is defined by the catechol structure, consisting of two neighboring hydroxy groups attached to an aromatic ring. The production and degradation of the active compounds is tightly regulated by various enzymes, which can be present in the neurons or the synaptic cleft and form wide and complicated metabolization networks. The three CAs are produced from the amino acids phenylalanine or tyrosine. [32] NE and E share a metabolization network that goes over various intermediates to vanillylmandelic acid or 3,4-dihydroxyphenylglycol (MHPG). DA is metabolized via two pathways to homovanillic acid (HVA). [33] 5-HT, however, is synthesized from the amino acid tryptophan and degraded to 5-hydroxyindoleacetic acid (5-HIAA). [34] Serotonin is also converted to the neurotransmitter melatonin, which is involved in initiating the sleep cycle, but cannot be detected with the ECD.

The activity of the neurotransmitters can be controlled either via the reuptake into neurons by specific transporters or degradation of the active substances in the synaptic cleft or glia cells. The degradation pathways vary between tissue and cell types depending on enzymatic content and activity. The enzymes monoamine oxidases (MAO) A and B, for example, are mostly present in presynaptic neurons, where they result in the oxidation of MA leaked from the synaptic vesicles. Catechol-O-methyl-transferase (COMT) is expressed mostly in postsynaptic neurons and glia cells inside and on outside membranes where it regulates degradation of MAs not transported back into presynaptic neurons. [33, 35] Therefore, an analysis containing a high resolution of the metabolic network is important, as it could point towards specific enzymatic effects and regulations in different tissues.

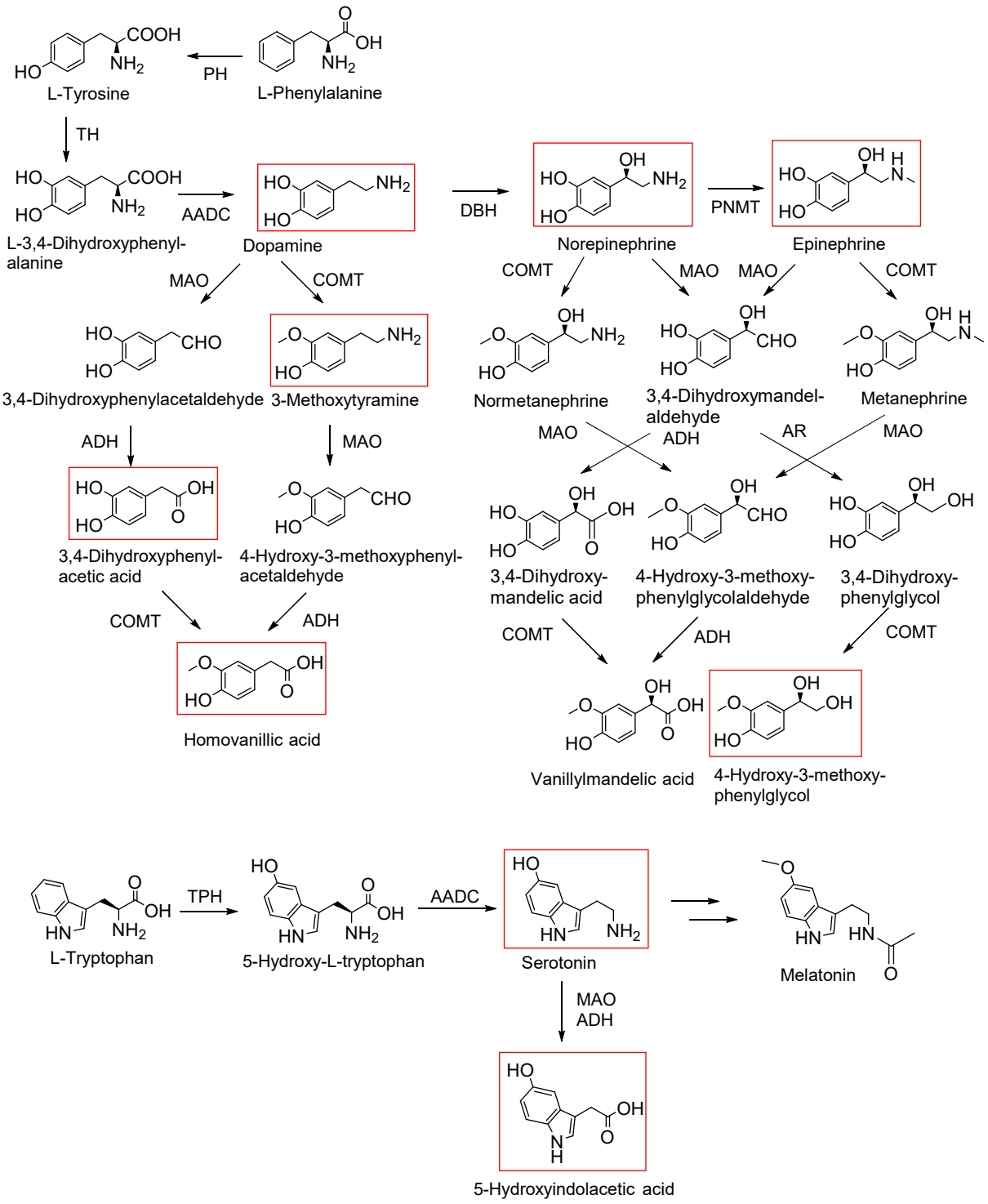

Figure 2: Metabolic pathway of MAs starting from tyrosine or tryptophan; PH: phenylalanine hydroxylase, TH: tyrosine hydroxylase, AADC: aromatic L-amino acid decarboxylase, DBH: dopamine β-hydroxylase, PNMT: phenyl ethanolamine N-methyltransferase, COMT: catechol-O-methyltransferase, MAO: monoamine oxidase, ALDH: alcohol dehydrogenase, ADH: aldehyde dehydrogenase, TPH: tryptophan hydroxylase, AR: aldehyde reductase; red boxes indicate compounds included in the developed method.

Another pathway starting from DA is the production of morphine (MO) (see Figure 3). This opioid is used as a strong pain medication and was previously thought to be present in urine due to dietary contents. However, it is now established that there is indeed an endogenous production of MO in mammals, starting with a Pictet-Spengler reaction of L-3,4-dihydroxyphenylacetaldehyde (L-DOPAL)

and DA, which results in the compound norlaudanosoline (NL), also called tetrahydropapaveroline. The function of this endogenous pathway is not yet fully understood, but proposed roles of endogenous morphine include action as neurotransmitter, involvement in neuroplasticity, nociception, memory, and inflammation. [36]

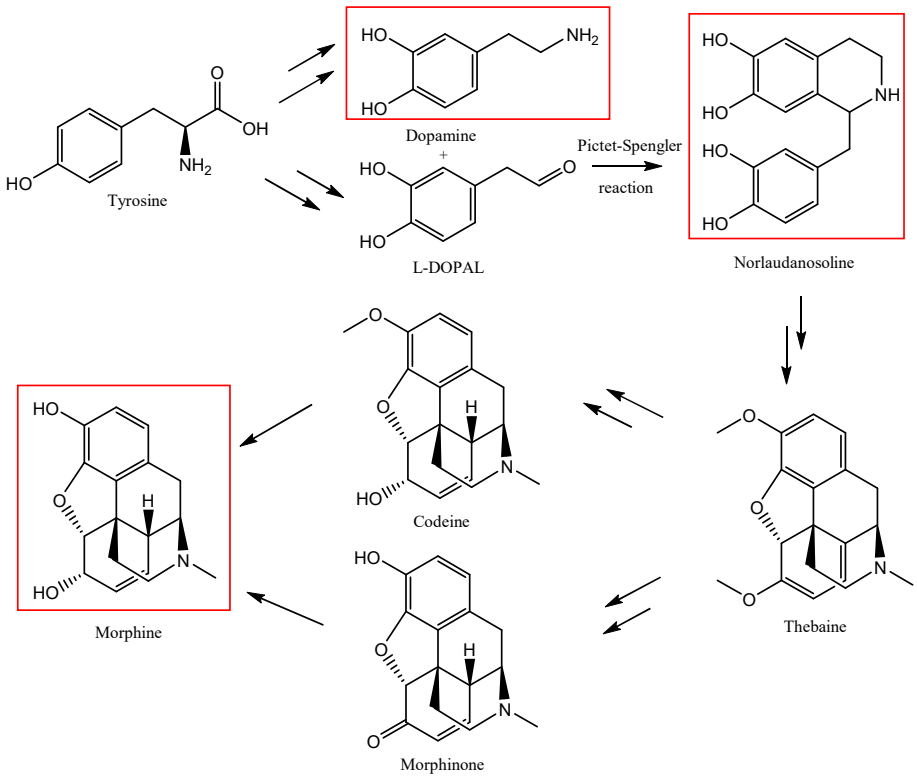

Figure 3: Endogenous formation of morphine from tyrosine; red boxes indicate compounds included in the developed method.

1.4. Neurotransmitters and diseases

Due to their fundamental function in the body, neurotransmitters are often implicated in the onset and progression of chronic diseases. However, often they cannot be identified as the root cause, as most of these diseases have multiple contributing factors, such as genetic predispositions or environmental changes. Yet, there can be no doubt that neurotransmitters have mechanistic effects on the phenotype of the afflictions. Therefore, knowledge of neurotransmitter levels and networks helps to understand the involved systems and might lead to the discovery of the root cause. They can also be used as an early indicator of the onset of diseases. Additionally, until genetic tools are developed and approved for human application, neurotransmitters often offer an accessible target for pharmaceutical treatment, e.g. either by supplementation or inhibition of receptors.

As an example, both 5-HT and NE pathways have been linked to symptoms of chronic depression. [37] One reason for a deficiency might be an increase in the degrading enzyme monoamine oxidase. [38] Antidepressants act on this and prevent metabolization or reuptake of the neurotransmitters and thereby increase and prolong their effect on the receptor site. However, this does not seem to be the only or determining factor, as these antidepressants take a few weeks to work, which points towards indirect effects of these neurotransmitters. [39] Many neurotransmitters have also been linked to various types of addiction. Dopamine, which has been related to the reward and motivation circuits, seems to be the most prominent. However, also serotonergic and adrenergic neurons seem to play a role. [40] Additionally, treatment of rats with NL caused them to increase alcohol consumption. [41] As exposure of neuronal cells to alcohol also causes release of endogenous MO, this pathway might also be linked to alcoholism or other addictions. [42]

Another affliction linked to MAs is Parkinson's disease. It is a neurodegenerative disorder, where dopaminergic neurons of the substantia nigra in the midbrain are degenerated. [43] Even though the exact causes are not known, there are both genetic and environmental factors, such as toxins, involved in the onset of the disease. The resulting loss of dopamine in the striatum of the basal ganglia on top of the midbrain causes many symptoms such as resting tremor, rigidity, postural instability, and bradykinesia, meaning slowing of movement and impaired dexterity. Patients may also experience other symptoms like sleep disorders, anxiety, depression, impaired cognition, hypotension, and nausea. These non-motor symptoms may not be related to loss of DA, but connected to other neurotransmitters, including NE and 5-HT. [44] Interestingly, patients treated with L-3,4-dihydroxyphenylalanine (L-DOPA) as a substitute for loss of dopaminergic neurons showed increased urinary levels of NL and MO. [45] This might indicate a connection between PD and a dysregulated endogenous MO pathway.

One of the most relevant diseases today is type II diabetes mellitus. It is increasing worldwide, with an estimated number of about 9 % of the population in the USA and about 7 % in Germany. [46, 47] During its course, less insulin is produced by the pancreas while the cells in the body become more and more insulin resistant, which increases blood glucose levels. This results in an increased prevalence of cardiovascular diseases, peripheral nerve damage that can lead to amputations, kidney failure, and various types of cancer. [48] While there are genetic factors, lifestyle and chronic obesity are the major risk factors for the development of the disease. Type II diabetes has also been linked to changes in neurotransmitter levels. For example, insulin resistance in the brain might cause an increased DA turnover and therefore mood disorders. [49] Additionally, in the periphery DA might be a contributing factor to insulin secretion and glucose tolerance. [50] 5-HT in the CNS has a suppressing effect on feeding and increase of its signaling is already used as a therapeutic target. [51] However, in the separate peripheral 5-HT systems, it decreases glucose uptake and energy

expenditure in brown adipose tissue, decreases glucose uptake and promotes gluconeogenesis in the liver, increases insulin secretion in the pancreas, and promotes cytokine production in macrophages, leading to insulin resistance. Therefore, in the periphery, 5-HT reduction might have potentially beneficial effects on diabetes. [52] Furthermore, in the periphery, diabetes patients show increased muscle sympathetic activity, as well as increased artery NE levels and impaired plasma NE clearance. [53] In the CNS, diabetes can also alter NE levels. [54]

In the research of these diseases, oftentimes genetically altered mice are used. In many cases, these genetic alterations change neurotransmitter levels and point to mechanistic effects. It is therefore of great importance to have the means to analyze neurotransmitter levels in various murine tissues to be able to detect these changes. For this reason, the following body of work concentrated on the development and application of improved methods for the analysis of neurotransmitter levels in brain and also peripheral tissues of laboratory mice.

II. Theoretical background

2.1. Instrumentation

2.1.1. High Performance Liquid Chromatography

One of the most widely used methods for the separation and analysis of single compounds is called high performance liquid chromatography (HPLC). Here, analytes are separated by differential interactions between a solid stationary phase, based inside a column, and a liquid mobile phase passed along the stationary phase at a steady flow by a pump of an HPLC instrument (Figure 4).

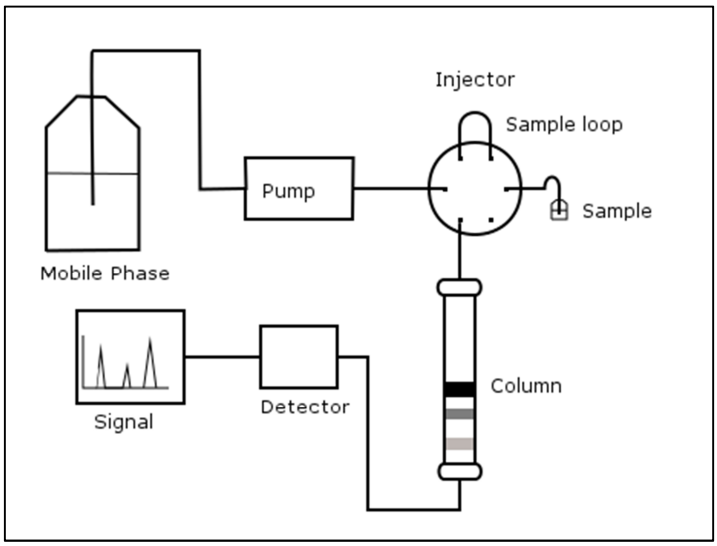

Figure 4: Schematic drawing of a HPLC instrument.

The injection of the sample is usually done by an autosampler that transfers the analytes automatically onto the column via a sample loop and a 6-way port, bypassing or directing mobile phase flow through the sample loop. After the separation on the column, compounds arriving individually at the detector cause a signal that is recorded by a computer and gives rise to a chromatogram, where the signal intensity is graphically plotted against time.

2.1.2. HPLC separation parameters

The separation of the analytes on the column is dependent on the interaction and therefore distribution of analytes between the mobile phase and the stationary phase. [55]

$$K_X = \frac{c_{stat}}{c_{mob}} \quad (1)$$

K_X is the distribution coefficient of compound X, while c_{stat} and c_{mob} are the concentrations of compound X in the stationary and mobile phase, respectively. As the mixture is passed along the column, the compounds diffuse in and out of the stationary phase according to their differential distribution coefficients and are therefore separated along the column. When K is higher, the compound interacts more with the stationary phase and elutes at a later time point due to the higher retention on the column. If the distribution coefficients for the given system setup are different enough, the compounds arrive separately at the detector and give rise to individual peaks, preventing difficulties in assigning and quantifying the peaks due to overlap (see Figure 5).

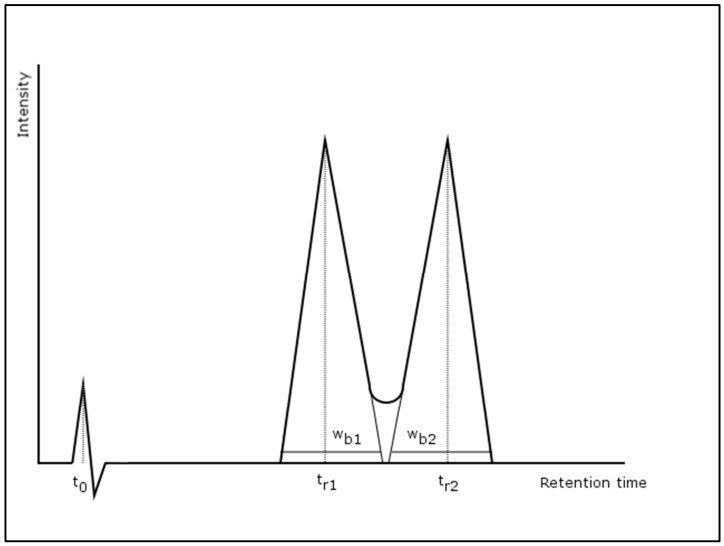

Figure 5: Resolution between peaks of chromatogram after HPLC separation.

The separation between peaks is called resolution and is defined as:

$$R_s = \frac{2(t_{r2}-t_{r1})}{w_{b1}+w_{b2}} \quad (2)$$

The width at the base of two peaks is compared with formula (2). A resolution of 1.5 and higher ensures that neighboring peaks are baseline separated and quantification by area can be done reliably. The resolution is dependent on three chromatographic parameters:

$$R_s = \frac{1}{4}\sqrt{N} \cdot \frac{\alpha-1}{\alpha} \cdot \frac{k}{1+k} \quad (3)$$

The first factor of equation (3) is called efficiency. It is a measure for dispersion of the compounds over the course of the column and therefore the peak width. N is the number of theoretical plates of the column. One plate is the distance on the column over which equilibrium between mobile and stationary phase is achieved. It is calculated by

$$N = 16(\frac{t_r}{w_b})^2 = 5.54(\frac{t_r}{w_{\frac{1}{2}}})^2 \quad (4)$$

where $w_{1/2}$ is the width of the peak at half its height. The higher the number of plates, the lower the dispersion and peak width, which causes better resolution. The plate number is influenced by the column dimensions, particle size, and quality of column packing. Also injection volume, flow rate, and

dead volumes, meaning voids caused by tubing, connections, or detector cell, influence the efficiency.

The second factor of equation (3) is called selectivity and is described by the separation factor α. It describes the differential interaction of compounds between the mobile and stationary phase and is determined by the retention capacity factors k (equation (5)).

$$\alpha = \frac{k_2}{k_1} = \frac{t_{r2} - t_0}{t_{r1} - t_0} \tag{5}$$

The term t_0 is the dead time, which is the time it takes a completely unretained compound to pass through the column. The selectivity of the method can be altered by the type of stationary phase, type of organic solvents in the mobile phase, additives, pH, and temperature.

The last factor of equation (3) is called retention and is a measure of the interaction of an analyte with the stationary phase. It is determined by the capacity factor, defined as the retention time of a compound in comparison with the dead time (equation (6)).

$$k = \frac{t_r - t_0}{t_0} \tag{6}$$

The retention is mostly influenced by the amount of organic solvent in the mobile phase, as it alters the affinity of compounds between the two phases.

The efficiency and therefore peak width is the result of the diffusion of compounds as they pass through the column. This is described by the Van Deemter equation (7) (see Figure 6).

$$H = A + \frac{B}{v} + C \cdot v \tag{7}$$

H stands for the height equivalent to a theoretical plate (HETP). The lower the HETP, the higher the plate number contained within a column and therefore the efficiency and resolution.

$$H = \frac{L}{N} \tag{8}$$

with L being the column length and N the number of theoretical plates in the column.

The first term of the Van Deemter equation, A, is called the Eddy diffusion. It sums up band broadening of the analytes due to differential flow paths through the column. The Eddy diffusion is independent from the linear velocity. However, smaller particles cause a more similar flow path than larger particles. Additionally, well packed columns without voids and a narrow particle size distribution lower the band broadening effect.

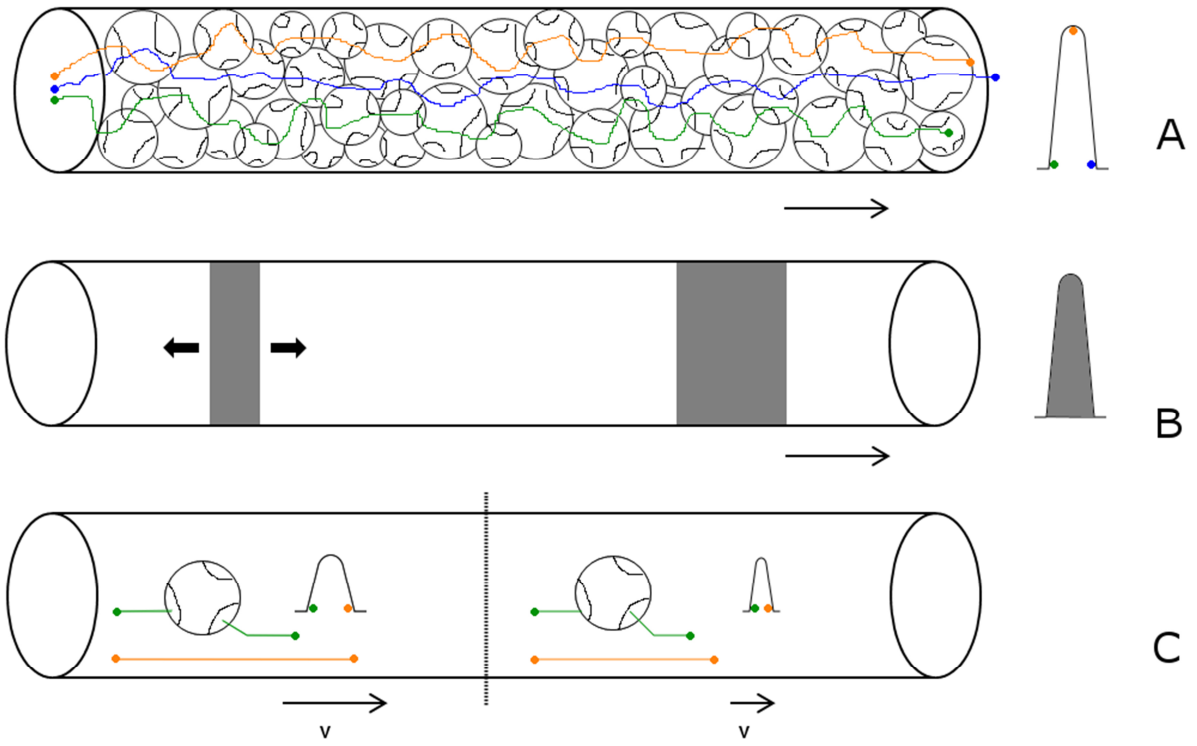

Figure 6: Contributions of the Van Deemter equation to peak width and resolution; A: Eddy diffusion, random flow paths of molecules through the column; B: longitudinal diffusion along the flow path; C: mass transfer between stationary and mobile phase.

The B term of the Van Deemter equation is the longitudinal diffusion. This is caused by movement of the analytes along their concentration gradient in both directions. The longitudinal dispersion is dependent on the flow rate. The higher the linear velocity is, the less time the molecules have for the dispersion and therefore the narrower the peaks are, causing better resolution.

The last term of the Van Deemter (C) equation describes the mass transfer between the mobile and stationary phase. This is due to interaction of the compounds with the stationary phase, but also due to diffusion in and out of the porous particles, where there is no flow of mobile phase. The mass transfer is inversely dependent on the linear velocity. The higher the flow rate, the more distance a molecule can travel with the mobile phase compared to one diffused into a particle. Therefore, with a lower flow rate, the resolution is increased. Also, smaller particles increase resolution due to a decrease of the mass transfer contribution, as the pathway the molecules have to take to diffuse in and out of the particles is smaller. Additionally, raising the temperature speeds up the diffusion processes and increases resolution.

An increase in flow rate causes contradictory contributions of the longitudinal diffusion and mass transfer to HEPT. With a higher velocity, the longitudinal diffusion is decreased, but the contribution of mass transfer is increased. An exemplary plot of the Van Deemter equation is shown in Figure 7, where the three factors have to be optimized to find the minimum plate height.

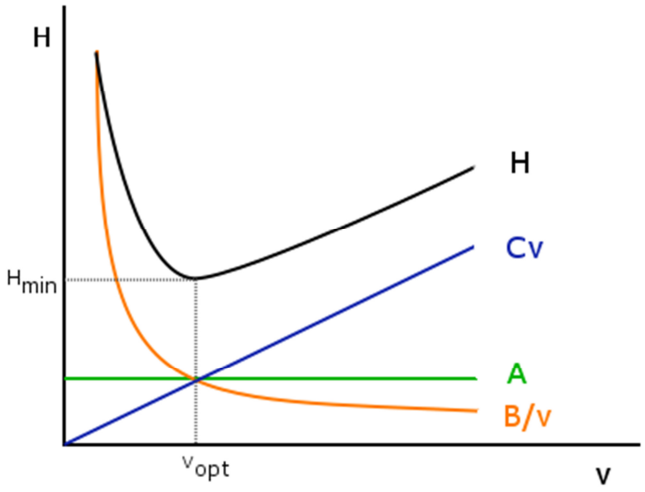

Figure 7: Van Deemter plot showing the dependency of the Van Deemter contributions on the linear velocity of the flow rate and their contribution to the minimum plate height; H: Height equivalent to theoretical plate, v: linear velocity, A: Eddy Diffusion, B: longitudinal diffusion, C: mass transfer.

2.1.3. Column chemistry

One of the major factors influencing retention in HPLC is the chemical structure of the stationary phase and the according mobile phase. [56] In the early variants, silica and alumina particles were used as stationary phases. These particles are hydrophilic, so polar compounds interact more and achieve higher retention. For the elution, nonpolar organic phases were used, which causes hydrophobic compounds to elute first. However, the range of possible applications is limited compared to other phases, as large non polar compounds are not retained and very polar or ionic substances are not eluted from the column.

Another mode of operation that has gained popularity due to its wide range of applications is called reversed phase (RP) chromatography. Here, the stationary phase consists of silica particles modified with an organic, nonpolar structure while an aqueous mobile phase is used. Therefore, polar compounds are eluted first, whereas nonpolar compounds are retained on the column. The most popular modification is the formation of octadecylsilane chains, called C18 phases. Other variants include C8 or phenyl based modifications (see Figure 8). Various columns of the same phase can also have different retention strengths, depending on whether silica groups remain or are modified in a second step with smaller alkyl chains such as trimethylchlorosilane, called endcapping.

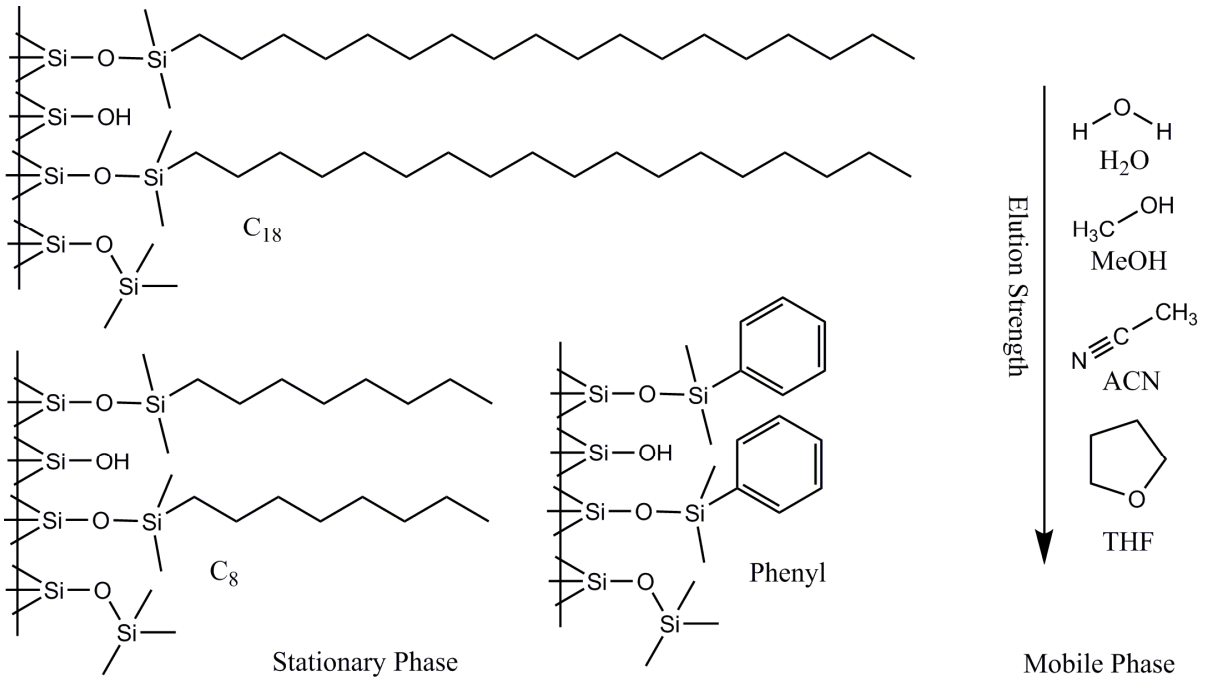

Figure 8: Common stationary and mobile phases in reversed phase chromatography; stationary phases shown partially endcapped.

Water as the most polar compound displaces hydrophobic substances into the stationary phase and therefore has the lowest elution strength for nonpolar compounds. Organic modifiers with a lower polarity can be added to increase elution strength. The most common are methanol (MeOH), acetonitrile (ACN), and tetrahydrofuran (THF). Additionally, the pH of the mobile phase can be adjusted to change the selectivity for charged analytes. When a compound is fully protonated, it interacts more with the stationary phase and is retained longer. When a molecule is deprotonated, its polarity is increased and it elutes faster. Very polar compounds are not retained by RP chromatography, however, the various stationary phases and modifications of the mobile phase allow for a much greater range of molecules to be separated than with normal phase chromatography. When an HPLC is equipped with a dual pump, it is possible to increase the organic modifier content over time in a gradient during an analytic run. This allows a wide range of polarity to be analyzed within one measurement, as in the beginning the mobile phase has a low elution strength and polar compounds can be retained on the column. Later, elution strength is increased so that nonpolar compounds can be eluted as well. This decreases time needed for the elution of all analytes.

2.1.4. Solid core particles

Usually, particles used in column chromatography are fully porous, which contributes to the mass transfer term of the Van Deemter equation. Smaller particles improve mass transfer and therefore reduce HEPT and increase resolution. They also improve analysis time as analytes move faster through the column. However, one major drawback of this approach is the increased back pressure in the system.

$$\Delta P = \frac{\eta L F}{K^0 d_c^2 d_p^2} \tag{9}$$

The back pressure is dependent on the viscosity η of the mobile phase, the flow rate F, the length of the column L, the column permeability K^0, the square diameter of the column d_c, and the square of the particle diameter d_p. Therefore, a decrease in particle diameter causes a quadratic increase in back pressure. Most conventional HPLC are not build for the back pressure of small particle sizes below 2 µm. Therefore, Ultra Performance Liquid Chromatography (UPLC) instruments have been built that allow back pressure in excess of 1000 bar. These instruments allow employment of small particles below 2 µm and result in very fast analysis time with a sharp resolution.

However, in recent years another type of particle has been introduced that allows a similar increase in resolution and analysis time without the increased back pressure. [57] These particles have a solid core with a small outer porous layer through which the analytes travel (see Figure 9). This reduces the mass transfer diffusion as well as the Eddy diffusion and results in the discussed advantages. Additionally, vendors state that these core shell particles allow a tighter control of the size distribution and column packing during the production process, which also improves the A and C term of the Van Deemter equation. Therefore, larger partially porous particles achieve the same efficiency as smaller fully porous particles at a much lower back pressure. Thus, these columns can be employed in laboratories without modern UPLC instruments and allow an increased throughput of samples on older conventional HPLC instruments.

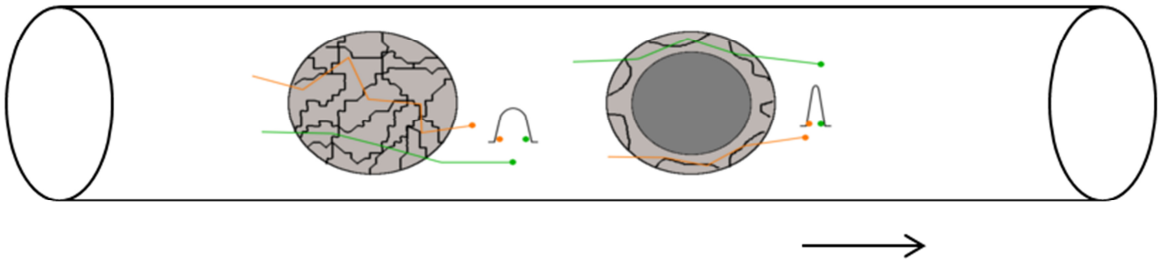

Figure 9: Comparison of mass transfer and Eddy diffusion between fully porous particles and particles with a solid core, resulting in increased resolution.

2.2. HPLC Detectors

2.2.1. Electrochemical detector

Oftentimes fluorescence, UV/VIS, or mass spectrometry detectors are coupled to HPLC instrument for the analysis of compounds after separation. However, one of the most popular choices for the measurement of MAs is the electrochemical detector (ECD) due to its high selectivity and sensitivity. Here, compounds are either oxidized or reduced and the resulting electron current to and from the electrode is detected. [58]

2.2.1.1. Electrochemical cell structure

In a galvanic cell, such as a battery, a redox reaction takes place spontaneously and results in an electric current between the two half cells, where oxidation and reduction take place separately. In an electrochemical detection cell, a voltage is applied to drive a non-spontaneous redox reaction. Such a cell consists of three electrodes (working, auxiliary, and reference electrode). At the working electrode, the analytes undergo either oxidation or reduction depending on the applied voltage. At the auxiliary electrode, the complementary part of the redox reaction takes place. These can be considered as the two half cells of an electrolytic cell. The Nernst equation describes the processes of the electrodes.

$$E = E^0 + \frac{RT}{z_e F} ln \frac{[Ox]}{[Red]} \quad (10)$$

E is the electrode potential, E^0 the standard electrode potential, R the universal gas constant, T the absolute temperature, z_e the number of transferred electrodes, and F the Faraday constant. From the equation it can be seen that when the cell potential is changed the concentrations of reactants has to change as well. As the standard electrode potentials are described for the reduction reaction, when the applied potential is positive the electrode acts as an oxidizing agent and the analytes at the electrode are oxidized, thus emitting electrons into the electrode. Conversely, if the potential is negative, the analytes are reduced and receive electrons from the working electrode. Therefore, a working electrode can be both an anode when oxidization takes place and a cathode when inducing reductions.

The potential of an electrode cannot be determined in absolute numbers, but only in comparison to a reference cell. [58] For the description of a standard electrode potential, a standard hydrogen electrode (SHE) is used as the reference and set to zero. However, these are not applicable in a standard HPLC detection system. The auxiliary cell could also be used to adjust the potential of the working electrode, however, the current flowing through both electrodes would change the potentials and make a consistent application difficult. Therefore, an additional reference electrode is usually installed, through which no current flows so that a constant potential can be applied at the

working electrode. The most common reference electrode is the Ag/AgCl electrode. A silver wire coated with silver chloride is put into a solution with a known concentration of potassium chloride.

The potential of the redox reaction

$$AgCl \rightleftarrows Ag^{+}\ Cl^{-}$$

is dependent on the solubility of Ag^{+} which is in turn dependent on the solubility of the counter anion Cl^{-}, which is limited by the concentration of the KCl solution. As only high concentrations of salt solution are used, the potential remains constant. This can be considered one half cell and can be used to determine the potential of the working electrode. At a saturated KCl solution (3.5 M), E^{0} of the Ag/AgCl electrode compared to the SHE is + 0.205 V. Therefore, it is important for the reporting of any electrochemical detection to mention the type of reference electrode that was used to adjust the applied potential at the working electrode. Over time there can be loss of anions, which shifts the potential of the working electrode. Then, reference electrodes have to be regenerated or replaced.

2.2.1.2. Working electrode

At the working electrode, multiple processes contribute to the resulting current. [58] Faradays law states that the flow of charge is proportional to the material quantity.

$$Q = nFN \tag{11}$$

Q is the charge, n the mole of electrons transferred, F the Faraday constant, and N the mole of material. Therefore, all processes contributing to a current at the working electrode through a chemical reaction are called faradaic processes. This includes the redox reaction of the analyte, but also reactions of impurities, electrolytes, electrode surface, oxygen, and water at extreme potentials. The latter are permanently present and contribute to the background current, which often is much higher than the current caused by analytes. However, due to the separation of compounds by HPLC, the background current can be filtered out and set to zero between arriving substances, so that only the analyte current can be picked up and enhanced electronically, giving rise to the peak signal. The remaining baseline noise is due to e.g. pump pulsation, electrode surface reactions, hydrodynamic flow in the cell, or power line noise. In modern instruments this noise is reduced drastically with precise pumps, flow cell design, and electronic filtering.

A non-faradaic process that contributes to the signal is the charging current. The interface between the electrode surface and the electrolyte solution can be construed as a double layer of charged particles. This double layer can act as a capacitator and store charge. Therefore, when a potential is applied to the electrode, there is a charging current that decreases rapidly with time as the layer reaches its full capacity. As long as the potential of the electrode and the solvent composition are

held constant, this capacitive current is nonexistent. This is the reason that the cell potential cannot be changed during a measurement and that no mobile phase gradient can be used with electrochemical detection, as both would change the capacity of the double layer and therefore result in an uncontrolled current. An isocratic elution, meaning constant mobile phase conditions, prevents this. The capacitive current is also the reason for the solvent front peak in chromatograms, as at the beginning of an injection the ionic strength of the mobile phase varies.

The response of the detector to the analytes is mostly dependent on the applied potential. If the potential is not high enough to oxidize or reduce a compound, there is no electron current that can be detected. This results in great selectivity of the ECD, as compounds that are not redox active or below the potential reaction limit do not contribute to the signal. As the reaction is dependent on the reaction potential of the analytes and the working electrode potential is set in comparison to a reference electrode, it is possible that analytes can also be reduced at a positive working electrode potential and vice versa. The signal intensity also varies from compound to compound due to the number of electrons transferred, the diffusion from the bulk solution to the electrode surface, and the type of electrode surface. One of the most popular materials is glassy carbon. These electrodes offer a wide potential window, are inert to solvent reactions, and have a low adsorption rate of compounds, called fouling. Other applied materials include gold, platinum, mercury or graphitic carbon. Also surface modifications and reactions have been used to vary the selectivity.

The type of electrode and its potential are chosen, so that the rate limiting step of the detection is not the chemical reaction but the mass transfer of the compound to the electrode surface. Mass transfer can occur through migration (movement of charged molecules under an electric field), convection (stirring), and diffusion (movement of molecules along a concentration gradient). Diffusion is the slowest and therefore the rate limiting step. Under these conditions, the maximal current achievable is described by the general equation

$$i_{lim} = nFAC(\frac{D}{\delta}) \tag{12}$$

with the number of transferred electrons n, the Faraday constant F, the surface area of the electrode A, the concentration of analyte C, the diffusion rate D, and the diffusion layer thickness δ. The diffusion part of the equation can take various forms depending on the geometry of the flow cell and is also dependent on the flow rate. However, for a given assembly of parameters, it becomes clear that the resulting current is directly proportional to the amount of analyte present in the flow cell. Therefore, the higher the concentration of a compound in a sample, the higher is the response of the detector and the signal intensity.

The optimal potential for any analyte has to be tested. During cyclic voltammetry, the analyte is present in an unstirred solution. Then, the potential is ramped up and down with time and gives rise to a cyclic voltammogram that shows both the potential at which the reaction and reverse reaction take place, since the product is not transported away. Some detectors are able to apply cyclic voltammetry during scan mode in combination with HPLC (where the analyte is spiked into the mobile phase) to adjust for variations in optimum potential due to flow conditions (see Figure 10 A).

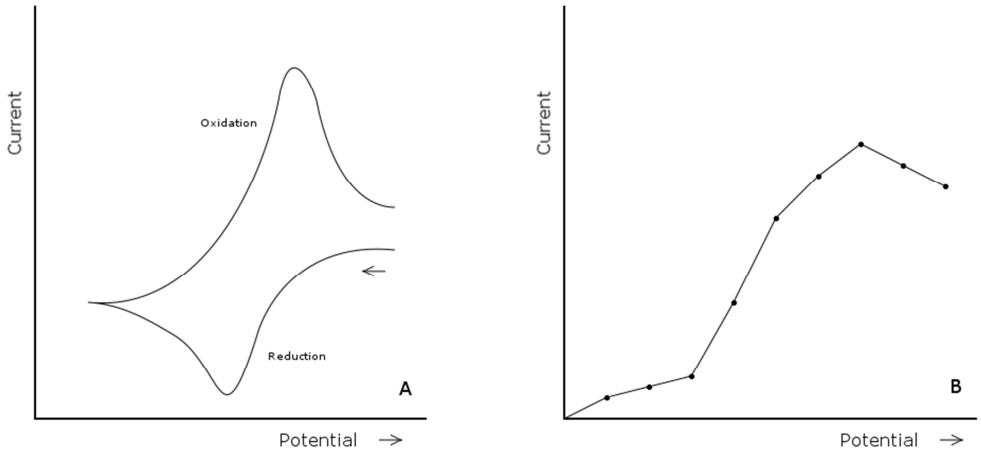

Figure 10: Schematic cyclic (A) and hydrodynamic (B) voltammogram for finding the optimal potential of the working electrode for maximum reaction of analyte at the electrode.

However, cyclic voltammetry instrumentation might not be available or multiple compounds need to be analyzed simultaneously. In these cases, such as in this work, hydrodynamic voltammetry is often applied. A standard solution at a constant concentration is injected at incrementally increased working electrode potentials. The result is a current-voltage curve that shows where the limited current is achieved and the response turns into a plateau (see Figure 10 B). The optimal current per analyte is chosen just shortly of the plateau to get the most sensitivity, but also prevent reaction of other compounds reacting at a higher potential.

2.2.1.3. Coulometric and amperometric electrochemical detector

Two major types of detectors can be used for electrochemical detection. [59] In amperometric analysis, the mobile phase flows through a cell in which the working and auxiliary electrodes are immersed. Only around 10 % of the analytes react as they come in contact with the electrode surface. This reduces sensitivity, as not all present molecules cause a response signal at the detector. However, at the same time less impurities and electrolytes are subjected to a redox reaction, which reduces baseline noise and thereby increases sensitivity. Additionally, analytes in the sample are not altered completely during the analysis and can be used further if necessary. Even though not all analytes react, the signal is still proportional to the concentration of compound in the mobile phase and can therefore be used for quantification purposes. Two variants of flow cell design are typically

used (Figure 11). In a thin layer flow cell, the mobile phase passes through a narrow channel. The counter electrode is placed opposite of the working electrode, to ensure uniform current between the two. In a wall jet cell, the mobile phase hits the working electrode orthogonally. This raises the amount of oxidized analyte, however due to occurring turbulences, the background noise is also higher. Additionally, the counter electrode has to be placed at a higher distance from the working electrode.

With coulometric detection, 100 % of the analytes are subjected to a reaction, as they flow through a porous membrane which acts as the working electrode (Figure 11). This raises sensitivity, as all analyte molecules cause a signal. In theory, at the same time more impurities and electrolytes react as well which increases the baseline noise and reduces the sensitivity. However, modern electronics together with high precision pumps can remedy this problem, so that a coulometric detector can apply its full capacity and can be more sensitive than amperometric detectors. However, all analytes are altered by the detector and the sample cannot be used further.

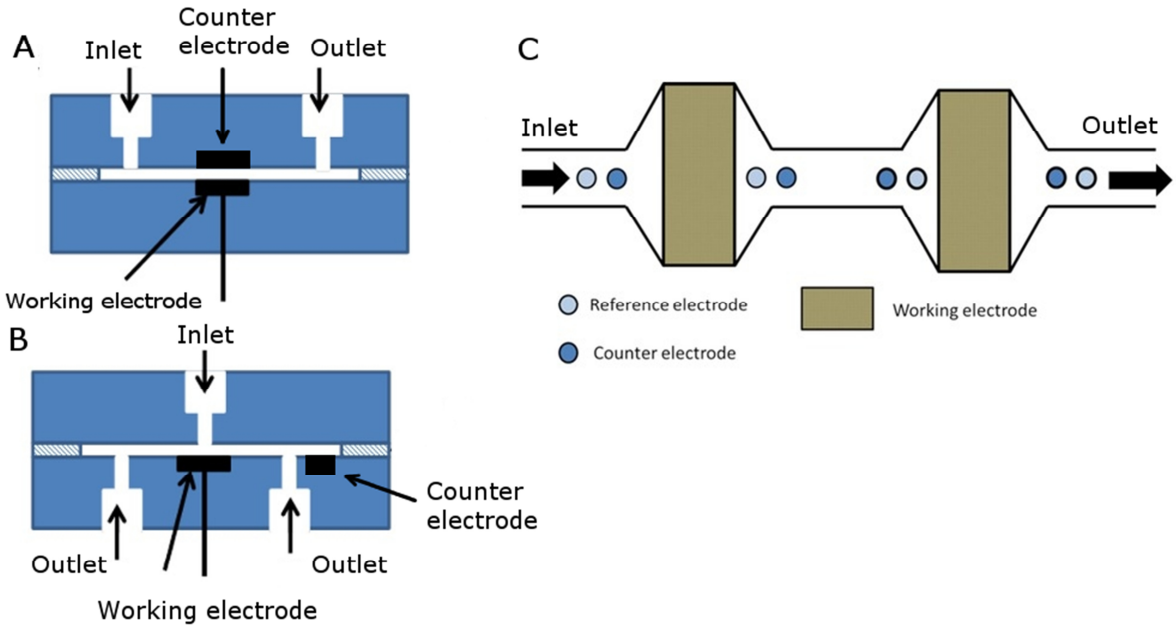

Figure 11: Different cell designs for amperometric and coulometric electrochemical detection; A: Thin layer amperometric flow cell; B: Wall jet amperometric flow cell; C: Dual coulometric cell (according to [59]).

Detectors can also have multiple cells at which different potentials can be applied. This can be used to increase selectivity, as for example compounds that have the same or similar chromatographic elution time but different redox potential can be detected separately at the detector when different potentials are applied. Also, with a coulometric detector one cell can be used to clean electrolyte impurities in the mobile phase to allow a better detection at the second cell. Other applications use the first cell to e.g. reduce all compounds to allow a reliable and sensitive oxidative detection at the

second cell [60]. This allows a high flexibility of the electrochemical detector in a wide array of applications.

2.2.1.4. Electrode reaction

Generally, hydroxy-, phenol-, catechol, quinone-, amine-, and thiol-groups are susceptible for redox reactions. As MAs and especially the subgroup of CAs contain one or multiple of these groups, electrochemical detection is especially suitable for their analysis due to the high selectivity and sensitivity. For example, for the catechol structure, two proton dependent electron transfers take place the electrode surface (Figure 12). [61]

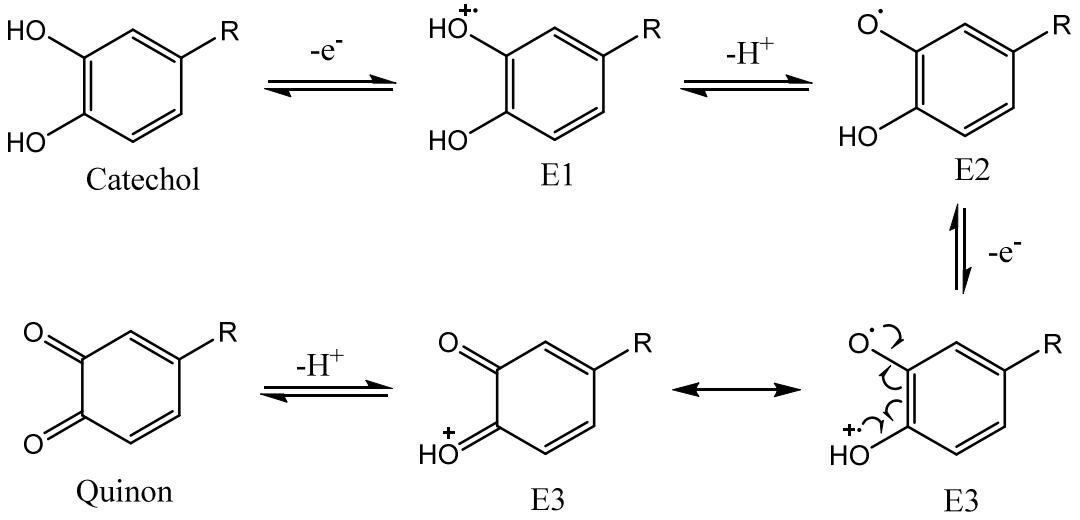

Figure 12: Possible oxidation of a catechol structure to the quinone via two proton dependent electron transfers.

The mechanism can be different according to the pH of the mobile phase. At higher pH one or both hydroxy groups are deprotonated and fewer electrons are transferred. Additionally, the intermediate E1 is not stabilized at pH levels above 5, and undergoes deprotonation first and then an electron transfer. At lower pH, E2 is stabilized and the electron transfer occurs first. In this case, the first electron separation is the transition state, requiring a higher potential. [61] The mechanism for the reaction of other redox active groups follows the same pattern. [62, 63] Therefore, the number of electrons transferred during the reactions depends on the number of active groups present in the analyte molecule. Additionally, neighboring groups and pH might influence the stability of intermediate products and also affect the intensity of the signal.

2.2.2. Mass spectrometry detector

Generally, nowadays the most popular and versatile detector is the mass spectrometer. [64] There, no chemical reaction as with electrochemical detection is observed, but the mass of the compounds is analyzed. To achieve this, analytes are ionized, and then separated according to their mass to charge ratio (m/z). For the separation of the ions, a collision free movement has to be ensured. Therefore, analytes have to be in the gas phase within a vacuum, free of other particles.

Consequently, a mass spectrometer consists of four general parts. First, there has to be an inlet into the instrument, after which an ion source needs to be employed. The compounds are then sorted in the analyzer and afterwards transformed into an electronic signal at the detector. The resulting plot of the m/z ratios to their relative abundance is called a mass spectrum. The identification of molecules can be done with the calculated masses or so called fragmentation patterns, where molecules are split into smaller parts.

When coupled to liquid chromatography, the eluent first has to be evaporated and molecules transferred into the gas phase before they can be analyzed with MS. The chosen mode of evaporation and ionization depends on the polarity and size of the analytes. For smaller non-polar to less polar compounds atmospheric pressure chemical ionization or atmospheric pressure photo ionization can be used, during which the mobile phase is turned into a fine spray by a nebulizer gas and then evaporated in a heater. The molecules are then ionized by a charged reagent gas or photons. For small to large polar compounds, electrospray ionization (ESI) is employed. The eluent is nebulized by a gas, however, at the needle tip an electrostatic field is applied which results in charged liquid droplets containing the molecules. Afterwards a drying gas dissolves the droplets. When the repulsive electrostatic forces within the droplets are stronger than the cohesive forces, a so called coulomb explosion occurs, which results in finer charged particles. This process is repeated until only charged molecules remain. This method is very soft and does not result in fragmentation of compounds. Afterwards, in all variants, the charged molecules are transported via electric forces into the vacuum zone.

Different types of mass analyzers exist which can be combined to allow high flexibility of analysis parameters. The simplest variant is a single quadrupole, which consists of four parallel metal rods. At two neighboring rods direct current (DC) and radiofrequency (RF) potentials are applied. At a certain voltage and frequency, only compounds with a specific m/z ratio achieve a stable flight path and can pass the rods. All other ratios collide with the rods and are removed. Therefore the instrument can be used in two ways: During singe ion monitoring (SIM), only one specific ion is allowed to pass. During scan mode, the voltage and frequency are varied, so that only one ion is allowed to pass at a time. Then the desired range of masses is scanned over short periods of time.

Triple quadrupole (QQQ) instruments combine three quadrupole mass analyzers. At the first and third DC and RF are applied, which allow SIM or scan mode. The central analyzer only uses RF to act as a collision cell, which causes fragmentation of the molecules. This allows different modes of operation. During selected reaction monitoring (SRM) a single ion is passed through Q1, fragmented in Q2, and a single fragmentation product is detected in Q3. With multiple reaction monitoring

(MRM) several fragmentation products of one or more precursor ions are detected in Q3. Also a scan of all masses can be done with Q3 after fragmentation of selected ions.

Another popular variant is the time of flight detector (TOF). The ions are propelled into a flight tube, where heavier molecules at the same charge reach lower velocities and therefore take longer to arrive at the detector. Therefore, due to the time of flight the m/z ratio can be determined. Often an ion mirror is placed in the middle of the flight path to repel the ions to the detector. This allows the construction of smaller instruments, as the length of flight is doubled in the same space. Oftentimes, these mass analyzers are employed in tandem with a preceding quadrupole (Q-TOF), to allow selection and fragmentation of specific masses.

For all mass analyzers, a specific device needs to be employed to count the number of arriving ions resulting in an electronic signal. Mostly electron multipliers, where the ions generate an increasing electron stream, or photomultipliers, where the same happens with generated photons, are used. The ion detectors have to recognize a low number of ions to achieve a high overall sensitivity. Additionally, the dead time of the detector and subsequent electronics need to be low, to allow the detection of m/z ratios arriving close together e.g. during time of flight, to achieve a high mass resolution. Mass resolution is defined as the ability of an MS instrument to separate two masses. At equal height with a valley between the peaks at a specified height (e.g. 10 %), it is defined as the weight of the second peak divided by the mass difference between peaks. Another definition is the mass of the peak divided by the width of the peak a certain height (e.g. 50 %). A high resolution is necessary to separately detect compounds close together in weight in complex mixtures. Together with high mass accuracy it results in reliable monoisotopic mass detection, which is required to reduce the number of possible candidates in compound identification.

2.2.3. Detectors used in the analysis of monoamines

Many detectors are available for the analysis of MAs. Some methods have employed a fluorescence detector utilizing the native fluorescence of the compounds. Here, analytes are excited by light, and emit photons when they undergo relaxation, which are then detected. [65] Other variants include derivatization reactions with various reagents to increase fluorescence and therefore sensitivity. [66, 67] The high selectivity of the detector usually allows short and non-extensive clean-ups, however there might be so called quenching due to sample components that lower detected fluorescence. Depending on the derivatization reagent, the sensitivity can go as low as the lower femtogram range. [68] Additionally, chemiluminescence methods have been used, where the excited state which emits photons is not caused by light but by a chemical reaction. They can also reach the femtogram sensitivity range. [69] Here, disadvantages are the additional reagent consumption and also lack of selectivity, as other sample components might be susceptible to a chemiluminescence reaction. [70]

UV absorption has also been used for the analysis of MAs. [71] However, generally UV/Vis methods lack the selectivity and sensitivity for the analysis of low concentration of compounds in biological tissues.

In recent years, analysis of MAs with mass spectrometry has gained popularity, since the widespread use of triple quad instruments and Q-TOFs has increased selectivity and sensitivity due to the available SRM/MRM modes and modern instrumentation. [72] However, since MAs are small and polar, they are not easily retained on RP columns. The alternative use of ion pairing reagents is difficult, as they are involatile and can contaminate the interface or MS cells. [73] Additionally, the small, polar molecules themselves are not very volatile and have a low ionization efficiency, which results in low sensitivity. [74] Chemical derivatization of the analytes before analysis increases retention on columns and ionization of the molecules, thereby resulting in a higher sensitivity into the lower femtogram range. [75] Since MS instruments detect most compounds and selectivity is achieved by MS/MS variations, for single cell instruments coeluting compounds can disturb measurements. Additionally, matrix components can cause ion suppression or enhancement. [76] Therefore, a more extensive sample preparation is necessary than for other detectors. However, the detection of a wider range of neurotransmitter classes, which is not dependent on specific chemical structures, is possible. [75, 77] Further, MS instruments allow structural identification through fragmentation experiments or direct identification if the resolution of the instrument is high enough. Another advantage is the possibility to use isotopically labeled internal standards. There, the same molecule as the analyte but with different isotopes such as ^{13}C, is added before the extraction. Both molecules behave the same during extraction and coelute within the same time window but can be separated in the MS due to the mass difference. Therefore the labeled IS can be used to correct for loss of analyte during the clean-up or ion suppression at the interface. The disadvantages of MS instruments are the high cost, high skill, and difficult maintenance. However, as a reliable and versatile instrumentation, MS has been used more widely in recent years for the analysis of MAs in different species from snails over mice to humans and in different matrices from urine to brain tissue. [78-81]

The major disadvantage of an ECD compared to MS instruments, is that no structural information, except that a redox reaction occurs, is elucidated. Therefore, identification of compounds can only be done by comparison of retention time to standards. This makes identification of unknowns especially difficult. Additionally, the use of labeled internal standards is not possible, as there is no differential reaction at the detector. For the use of IS, compounds structurally similar to the analytes have to be found and tested for equal behavior during the extraction procedure. Another detriment is the dependence on redox active groups within the molecule for detection. Therefore, neurotransmitters outside of MAs are often not accessible by this detector. However, derivatization reactions can also

be employed here, to add redox active components in a quantitative way. [82] Furthermore, this high selectivity is also one of the biggest advantages of ECD, as no extensive sample clean-up is necessary, which lowers laboratory time and cost and raises sample throughput. The ECD is also very sensitive, often reaching the femtogram range. Depending on analytes, flow cell, and electrode material, amperometric electrodes can be prone to fouling, however, their maintenance is not complicated and can be done fast. Modern coulometric detectors don't have to be polished and are very low in maintenance. ECDs also have a low cost, compared to MS detectors, which makes this variant more affordable for small analytical laboratories, where no modern MS instrumentation is available. Therefore, despite other detector variations and developments, ECD remains the most popular choice for the analysis of MAs according to the number of publications on Web of Science. In recent years, it has been used in various matrices and species for the detection of MAs in research and clinical settings. [83-88]

2.3. Extraction techniques

For most detectors, samples have to be purified to get rid of disruptive compounds and matrix components to achieve an accurate and reproducible analysis. Therefore, sampling and clean-up procedures are an important part of any analytical method. Due to its selectivity for redox active substances, the clean-up does not have to be as elaborate for an electrochemical detector. However, to detect MAs out of biological tissues, the compounds have to be brought into a liquid phase to be compatible with HPLC. This is done with liquid extraction techniques. Most commonly, an acid, sometimes with additional antioxidants, is added to solid tissue samples, which are then homogenized with ultrasonication. [89-91] Here, cell membranes are broken by ultrasonic waves, sent by a metal rod, and compounds are released into the liquid phase. The acid additionally precipitates proteins, which are then separated together with fat particles from the solution via centrifugation to prevent blocking of the HPLC column and disturbance of the detector. For liquid matrices such as plasma and urine, this procedure might also work for the precipitation and removal of proteins, however, the resulting solution volume might be too high and lower the concentration of analytes below the limit of quantification. Here, for clean-up and also concentration purposes, a technique called solid phase extraction (SPE) is often employed.

For extraction, the liquid sample is loaded onto a column containing solid particles with specific chemistry, similar to an HPLC column. The analytes bind to the particles, and other compounds and impurities are removed with a washing solution. Then, a specific elution reagent is added to release the analytes from the particles and wash them down as well. When a lower volume of eluting reagent than the volume of the sample is added, the concentration of analytes is increased.

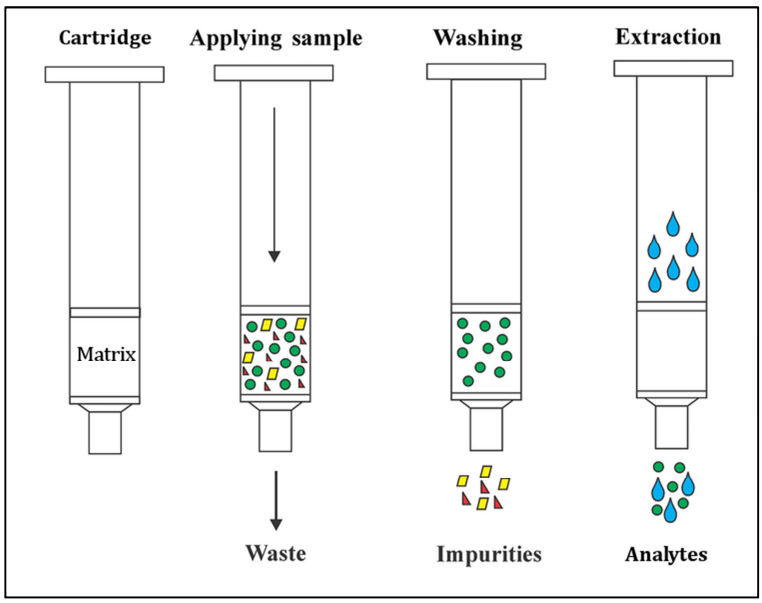

Figure 13: Procedure of a solid phase extraction for the purification and concentration of analytes in a liquid matrix (adapted from [92]).

A popular type of SPE used for CAs, is alumina oxide. [93, 94] It selectively binds the catechol moiety and retains the compounds during the washing steps. The major drawback, however, is that only CAs can be analyzed this way and most of their metabolites are washed away and lost for the analysis. Other types of SPE include C8 or C18 variants, cation exchangers, and phenylboronic acid. [95-97] Disadvantages of this method are the constant use of expensive consumables, high amount of solvent use, and time intensive laboratory work, which prevents high throughput without automated machines.

Another common extraction procedure is liquid liquid extraction (LLE). [98] A solvent that is not miscible with the liquid sample is added and the solution is shaken. Afterwards the two phases separate and can be taken individually. The analytes prefer one phase over the other depending on their chemistry or lipophilicity and can be separated from other compounds and interfering matrix components. The organic phases containing the analytes can be evaporated and the analytes reconstituted in a solvent compatible with the HPLC mobile phase. This procedure works well for non-polar compounds, however it is also labor intensive and consumes a high amount of solvents.

In order to remedy this problem, Rezaee *et al.* developed a variant called dispersive liquid liquid micro extraction (DLLME). [99] Here, a mixture of two solvents is added to the liquid sample. One, called the extractant is not miscible with the sample phase and serves the same purpose as in conventional LLE. The other, called the disperser, is miscible with both the extractant and the sample phase. Rapid injection of the extractant/disperser mixture into the sample results in a fine dispersion of extractant droplets.

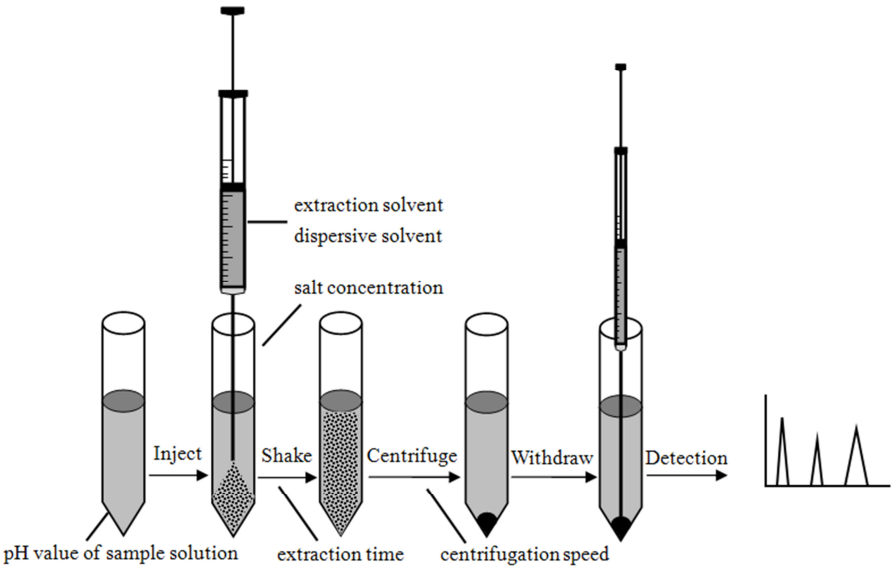

Figure 14: DLLME procedure with a high density extractant found at the bottom of the tube after centrifugation; procedures with lower density extractants are possible, where the extractant floats on top of the solution (adapted from [100]).

The analytes diffuse into the droplets and due to their fine distribution and high surface area, a very fast equilibrium and therefore extraction is achieved. Afterwards, the dispersion is centrifuged. When the extractant has a higher density than water, it can be found at the bottom of the tube in the form of a small droplet than can be taken directly with a syringe. This variant works well for non-polar compounds with high logP values that favor the organic phase over the aqueous phase. The major advantages of this method are the fast extraction and the low amount of necessary solvents, making it inexpensive, environmentally friendly, and suitable for a high throughput of samples. In its original form, tetrachloroethylene was used as the extractant, mixed with acetone as the disperser for the extraction of polycyclic aromatic hydrocarbons out of a water sample.

Other extractants commonly used are carbon tetrachloride, chlorobenzene, dichloromethane, and chloroform. [101] They have a low solubility in water, have good extraction capabilities for non-polar compounds, and have a higher density than water and can be found at the bottom of the tube after centrifugation. Due to their chlorination, they possess a high toxicity and are not environmentally friendly. Other less hazardous extractants, however, often have a lower density than water. Therefore, they are found at the top of the aqueous phase, and special equipment has been developed, that allows withdrawal of lower density extractants. Mostly, special self-made vessels are employed that have a narrower upper end in which the extractant resides after centrifugation. Due the narrower cone, the small amount of extractants consists of a broader band and can be taken more easily with a syringe. Since often the volume of sample, disperser, and extractants does not result in an exact placement in the narrow part, containers with a side opening have been

introduced. [102] After centrifugation, water can be added through that opening, and the floating extractant is pushed into the narrow end. Another possibility is the use of a conventional plastic pasteur pipettes. Turned upside down, the reservoir serves as the container and can be pushed to extend the solvents into the upper narrow tip. [103] Additionally, for some extractants with a melting point near room temperature, it is possible to cool the solution after centrifugation, resulting in a solid floating drop of extractant on top of the aqueous phase that can be taken easily. Mostly long chain alcohols such as undecanol and dodecanol have been used this way. [102] However, when the aqueous phase is not too voluminous and there is enough extractant, it is also possible to abandon home-made devices and just remove the lower aqueous phase with a long syringe needle and leave the extractant in the container.

Another variant of extractants are ionic liquids. The dispersion is assisted by a disperser, heat, ultrasound, or microwaves. [104] These allow more versatile methods, also applicable for less lipophilic small organic compounds. The main advantages are the low miscibility with water, low volatility, and the direct compatibility of ionic liquids with most aqueous mobile phases.

The selection of the correct disperser is also very important for the success of the DLLME method. It has to be soluble in both the extractant and the sample phase and cause a stable dispersion upon injection. Usually, MeOH, ethanol, acetone, or ACN fulfill this requirement and are most often chosen. [101] Additionally, the volume has to be in the correct proportion to the sample and extractant volume. If the volume is too low, no dispersion occurs. If it is too high, it raises the solubility of analytes in the aqueous phase and lowers extraction efficiency. The volume of the resulting extractant droplet is also dependent on the disperser volume. In the interest of removing the limitations and making the method even more environmentally friendly through the reduction of disperser volume, various techniques have been applied. They include the assistance of ultrasonication, temperature, and addition of surfactant to increase emulsifying strength. [105] Furthermore, pH and salt concentration also play an important role. Depending on the pH, functional groups of organic molecules may be protonated or ionized, thereby affecting the affinity to the aqueous sample phase. [106] Raising the salt concentration of the sample may also alter extraction efficiency through the salting-out effect. [107]

DLLME has mostly been applied to aqueous environmental water samples, due to its easy application in this matrix. [108] Using DLLME for biological samples is more difficult as matrix components such as proteins might affect and disturb extraction efficiency. Additionally, direct application to solid tissues is not possible and intermediate steps must be introduced. However, this disadvantage also applies to other techniques such as SPE or LLE. Therefore more and more publications are applying DLLME to biological and food matrices. [109]

2.4. Design of Experiment

In the development of a DLLME method multiple parameters have to be optimized. Traditionally, method development optimizes the conditions of one parameter, while keeping the others fixed. This one-factor-at-the-time (OFAT) approach requires a lot of experiments and finds an optimum only through coincidence. Further, interactions between factors cannot be recognized. Therefore, using a statistical experimental design for method optimization is very useful. An approach called Design of Experiment (DoE) has gained wide popularity in DLLME development. [110] Here, experimental points are planned and combined to create a test space, which is statistically evaluated to find the effects of all inputs (experimental factors) on the output (results) (see Figure 15). In comparison to the OFAT, interactions between factors can be found while the number of necessary experiments is drastically reduced.

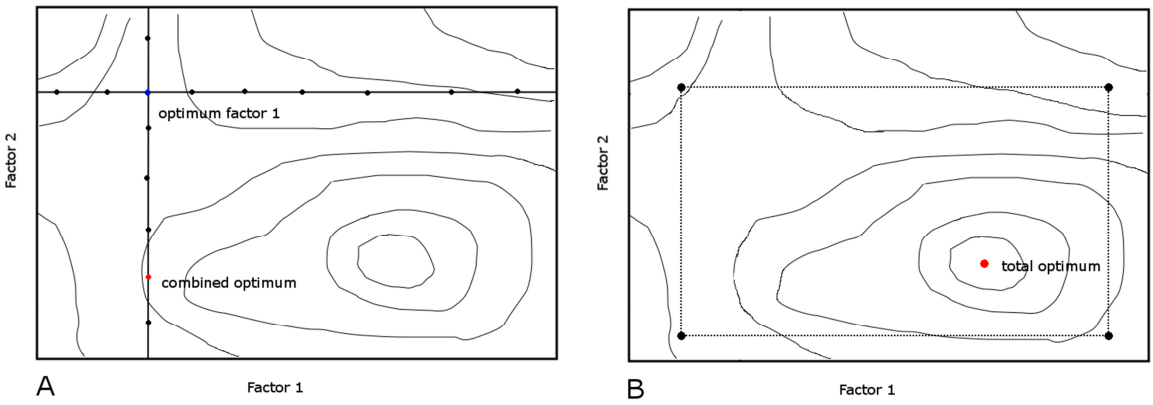

Figure 15: Exemplary method optimization shown by response surface plots; A: One-factor-at-the-time approach, first optimization of factor 1, then optimization of factor 2, combination results in a false optimum; B: DoE approach, experimental points create test space, statistical analysis finds total optimum and interaction between factors.

Multiple approaches for the creation of the test space are available. For the screening of factors, often a full factorial design is used. Here, each factor is assigned two levels and all combinations of levels are experimentally analyzed. The number of resulting experiments therefore is 2^k, with k being the number of factors. If multiple factors need to be analyzed, the workload is high. In order to avoid this, a fractional factorial design can be used, where also two levels are assigned per factor, but not all combinations are experimentally tested. This decreases the workload, however, resolution as well, meaning that possibly not all interaction between factors can be discovered. A resolution of V shows an overlap between major effects of factors and four factor interactions or 2 factor and 3 factor interactions. A resolution of III could not discover interactions between major effects and two factor interactions, and would therefore only show effects of the single factors. However, as interactions of more than two factors are rare, a reduction in number of experiments might be worth the reduction of resolution to above III, if the number of factors is high. Full resolution is achieved

with a full factorial, where all interactions can be analyzed. However, if only two levels are analyzed, non-linear interactions might not be discovered. Therefore, a center point is added, where all factors are at half the distance between the two levels. If this center point shows a deviation from the statistical expectation, at least one of the factors shows a non-linear effect on the result. A repetition of the center point also shows the general variability of the experiments without repeating the whole design.

In a response surface design, the factorial approach is extended through additional points, to analyze non-linear quadratic effects of the factors and to optimize parameters. The resulting response surface plot (RSP) indicates the curvature of the effects and shows the optimum visually. Most commonly, the central composite design (CCD) is employed. Here, each factor is extended with axial points beyond the two levels, while keeping the other factors at the center point level, resulting in a star shaped design. The number of experiments with a two level factorial design is calculated with

$$N = 2^k + 2k + C_0 \tag{13}$$

with k being the number of factors and C_0 the number of center point runs.

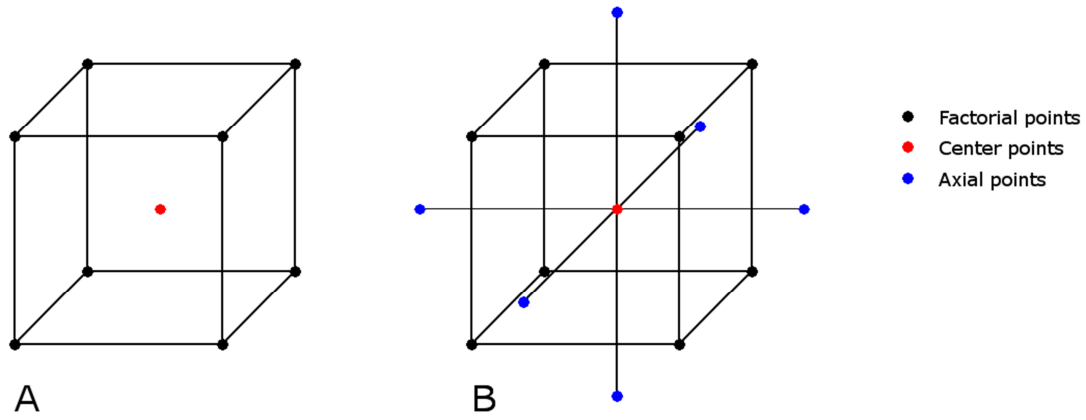

Figure 16: Comparison of full factorial design (A) and central composite design (B) at three factors with two levels.

Two important characteristics a design should have are orthogonality and rotatability. Orthogonality is achieved when the sum of products of levels between column vectors is zero, and ensures that columns are independent of each other. Rotatability is given when the prediction variance is the same for all points at the same distance from the center. In that case, however, the variance of factorial points compared to axial star points is different. A spherical design is not rotatable, however has the same prediction error for factorial and axial points. A rotatable design should be chosen when the optimum might not lie directly in the center of the test space but closer to the edges, making equal variances of all points at the edges favorable. These characteristics are decided by the distance α of the axial points from the center point. If α = 1, a three level factorial design is formed.

Setting $\alpha = \sqrt{k}$ results in a spherical shape, where all points are equidistant from the center. Rotatability can be achieved by choosing $\alpha = [2^k]^{1/4}$. For orthogonality, the distance of the axial points is also dependent on the number of center points, resulting in $\alpha = (2^k + n_s + C_0)^{1/4}$ with n_s being the number of star points and C_0 the number of center points. Both orthogonality and rotatability can be achieved at the same time. However, when this not the case, the experimenter has to decide which characteristic is more important to the results. After performing the experimental design, reliability of the model has to be confirmed by further experiments around the calculated optimum. Still, in contrast to the conventional OFAT approach, DoE results in a lower number of experiments during method development and does not rely on luck to find the true optimal combination of factors.

III. Scope of work

The first part of the presented work concentrates on the development of an analytical method for the analysis of monoamine neurotransmitter in peripheral murine tissues. This comprises a suitable tissue clean-up and extraction procedure as well as the development of a fast instrumental method applicable to a high throughput of samples. After complete validation, the method should be applied in cooperations within the Helmholtz Center to show the benefit in research of diseases such as diabetes.

The data of these cooperations should be analyzed to find indications in the levels between wild type and treated/knockout mice that point towards the identity of unknown compounds present in the analyzed samples. In order to confirm to the structure of the unknowns, a workflow for the identification with a mass spectrometry instrument needs to be developed. This includes extraction after HPLC analysis, chemically tagging the analyte to increase volatility for the mass spectrometer, and optimizing the parameters of the mass spectrometer.

A third part focuses on the extension of the analytical portfolio to lipophilic compounds. Norlaudanosoline, an intermediate in the endogenous formation of morphine is chosen as a model compound in brain tissue. In order to access the suspected low concentration, a pre-concentration step needs to be added. Dispersive liquid liquid microextraction is a suitable method, where a new variant needs to be developed for the inclusion of both norlaudanosoline and morphine.

IV. Materials and Methods

4.1. Materials

A complete list of equipment, consumables, and chemicals can be found in Appendix 7.3. All instruments were qualified and calibrated. All chemicals were purchased in the highest available purity.

For the analysis of MAs and MO/NL three HPLC instruments coupled to an ECD were used. An UPLC with an MS detector was tested for the identification of unknown compounds from the ECD instruments.

4.1.1. System I

This system from Dionex consisted of a gradient pump (GP40), an autosampler (AS50) with an automatic injection valve and a 100 µL sample loop, and an electrochemical detector (ED40) with a glassy carbon working electrode (see Figure 17). The potential of the detector was set against an Ag/AgCl reference electrode. The mobile phase was degassed under vacuum in an ultrasonic bath prior to use. Before and after each measurement the syringe and the injection loop were flushed with 250 µL of a solution of degassed 10 % methanol in HPLC grade water. The sensitivity display range was set to 10 µA and the data transfer rate to the computer to 5 Hz. The software PeakNet 5.2 (Dionex) was used to control the system and process chromatograms.

Figure 17: HPLC system I (Dionex) with ECD (Picture: Joachim Nagler).

4.1.2. System II

This HPLC–ECD system from Dionex comprised a gradient pump (GP50), a cooled autosampler (AS50), set to 4 °C, with an automatic injection valve, a 25 µL or 100 µL sample loop, and an electrochemical detector (ED50A) with a glassy carbon working electrode (see Figure 18). The potential of the detector was set against an Ag/AgCl reference electrode. The mobile phase was degassed under vacuum in an ultrasonic bath prior to use. Before and after the measurements the syringe and the injection loop were flushed with 250 µL of a solution of degassed 10 % methanol in HPLC grade water. The sensitivity display range was set to 10 µA and the data transfer rate to the computer to 10 Hz. The software Chromeleon 6.5 (Thermo Fisher) was applied to control the system and process chromatograms.

Figure 18: HPLC system II (Dionex) with ECD (Picture: Joachim Nagler).

4.1.3. System III

This Ultimate 3000 HPLC system from Thermo Fisher (see Figure 19) comprised an isocratic pump (IS0-3100A), a cooled autosampler (WPS-3000(T)SL), set to 4 °C, with an automatic injection valve and a 100 µL sample loop, and an electrochemical detector (ECD-3000RS usable with 6011 RS coulometric or 6041RS amperometric analytical cell (in both cases potential set against a Pd reference electrode)). The mobile phase was degassed under vacuum in an ultrasonic bath prior to use. Before and after the measurements the syringe and the injection loop were flushed with 300 µL and the needle washed externally with 100 µL of mobile phase. The sensitivity display range was set to 10 µA and the data transfer rate to the computer to 25 Hz. The software Chromeleon 7.2 SR3 (Thermo Fisher) was applied to control the system and process chromatograms.

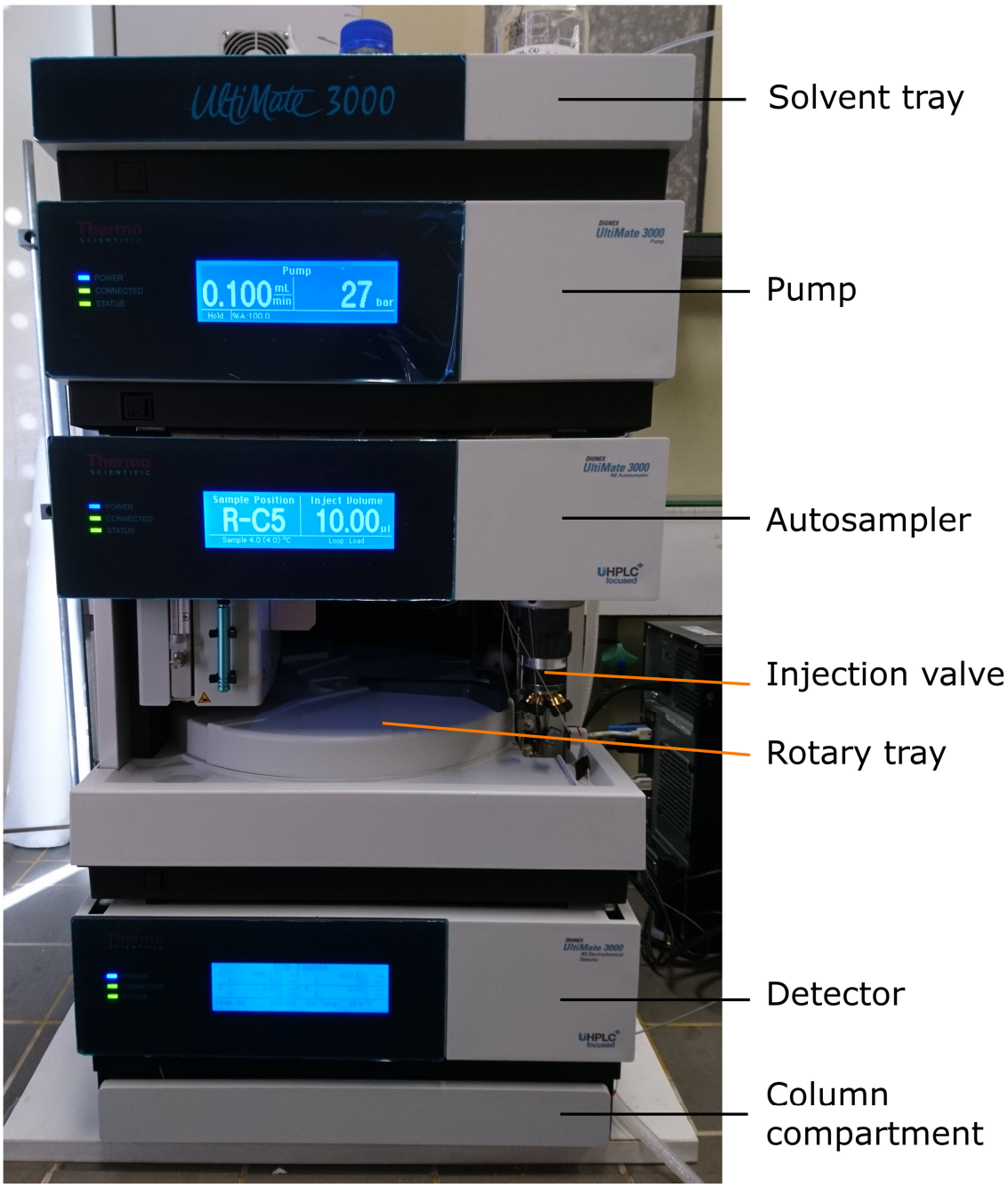

Figure 19: System III, Ultimate 3000 (Thermo Fisher) with ECD (Picture: Joachim Nagler).

4.1.4. System IV

The nanoAcquity UHPLC system from Waters (see Figure 20) was equipped with a gradient pump (Binary Solvent Manager) and a cooled autosampler (Sample Manager), set to 10 °C, with a 5 µL sample loop and a heatable column holder, set to 40 °C. A C18-column (ACQUITY UPLC M-Class HSS T3 1.8 µm, 300 µm x 150 mm) with a flow rate of 5 µL/min was used. The HPLC was coupled to a hybrid quadrupole time-of-flight mass spectrometer from Waters-Micromass (QTOF2) equipped with a micro scale ESI interface. The mass calibration of the MS was carried out by direct infusion of 0.1 % v/v phosphoric acid in 50:50 acetonitrile:water (v:v) with a syringe pump. The MS was run in positive ionization mode with a gradient between solvent A (subboiled ultrapure water with 0.1 % v/v formic

acid) and solvent B (ACN with 0.1 % v/v formic acid). Both solvents were degassed prior to use with an ultrasonic bath. After each injection, the needle was washed with 300 µL ACN and 900 µL mixture H_2O/ACN (99/1). The MassLynx software version 4.1 (Waters) was applied to control the MS system, while the nanoAcquity UPLC console version 1.41.2872 was used for control of the chromatography system.

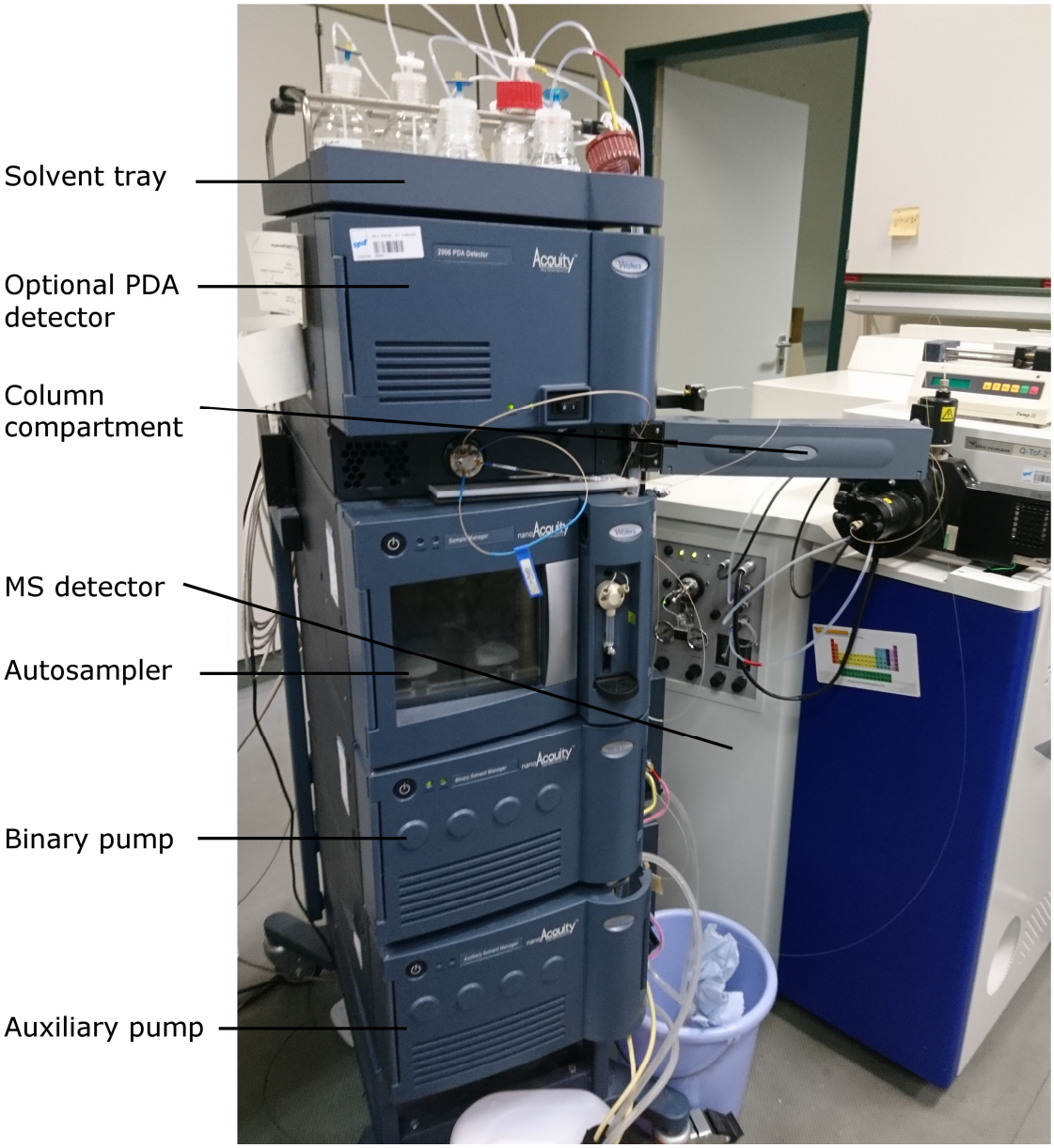

Figure 20: System IV, nanoAcquity with MS detector (Waters) (Picture: Joachim Nagler).

4.2. Methods

4.2.1. Calculations

On system I, due to deficiencies of the software, the resulting peak areas had to be transferred to and computed with an excel sheet.

First, a calibration standard consisting of analytes and IS was measured. A one point calibration curve was used, exploiting the perfect linearity of the detector in the expected range. The resulting calibration curve can be plotted and equation (14) retrieved:

$$\frac{Resp.\ Analyte_{\ calibration}}{Resp.\ IS_{\ calibration}} = m \cdot \frac{Conc.\ Analyte_{\ calibration}}{Conc\ IS._{calibration}} \tag{14}$$

From this, the slope of the calibration curve m can be calculated with equation (15):

$$m = \frac{Resp.\ Analyte_{\ calibration} \cdot Conc.\ IS_{\ calibration}}{Resp.\ IS_{\ calibration} \cdot Conc.\ Analyte_{\ calibration}} \tag{15}$$

With m, the concentration of the analyte per injection can be calculated with equation (16). The amount of IS found in the injection, compared to the known amount in the calibration, is used to adjust for loss of sample during sample clean-up.

$$Conc.\ Analyte_{\ sample\ inj.} = \frac{Resp.\ Analyte_{\ sample} \cdot Conc.\ IS_{\ theoretical\ in\ sample\ inj.}}{Resp.\ IS_{\ sample} \cdot m} \tag{16}$$

While the amount of analyte is adjusted above, the recovery of the internal standard can be calculated with equation (17).

$$R = \frac{Resp.\ IS_{sample} \cdot Conc.\ IS_{\ calibration} \cdot}{Resp.IS_{\ calibration} \cdot Amount\ IS_{added\ to\ sample}} \tag{17}$$

Equation (18) calculates the total amount of analyte present in the whole sample.

$$Amount_{\ total\ sample} = Conc.\ Analyte_{\ sample\ inj.} \cdot \frac{Vol._{sample\ Inj.}}{Vol._{total\ Sample}} \tag{18}$$

The total amount divided by the total tissue weight of the sample results in the mass concentration of the analyte (Equation (19)).

$$Mass\ Conc._{total\ sample} = \frac{Amount_{\ total\ sample}}{Weight_{\ total\ sample}} \tag{19}$$

On Systems II and III the software Chromeleon was used. It was ordered to use the setting Variable/IS for the calculation, where results are adjusted according to the recovery of the IS with equation (20).

$$Amount_{j,k} = f(Response_{j,k}) \times (\frac{Dilution\ Factor_j}{Weight_j}) \times Factor_k \times IS\ Factor_{j,k} \tag{20}$$

f is the inverted calibration function, $Response_{j,k}$ the amount detected for component k in injection j, *Dilution Factor* and *Weight* are factors defined in the injection list (set to 1), $Factor_k$ is a scaling factor (set to 1), and $IS\ Factor_{j,k}$ is the correction factor for the recovery. (equation (21)).

$$IS\ Factor_{j,k} = \frac{Amount_{j(injection\ List)}}{Amount_{j,\ IS\ (k)}} \quad (21)$$

The amount of IS is calculated with the same formula as the other components but without the weight correction.

4.2.2. Method validation

4.2.2.1. Blank

On each system, a blank of $HClO_4$ was injected to confirm that no impurities or underlying disturbances are present in the chromatograms.

4.2.2.2. Linearity

Linearity refers to the range where the response of the detector is directly proportional to the concentration of the analytes in the sample. In order to test linearity, standard solutions with a concentration of 0.1 ng, 0.5 ng, 1 ng, 5 ng, 10 ng and 20 ng per injection volume were measured in triplicates for each of the three systems. The values were plotted into a calibration curve and the coefficient of determination (R^2) extracted. A value above 0.99 was deemed acceptable.

4.2.2.3. Limit of detection and limit of quantification

The limit of detection (LOD) is defined as the concentration of analyte at which the signal can still be distinguished reliably from the baseline noise. A signal to noise ratio of 3:1 is generally agreed upon. A blank injection of LC-MS grade H_2O was used for the height determination of the noise. For each system, a standard solution of analytes with a concentration of 1 ng/injection was diluted until the LOD was found for each analyte according to the definition above.

The limit of quantification (LOQ) is defined as the concentration of analyte at which the analyte can be quantified with sufficient precision. A signal to noise ratio of 10:1 is recommended. The LOQ was determined during the same series as the LOD.

4.2.2.4. Accuracy

Accuracy is defined as closeness of the measured value to the real amount of analyte in the sample. The accuracy of the extraction methods was tested with spiking experiments in biological tissues, where a known amount of analyte standard is added to the samples before the clean-up and the calculated amount compared to the expected result.

For the analysis of MA, the method was validated in eWAT, gastrocnemius muscle, and in hypothalamus of C57Bl/6J mice. Four sample tissues were pooled the day of analysis, homogenated,

diluted threefold to achieve sufficient material, and aliquoted. The aliquots were spiked with standard to achieve three different concentrations of 0.5 ng, 1 ng, and 5 ng per injection and injected into the system in triplicates on three days. A blank sample without addition of standards was analyzed in triplicate each day to adjust the results for present endogenous compounds.

The validation for the analysis of MO and NL was performed in the thalamus brain region of C57Bl/6J mice. Four sample tissues (two Dusp8tm1a het, one Dusp8tm1a WT, one Ghrelin KO and one Ghrelin;GHSR dKO, male C57Bl/6J) were pooled and homogenized together to reduce any effect the genotypes might have on the analysis. Samples were pooled on the day of analysis, homogenated, diluted threefold, and aliquoted. The aliquots were spiked with standards for a concentration of 0.5 ng, 1 ng, and 5 ng per injection and extracted with DLLME in triplicates on three days. A blank sample without addition of standards was analyzed in triplicate each day to adjust the results for endogenous compounds present.

4.2.2.5. Precision

Precision is defined as the reproducibility of measurements, meaning how close the values of repeated measurements group together. The inter and intraday precision of each HPLC system was tested by five injections of standard solutions at a concentration of 1 ng/injection, on the same day and on five consecutive days, respectively.

The precision of the whole methods in biological tissues was determined at the same time as the accuracy.

4.2.2.6. Recovery

The recovery is defined as the amount of analyte found in the analysis after the extraction procedure. For the calculation, internal standards are added at the beginning of the clean-up in a known amount. As these internal standards have a similar configuration to the analytes, it is accepted that the recovery of the analytes in the sample is similar to the IS. The analyte values are adjusted for the recovery by the chromeleon software, however no recovery value is given. For the calculation of recovery, equation (22) was used within an excel sheet.

$$R = \frac{(Amount\ IS_{\ injection} \div Volume_{\ Injection}) \times Volume_{\ total}}{Amount\ IS_{\ added}} \quad (22)$$

4.2.3. Monoamine analysis

4.2.3.1. Standard preparations

300 mL HPLC grade water was put into a 500 mL volumetric flask, 12.85 mL of $HClO_4$ (70%) added, and the flask filled to the mark with water, in order to achieve a concentration of 0.3 M.

12.35 mg MHPG hemipiperazinium salt, 10 mg 3,4-dihydroxyphenylacetic acid (DOPAC), 10 mg HVA, 10 mg 5-HIAA, 12.2 mg 3-methoxytyramine (3-MT) hydrochloride, and 12.1 mg 5-HT hydrochloride were weighted into a 10 mL volumetric flask and dissolved with 10 mL 0.3 M $HClO_4$ to achieve a standard stock solution at a concentration of 1 µg μL^{-1}. Standard solutions of the catecholamines NE, E, and DA as well as the internal standard 3,4-dihydroxybenzylamine (DHBA) were commercially available at a concentration of 1 µg μL^{-1}.

For working standard solutions, 100 µL of the standard stock solution and 100 µL of the commercially available catecholamine standard stock solution were pipetted into a 100 mL volumetric flask and the flask filled to its mark with 0.3 M $HClO_4$, resulting in a concentration of 1 ng μL^{-1}. 100 µL of the commercially available IS standard stock solution was pipetted into a 100 mL flask and the flask filled up to its mark with 0.3 M $HClO_4$, resulting in a working IS standard solution at a concentration of 1 ng μL^{-1}. The flasks were wrapped with alumina foil and stored in a fridge at 4 °C.

For daily calibration, 10 µL of the MA working standard solution and 10 µL of the IS working standard solution were pipetted into a sample vial and diluted with 180 µL 0.3 M $HClO_4$ to achieve a standard solution at a concentration of 1 ng/20 µL injection volume that was immediately injected into system II and III. For system I, the amount of standard was doubled each, for a concentration of 1 ng/40 µL injection volume.

4.2.3.2. Tissue homogenization and extraction

Different extraction procedures were employed for each of the murine tissues. In order to achieve a full homogenization, it was best to store tissues in 1.5 mL Eppendorf tubes with a pointed lower end after dissection. If tissues were stored in 2 mL, they were transferred into 1.5 mL tubes before homogenization. Samples needed to be kept on ice during the transfer to prevent loss of sample material.

Brain

200 µL of 0.3 M $HClO_4$ and 4 µL of IS (1 ng μL^{-1}) were added to the brain region samples (10 – 15 mg). They were thawed on ice and homogenized via ultrasonication for 30s on ice. The homogenate was centrifuged at 4 °C with 7900 g for 10 minutes, an appropriate aliquot of supernatant was taken, transferred into a HPLC vial, and injected into a HPLC system. The remaining supernatant was transferred into a storage vial and stored at -80 °C.

Muscles (Soleus, gastrocnemius, extensor digitorum longus)

The muscles were transferred onto a piece of alumina foil, which was folded and placed in a mortar cooled with liquid nitrogen. The tissues were ground into powder with a cooled pistil, transferred into a 1.5 mL Eppendorf tube with a cooled spatula, and stored at -80 °C until further analysis.

200 µL of 0.3 M $HClO_4$ and 4 µL of IS (1 ng μL^{-1}) were added to powdered soleus (10 – 20 mg) and extensor digitorum longus (EDL) (20 – 30 mg), while 400 µL of 0.3 M $HClO_4$ and 4 µL IS (1 ng μL^{-1}) were added to gastrocnemius (150 – 190 mg). The muscles were thawed on ice and homogenized via ultrasonication for 2 × 30s on ice. Small amounts of tendon were possibly present and could not be homogenized. The resulting homogenate was centrifuged at 4°C with 7900 g for 10 minutes, an appropriate aliquot of supernatant was taken, transferred into a HPLC vial, and injected into a HPLC system. The remaining supernatant was transferred into a storage vial and stored at -80 °C.

Pancreas

200 µL of 0.3 M $HClO_4$ and 4 µL of IS (1 ng μL^{-1}) were added to the pancreas samples (130 – 200 mg). After thawing on ice, they were homogenized via ultrasonication for 30s on ice. The resulting thick homogenate was centrifuged at 4°C with 7900 g for 10 minutes. An appropriate aliquot of supernatant was taken, transferred into a HPLC vial, and injected into a HPLC system. The remaining supernatant was transferred into a storage vial and stored at -80 °C.

Liver

400 µL of 0.3 M $HClO_4$ and 4 µL of IS (1 ng μL^{-1}) were added to the liver samples (130 – 200 mg). The samples were thawed on ice and homogenized via ultrasonication for 30s on ice. The resulting thick homogenate was centrifuged at 4°C with 7900 g for 10 minutes. An appropriate aliquot of supernatant was taken, transferred into a HPLC vial, and injected a HPLC system. The remaining supernatant was transferred into a storage vial and stored at -80 °C.

Brown and white adipose tissue

200 µL of 0.3 M $HClO_4$ and 4 µL of IS (1 ng μL^{-1}) were added to the white adipose tissue (WAT, 100 - 120 mg) samples. 400 µL of $HClO_4$ and 4 µL of IS (1 ng μL^{-1}) were added to brown adipose tissue (BAT, 50 -350 mg), unless the available amount was below 100 mg. Then only 200 µL $HClO_4$ was added. The samples were thawed on ice and homogenized via ultrasonication for 30 s on ice. The homogenate was centrifuged at 4°C with 7900 g for 10 minutes.

For BAT, the resulting fat layer was on the bottom of the tube and the supernatant could be taken directly. For WAT, the fat layer on top of the solution. It was pierced with a cannula fitted to a syringe and the solution below was drawn while taking care not to disturb the fat layer. The solution was filtered through a 4 mm, 0.2 µm PTFE syringe filter to remove any fat particles. Care was taken to press the syringe and filter together onto the top of the vial, to prevent separation and loss of sample

due to the high pressure build up. The syringe was removed, air drawn, the filter reconnected, and the air pushed through the filer to remove remaining sample from the filter. An appropriate aliquot of samples was transferred into a HPLC vial and injected a HPLC system. The remaining solution was stored at -80 °C in a storage vial.

Cell culture

4 µL of IS (1 ng μL^{-1}) was added to 200 µL of cell medium. The solution was transferred into a 0.5 mL centrifuge filter unit and centrifuged at 4 °C with 17530 g for 30 min. 100 µL of 0.3M $HClO_4$ and 4 µL of IS (1 ng μL^{-1}) were added to the cell pellet. The solution was transferred into a 0.5 mL centrifuge filter unit and centrifuged at 4°C with 17530 g for 30 min. An aliquot of filtrate was transferred into a HPLC vial and injected into a HPLC system. The remaining filtrate was stored at -80 °C in a storage vial.

Instrumental conditions

System I

For the analysis of MAs on system I, the potential of the detector was set to 0.7 V. The separation was carried out on a reversed phase C18column (Atlantis T3, 3 µm, 3.0 mm x 150 mm) at an isocratic flow rate of 0.5 mL min^{-1}. A C18security cartridge preceded the column. A commercial mobile phase from RECIPE with 5.5 % v/v added ACN was used. The column and detector ovens were set to 30 °C. The injection volume was 40 µL.

System II

For the analysis of MAs on system II, the potential of the detector was set to 0.7 V. Separation of the compounds was conducted at an isocratic flowrate of 1 mL min^{-1} on a solid core particle reversed phase C18column (Accucore XL C18, 150 × 4.6 mm, 4 µm). A security cartridge of the same material preceded the column. The RECIPE mobile phase with 0.25 % v/v added ACN was used, after lowering the pH value to 3.85 using $HClO_4$ (70%). The column and detector compartment was set to 40 °C. The injection volume was set to 20 µL.

System III

For the analysis of MAs on system III, the potential for the two coulometric detector channels was set to 0.4 V and 0.7 V. For separation, a reversed phase C18column (Atlantis T3 100Å, 3 µm, 4.6 mm X 150 mm) was used at an isocratic flow rate of 1 mL min^{-1}. A C18-security cartridge preceded the column. The RECIPE mobile phase with 5.5 % v/v added ACN was used. The column oven was set to 30 °C.

4.2.4. Morphine and norlaudanosoline analysis

4.2.4.1. Standard preparation

1.28 mg of NL hydrobromide was weighted into a 10 mL volumetric flask and dissolved in 10 mL 0.3 M $HClO_4$ to reach a standard stock solution at a concentration of 100 µg mL^{-1}. 1 mg of higenamine (HG) was weighted into a 10 mL volumetric flask and dissolved in 10 mL MeOH for a standard stock solution solution at a concentration of 100 µg mL^{-1}.

10 µL of commercial MO standard stock solution (100 µg mL^{-1}) and 10 of NL standard stock solution were pipetted into a 1.5 mL tube and diluted with 480 µL of 0.3 M $HClO_4$ to produce a working standard solution at a concentration of 2 ng μL^{-1}. 1 µL of a commercial nalorphine (NP) standard stock solution (1 mg mL^{-1}) and 10 µL of HG standard stock solution were pipetted into a 1.5 mL tube and dissolved in 489 µL $HClO_4$ for a working standard solution at a concentration of 2 ng μL^{-1}.

Each day, 5 µL of NP/HG working standard and 5 µL of MO/NL working standard were pipetted into a sample vial and dissolved in 90 µL of 0.3 M $HClO_4$ to produce a calibration standard with a concentration of 1 ng per injection.

4.2.4.2. Extraction procedure

Brain samples were thawed on ice and 105 µL of 0.3M $HCLO_4$ and 5 µL of internal standard solution added. The mixtures were homogenized via ultrasonication on ice for 10 s and centrifuged for 5 min at 4°C with 4000 g. The supernatants were transferred into 1.5 mL collection tubes. 300 µL tributyl phosphate (TBP) was injected rapidly into the supernatant with a Hamilton syringe. The solution was shaken until a cloudy dispersion was formed and centrifuged for 10s at room temperature with 3500 g. The lower water phase was taken and discarded. The remaining TBP phase was taken and transferred into a 10 mL conical tube. 5 mL of pre-cooled (4 °C) cyclohexane was added to theTBP in the 10 mL tube. 60 µL of pre-cooled (4°C) MeOH was added with a Hamilton syringe and the tube briefly shaken. The resulting cloudy dispersion was centrifuged for 1 min at 4°C with 3200 g. The lower MeOH phase was carefully taken with a 10 µL Hamilton syringe and transferred into a storage vial. An aliquot was transferred into a HPLC vial and injected into system III.

4.2.4.3. Instrumental conditions

System III was used for MO/NL analysis, with the potential of the two coulometric detector channels set to 0.5 V and 0.7 V. For the separations, a reversed phase C18column (Atlantis T3 100Å, 3 µm, 4.6 mm x 150 mm) was used at a flow rate of 1 mL min^{-1}. A C18-security cartridge preceded the column. The RECIPE mobile phase with 15 % v/v added MeOH and 5 % v/v added ACN was used.

The column oven was set to 30 °C. The injection volume was 10 µL for calibration and method development and 20 µL for brain samples.

4.2.4.4. Design of Experiment

The DoEs used during method development for the extraction of MO and NL were constructed with R package Rcmdr version 2.4-4. Central composite designs were used with orthogonal position of star points. Response surface models were created with the standard proposed formula, integrating first order interactions, two factor interactions, and quadratic interactions. Models were statistically analyzed and plotted graphically either as 3D perspective plots or contour plots.

4.2.5. Unknown compound identification

4.2.5.1. Extraction of compound with HPLC

For the extraction of an unknown compound out of biological samples, a 100 µL sample loop and injection was used in system II. A cleaned-up sample was injected to check the exact retention time of the desired compound. A new measurement was started and immediately after injection the detector was switched off, to prevent oxidation of the compound. At the retention time where the desired peak starts in the chromatogram, the outflow of the column was collected in a 4 mL amber vial. The time delay from the detector to the end of the outflow capillary can be calculated with:

$$t = \frac{V_{cyl}}{Q} = \frac{\pi \cdot r^2 \cdot h}{Q} \tag{23}$$

V_{cyl} is the cylinder volume of the capillary, with r being the radius and h the height, while Q is the flowrate of the mobile phase. The time for typical capillaries and lengths lies in the range of a fraction of a second and can be neglected.

4.2.5.2. Derivatization reaction

10 µL of 100 mM sodium carbonate was added to 30 µL standard solution in RECIPE mobile phase (1ng μL^{-1}) or 30 µL of extracted compound solution. The mixture was briefly vortexed and 10 µL of benzoylchloride solution (2 % v/v in ACN) was added and the solution briefly vortexed for derivatization of analytes (see Figure 21). An aliquot was transferred into MS sample vial with a conical insert.

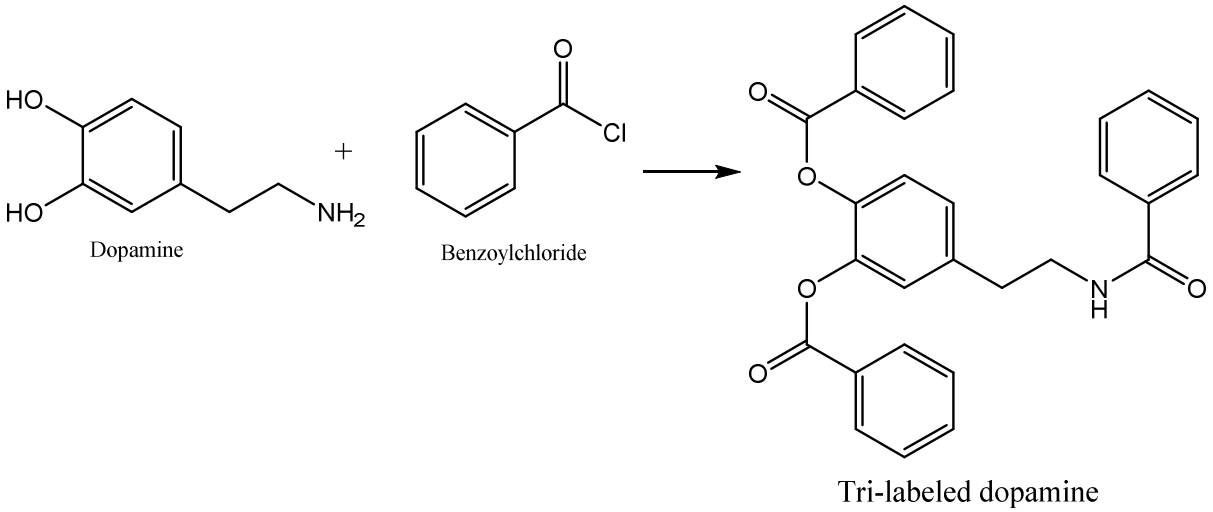

Figure 21: Derivatization of dopamine with benzoylchloride.

4.2.5.3. Instrumental conditions

The unknown compound identification was done on system IV with the MS detector. Positive ionization mode was used with a scan from 100-1000 kDa for 30 min and a scan time of 2.5s. 2.5 kV and 35 V capillary and cone voltage as well as 10 eV collision energy were applied. The injection volume was 5 µL.

Table 1: Solvent gradient for elution of derivatized MAs.

Time [min]	0	0,1	0,15	14	14,5	18	19	30
A [%]	100	85	83	45	30	0	100	100
B [%]	0	15	17	55	70	100	0	0

V. Results and Discussion

5.1. Instrument validation

The validation of an instrument is an important step during method development to ensure high confidence in results. Important parameters of the instrument are linearity, precision, the proper voltage applied to the electrode for each analyte, and LOD/LOQ for the respective analytes. In this work, three HPLC/ECD instruments were used for the analysis of MAs in murine tissues, where parameters are subject to variations between instruments and have to be checked for each.

5.1.1. System I

The validation of system I was performed during an earlier method development for MAs in brain regions and can be found in Appendix 7.4.

5.1.2. System II

5.1.2.1. Voltammetry

As system II employed the same detector as system I, the same voltage of 700 mV was used for the detection of MAs and was not optimized further.

5.1.2.2. Linearity

Linearity is the range where the detector gives a proportional response to the concentration of analyte in the sample. Outside this range, a change in analyte concentration does not result in an equal change of the detector response, making it imperative to either stay within the appropriate concentration or adjust the calibration function accordingly. Appendix 7.5 shows the linearity of MAs on system II. The response is linear in the range from the LOQ to 20 ng per injection. All of the R^2 are above the accepted value of 0.99.

5.1.2.3. Limit of detection/quantification

The limit of detection is the concentration level at which analytes can be distinguished reliably from the baseline. It is important to set this level beforehand to avoid subjective bias in the moment of analysis and to reduce the chance of false positive signals. The limit of quantification is the concentration level at which reliable quantification of the analytes is possible, as between LOD and LOQ the variation of peak area is higher due to fluctuations from the noise.

The LOD for all MAs analyzed on system II was between 0.5 and 2.5 pg μL^{-1}. Here, despite the highest response in the detector, 3-MT does not achieve the lowest LOD. This is due to the elution pattern of this peak. It elutes late in the chromatogram and has a broader peak shape than the other earlier eluting compounds (Appendix 7.6). The broader peak shape dissipates into the baseline noise earlier and cannot be distinguished anymore.

All measured LODs are in the single digit picogram range per microliter, displaying a very low sensitivity suitable for the analysis of neurotransmitters in biological tissues.

Table 2: LOD/LOQ of MAs on system II.

Analyte	MHPG	DOPAC	NE	E	5-HIAA	HVA	DA	3-MT	5-HT
LOD [pg µL-1]	2.5	0.5	1.25	1.25	2.5	1.25	1.25	2.5	2.5
LOQ [pg µL-1]	7.5	1.5	3.75	3.8	7.5	3.75	3.75	7.5	7.5

5.1.2.4. Precision

Precision is the reproducibility of measurements. Not only response of the detector, but also variations of injected volume by the autosampler and column properties affect the precision.

The precision of the instrument was very reliable. Intraday it was below five percent over five runs. Interday it was a bit higher, but still below 10 %. As pre-prepared standard solutions degrade very fast (see 5.2.2.2), each day a new standard was prepared from the standard stock solutions. The higher variations in the interday measurements are most likely a result of small variations of this daily preparation. The results show that the system does not have a great variation between measurements and that samples can be compared reliably.

Table 3: Intra- and interday precision in standard solution at a concentration of 1 ng 20 µL^{-1}; measurements were done in replicates of five.

Analyte	Intraday [pg]	RSD	Interday [pg]	RSD
MHPG	969	2.2	983	7.9
DOPAC	1053	3.0	962	5.2
NE	1056	3.1	971	5.8
E	1052	2.8	963	5.9
5-HIAA	1018	1.1	953	3.9
HVA	1056	2.9	961	5.6
DA	1049	2.7	951	5.8
3-MT	1047	3.5	972	6.9
5-HT	1019	1.0	986	3.8
IS	946	3.4	936	9.2

5.1.3. System III

5.1.3.1. Voltammetry

For both the amperometric and coulometric detector cell, the most suitable potential for the detection of MAs had to be established. The amperometric detector was tested between 600 and 800 mV. At 800 mV, NE and E gave the highest response, however, both 3-MT and 5-HT were not detectable. At 600 mV, NE, E, HVA, and 3-MT gave a slightly higher signal, however the broadest and therefore lowest sensitivity peak 5-HT had the highest signal at 700 mV, which was chosen as the applied potential for the amperometric cell.

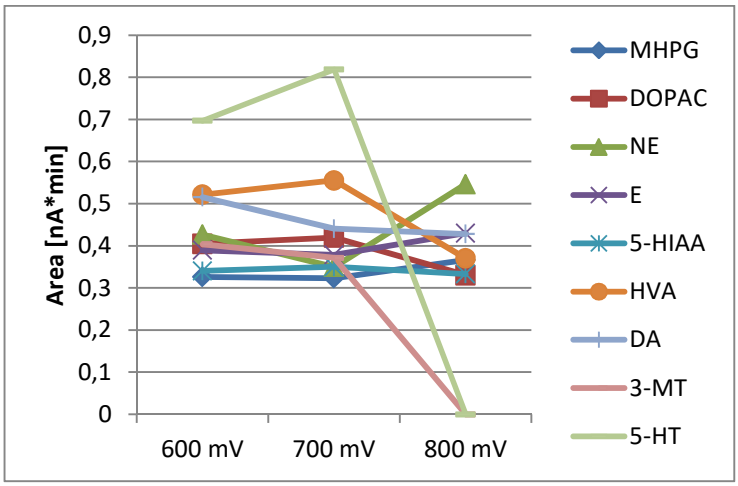

Figure 22: Voltammetry of the amperometric detector, analyzed with separate injection of MA standard solution at 1 ng per injection with different voltages and sufficient equilibration time between measurements.

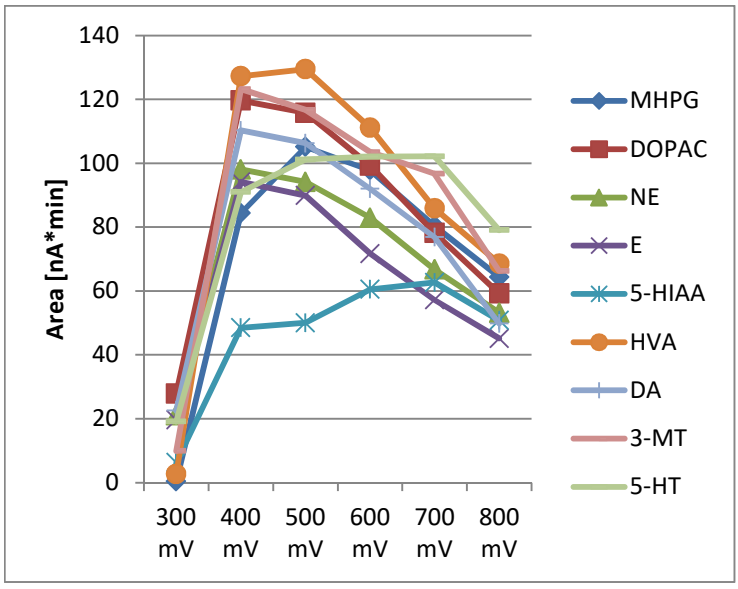

Figure 23: Voltammetry of the coulometric detector, analyzed with separate injection of MA standard solution at 1 ng per injection with different voltages and sufficient equilibration time between measurements.

For the coulometric detector a lower voltage was chosen. 700 mV gave the highest signal for 5-HIAA, however, the other analytes were reduced. 500 mV was better for MHPG, 5-HIAA, HVA, and 5-HT. As the remaining five compounds were optimal at 400 mV, with little trade of for the former, it was chosen as the applied potential.

The optimal potential of the coulometric detector was also determined for MO and NL. Due to the reduced sensitivity, the amperometric cell was not tested. Generally, NL has a higher response to the detector, due to its multiple hydroxy groups that can be oxidized. The optima of both compounds lie close together, with 400 mV for NL and 500 mV for MO. The latter was chosen as the voltage for the method, as though the response of NL dipped slightly, it still had a considerably higher peak area than MO.

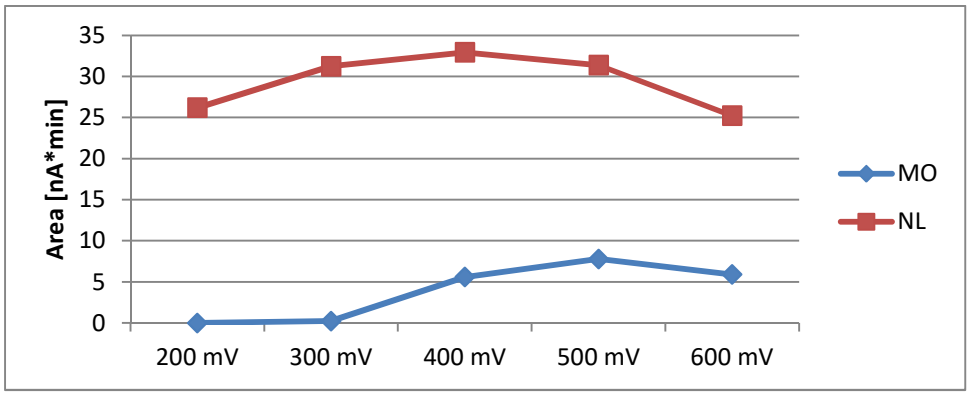

Figure 24: Voltammetry of MO and NL with coulometric detector, analyzed with separate injection of MA standard solution at 1 ng per injection with different voltages and sufficient equilibration time between measurements.

5.1.3.2. Linearity

System III also shows linearity in the range from the LOQ to 20 ng per injection with R^2 above 0.99 for all MAs (Appendix 7.5). Interestingly, in the coulometric detector HVA causes the highest response. Similarly, all other analytes are also shifted in their response compared to the amperometric detector, possibly due to differential mass transfer effects to detector, which do not apply to the coulometric cell with its full oxidation of analytes at the membrane.

The linearity of the system was also tested for MO and NL. The response of both compounds was linear from the LOQ to 20 ng per injection as well with R^2 above 0.99 (Appendix 7.5).

5.1.3.3. LOD/LOQ

In the coulometric detector the analytes flow through a membrane where the voltage is applied. Therefore, all of the analytes are oxidized and the detector should give rise to higher signal than the amperometric detector, where the analytes flow through a small cell and only about 10 % of analytes come in contact with the electrode. However, in the coulometric cell not only the analytes but also other compounds are oxidized in greater amounts, so baseline noise might be higher and, therefore, amperometric detectors more sensitive. For system III, both a coulometric and an amperometric detector cell were available and tested for the LOD and LOQ of MAs.

Table 4: LOD/LOQ of MAs on system III with coulometric detector.

Analyte	MHPG	DOPAC	NE	E	5-HIAA	HVA	DA	3-MT	5-HT
LOD [pg µL-1]	0.3	0.2	0.2	0.3	0.6	0.3	0.3	1.3	1.3
LOQ [pg µL-1]	0.9	0.6	0.6	0.9	1.8	0.9	0.9	3.9	3.9

Table 5: LOD/LOQ of MAs on system III with amperometric detector.

Analyte	MHPG	DOPAC	NE	E	5-HIAA	HVA	DA	3-MT	5-HT
LOD [pg µL-1]	5	5	5	10	10	10	10	20	20
LOQ [pg µL-1]	15	15	15	30	30	30	30	60	60

In the present case, the amperometric detector had a 15 to 30 times higher LOD than the coulometric detector. HPLC grade materials were used for the standard preparation, so no disturbing compounds were present. Additionally, the vendor designed the system to produce as little background noise as possible. The tubing was made of PEEK plastic materials and no metal parts were used. This prevents not only loss of analytes due to chelating binding to the metal, but also possible leakage of ions that could cause noise. The electronics were also optimized, resulting in a reduced electronic fluctuation of the baseline. This lowers the baseline noise in the cell and the coulometric detector can develop its full potential with the higher amount of oxidized compounds.

Compared to the amperometric detector in system II, the one in system III has a two to tenfold higher LOD. Most likely, this is not an effect of the detector itself but of the chromatography. On system III, a larger column with a longer elution time was used. Therefore, the peaks are also broader with less height, and vanish into the baseline earlier. This is especially apparent in 3-MT and 5-HT, the latest eluting peaks, which both have a much higher LOD in system III. However, in comparison to the coulometric detector, the amperometric detector in system II has two to eightfold higher LOD, making the coulometric detector far superior in terms of analysis of small amount of analytes. Most likely, the sensitivity of the both detector cells could be further improved by employing small particle or solid core particle columns to reduce band broadening effects.

Table 6: LOD/LOQ of MO and NL on system III with coulometric detector.

Analyte	MO	NL
LOD [pg µL-1]	3.6	1.3
LOQ [pg µL-1]	10	3.6

The LOD and LOQ for NL were in the same range as some of the monoamines, while for MO they were a bit higher, but still in the same order of magnitude. The low sensitivity of single digit pg per µL allows the detection of very low amounts of analyte present in biological samples.

5.1.3.4. Precision

System III was also optimized by the vendor to result in a much higher precision. The variation between intraday measurements was below one percent for all analytes except 5-HIAA. The interday variation was higher but still below five percent. Given the very high intraday precision this is most likely an effect of daily standard preparation.

Table 7: Intra and interday precision in standard solution at a concentration of 1 ng 20 µL^{-1}; measurements were done in replicates of five.

Analyte	Intraday [pg]	RSD	Interday [pg]	RSD
MHPG	1032	0.4	975	4.3
DOPAC	1049	0.2	993	4.2
NE	1021	0.2	974	4
E	1020	0.1	965	4.6
5-HIAA	965	3	958	4.5
HVA	1013	0.4	969	4.2
DA	1017	0.3	969	4
3-MT	1025	0.9	983	3.7
5-HT	990	0.9	975	4.3
IS	1008	0.2	993	4.2

5.2. Monoamine analysis

5.2.1. Method development

Previously, MAs were measured in single murine brain regions on system I with a RECIPE mobile phase with 5.5 % v/v ACN at a flow rate of 0.5 mL min^{-1}. The separation of the compounds was carried out on an Atlantis T3 C18 3.0 x 150 mm column with a particle size of 3 µm at a temperature of 30 °C, resulting in a total run time of 40 min.

With extension of the analysis of MAs to peripheral murine tissues, a much higher number of samples per animal were expected in routine analysis. Due to the selective detection mode of ECD no extensive clean-up procedure was necessary to remove disturbing compounds, making the analysis time on the HPLC the bottle neck of the method. Therefore, a faster measurement time was needed to allow a higher throughput of samples. Usually, a faster time is achieved by employing smaller particle sizes and column dimensions, which requires suitable HPLC instruments capable of handling the resulting higher backpressure. However, solid core particle columns achieve a comparable separation to small dimension particle columns at lower backpressure and can therefore be employed on older instruments.

5.2.1.1. Chromatographic conditions System II

In order to achieve a reduced run time on system II, a solid core particle column Accucore XL C18 with 4 µm particle size and 4.6 x 150 mm dimensions from Thermo Fisher with an according guard column was tested.

A RECIPE mobile phase with 5.5 % ACN and a flow rate of 0.5 mL min^{-1} resulted in a much shorter run time of 20 min, however, the peaks of HVA and IS as well as E and 5-HIAA were overlapping. 0.5 % ACN had a run time of 36 min, with separation of HVA and IS but not the other pair. Raising the flow rate to 1 mL min^{-1} shortened the run time to 18 min within the pressure limits of the instruments, but the same separation pattern between analytes was present. 0.25 % ACN slightly raised run time to 19 min, but did not change co-elution of E and 5-HIAA.

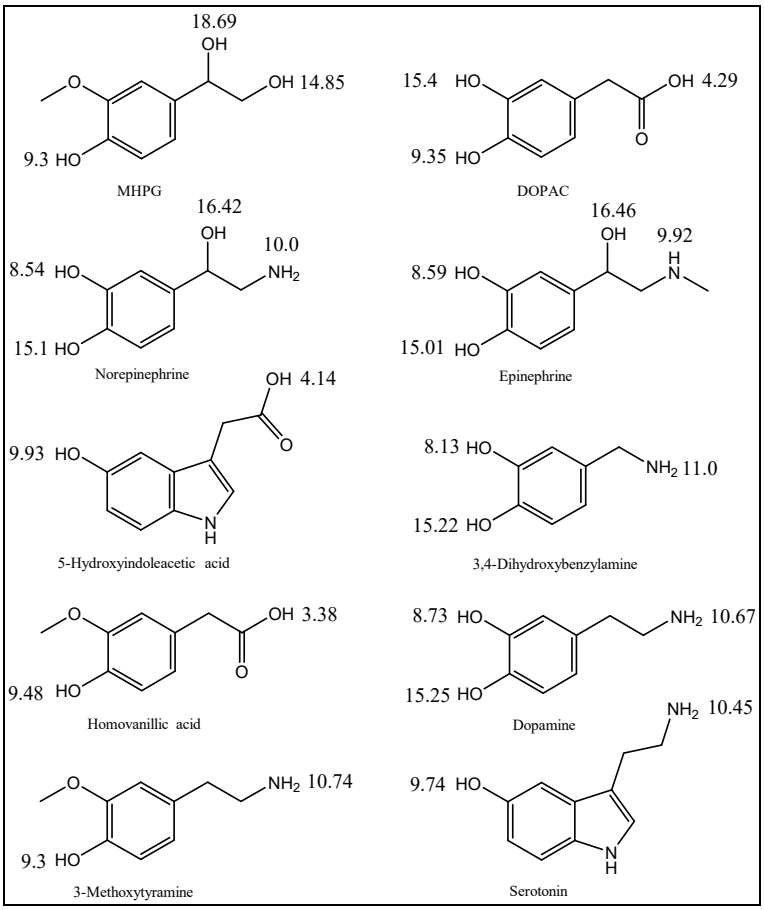

Figure 25: pKa values for protic groups of analytes; calculated with Chem 3D 16.0.

The pH level of the mobile phase also affects the elution pattern of the column, as the ionization of compounds can change the interaction between stationary and mobile phase, causing a shift in retention time. Figure 25 shows the pKa values of MA analytes. When the pH levels matches the pKa, half of the compound is present in the protonated form while the other half is deprotonated and in ionized form. At a pH of pKa ± 1, 90 % of the compounds are in the according form. A compound in its ionic form is more polar, and therefore less likely to interact with the C18 chains of the column particles, eluting faster than its protonated form.

The pH of the degassed mobile phase with added organic content was 4.3, where most of the compounds protic groups were fully protonated. However, the carboxyl groups of DOPAC, 5-HIAA, and HVA are close to this value and can be affected by a pH change. Lowering the pH value to 4.15 achieved the same run time as before with 19 min, with a better separation of E and 5-HIAA, however still slightly overlapping. As the pH was closer to the pKa of the carboxyl group of 5-HIAA,

more of this group was protonated and interacted more with the stationary phase and, therefore, eluted later. Lowering the pH to 4.05, further protonated 5-HIAA and achieved separation from E. Altogether, full separation of all compounds was therefore achieved with an addition of 0.25 % organic modifier and adjusting the pH to 4.05.

However, during summer an increase in outside temperature caused an increase in room temperature that the column compartment could not regulate due to a missing cooling function. At the higher internal temperature of the compartment of 31 °C, the viscosity of the mobile phase was decreased and allowed better diffusion of the compounds and a faster run time. Further, a higher temperature causes a decrease of pKa and altogether overlapped of E and 5-HIAA again. In order to avoid influence of the room temperature to the column compartment during summer time, its heating was raised permanently to 40 °C. With organic content of 0.25 % ACN at pH 4.05, a run time of 14 min but also overlapping 5-HIAA/E and IS/HVA occurred. Lowering pH to 3.95 achieved complete separation of all peaks at a run time of 13.5 min. A striatum brain sample was extracted as an exemplary biological tissue and showed no unknown peaks overlapping with any of the desired analytes. At higher standard concentration, 5-HIAA and E still showed some overlap, which was completely resolved by lowering the pH to 3.85. The total run time was 13 min, which meant a threefold reduction of analysis time on the instrument compared to the previous method with a fully porous particle column.

5.2.1.2. Tissue Extraction

Due to the high selectivity of the ECD, no extensive clean-up procedures were necessary for the analysis of MAs out of brain tissue. Samples were thawed and perchloric acid was added to precipitate proteins and act as an antioxidant. The sample was then homogenized with ultrasonication on ice and afterwards centrifuged. The resulting supernatant was then transferred into a HPLC vial and injected into a HPLC system. This works very well for brain tissue, as it consists mostly of lipids and does not have resilient protein structures, such as muscles or collagen. However, peripheral tissues show a different composition of macromolecules and need slight variations in the extraction procedure.

For fat tissue, whether brown or white, homogenization with ultrasonication worked well. However, after centrifugation, WAT precipitate was above the solution and drawing of the solution with a pipette caused disturbance of the pellet. Fat particles were drawn with the liquid, which could cause blocking of the column upon injection into the HPLC. Further, even though the brown fat pellet was on the bottom of the solution after centrifugation, the pellet was not very stable and fat particles were easily drawn into the pipette tip. In order to remove the fat particles, the solution was passed through a syringe filter after homogenization and centrifugation. A PTFE syringe filter with a pore size of 0.2 µm and a diameter of 4 mm was chosen. The PTFE membrane is hydrophobic and does,

therefore, not interact with the MA analytes. Additionally, the membrane has a high chemical resilience and is not degraded by perchloric acid contained in the homogenate. A 1 mL syringe fitted with a cannula was used to draw the supernatant, which was then passed through the filter after fitting it onto the syringe. Care needed to be taken not to draw too much fat into the syringe, as blocking of the filter was possible. However, even with little fat particles in the solution a high pressure built up occurred. Therefore, it was necessary to apply constant pressure to the syringe and the syringe filter on the top of the storage vial sitting on the bench. If too little pressure was applied to the filter, a sudden separation of the filter from the syringe was possible, resulting in loss of sample and health hazards due to acidic solvent splashes. Further, it was possible that not all of the solvent was passed through the filter. In order to mitigate sample loss here, it was best to draw a pocket of air into the syringe before drawing in the solution. The air pushed more solvent out of the filter into the storage vial. To remove all of the solvent from the filter, the syringe was separated, air drawn in, and pushed through the filter again. This procedure was repeated until no further filtrate could be collected. The filtration step did not result in any loss of analyte when a standard solution was subjected to the process. Also, a blank solution of perchloric acid pushed through the filter did not result in the occurrence of impurities in HPLC chromatograms.

For muscle, the simple homogenization procedure applied to brain and fat tissue was not sufficient. Ultrasonication was not powerful enough to destroy the muscle fibers completely and solid parts of tissue remained in the solution. This also meant that possibly not all of the cells were opened up and analytes might remain in the tissue and not be extracted into the aqueous phase. Therefore, homogenization of the muscle with a turrax homogenizer was tested. This device is a stirrer with a fast rotating blade. The mechanical shearing forces of the disperser tool should homogenize the muscle. However, parts of the muscle got stuck to the blade and were difficult to remove. This would require constant interruption of the homogenization process and might also possibly cause cross contamination. Next, solid biopulverizer beads in a 2 mL solvent tube were tested. Here, the tissue and solvent are added to the beads, and the beads shaken or vortexed. The mechanical forces of the beads connecting with the tissue at high speed cause breaking of the cells and release the analytes into solution. Usually, a special bead homogenizer is used, which allows shaking of the tubes with the beads at high velocities. However, such an instrument was not available in our laboratory and the vortexer and shakers were not powerful enough to homogenize muscle tissue with the tested standard glass beads.

The remaining possibility was the labor intensive manual grinding of the tissues with a mortar and pistil. A mortar cooled with liquid nitrogen was employed to prevent thawing and sample loss or cross contamination. Here, a reservoir for liquid nitrogen is located below the grinding bed, which cools the whole apparatus. Before grinding of the tissue, all necessary tools were also cooled on dry

ice to prevent thawing of the samples. Muscles were then placed into a folded piece of alumina foil to prevent contamination of the mortar and pistil. The foil was placed in the cooled mortar and the muscles ground into powder with the pistil. The sample was then transferred into a storage vial with a spatula and stored at -80 °C until further processing. Muscles treated in this manner could be homogenized completely by ultrasonication. This processing showed improvement of extraction of analytes out of muscles.

Liver could be homogenized by ultrasonication alone. The resulting homogenate consisted of turbid slurry, however, after centrifugation a pellet was formed and the supernatant was separated. Previous pulverization of the liver tissue with a mortar did result in less turbid slurry, however, the resulting chromatograms did not show any difference. Pancreas did also not cause any issues during the homogenization procedure. Therefore, muscle was the only tissue that required pulverization before the homogenization process.

For bigger tissues such as gastrocnemius and liver, different amounts of solvent were tested. At a higher amount, the analytes are diluted more, however homogenization works better. 200 µL and 400 µL added to gastrocnemius were tested. At the same homogenization and extraction rate, the amount should be doubled exactly in the lower volume solvent. However, at half of the solvent only roughly three quarters of the theoretical amount were present showing a better extraction with 400 µL. Therefore, 400 µL of perchloric acid were added to the gastrocnemius and liver to facilitate better extraction of analytes.

It was also found that the form of the homogenization tube has a substantial influence on the effect of the process. When a 2 mL tube with a leveled lower end was used, the sonication was not as efficient and in the case of muscle tissues not sufficient to cause full homogenization. When smaller 1.5 mL tubes with a conical lower end were used, the procedure was successful under the conditions described above. The ultrasonication procedure relies on a process called cavitation. The ultrasonic waves of the device consist of a compression phase with high pressure and a rarefaction phase with a low pressure in accordance to the frequency. During the rarefaction cycle, vacuum bubbles form and expand in the liquid. During the compression phase these bubbles implode and release high temperature and pressure, also sending out liquid jets. This process is called cavitation. The resulting forces cause the cell membranes to break and release their content. It seems that in the bigger tube with the leveled end and higher circumference the pressure and jet streams can disperse more and therefore not transfer their energy to the tissue. In the conical tubes, the solution is more confined and the destructive forces can develop their full potential. The high temperature during the cavitation process is also the reason for necessary cooling of the sample during the ultrasonication step. To ensure that the analytes are not degraded due to the high temperatures, standard solutions

were subjected to ultrasonication for different lengths of time, where no loss of analyte was detectable.

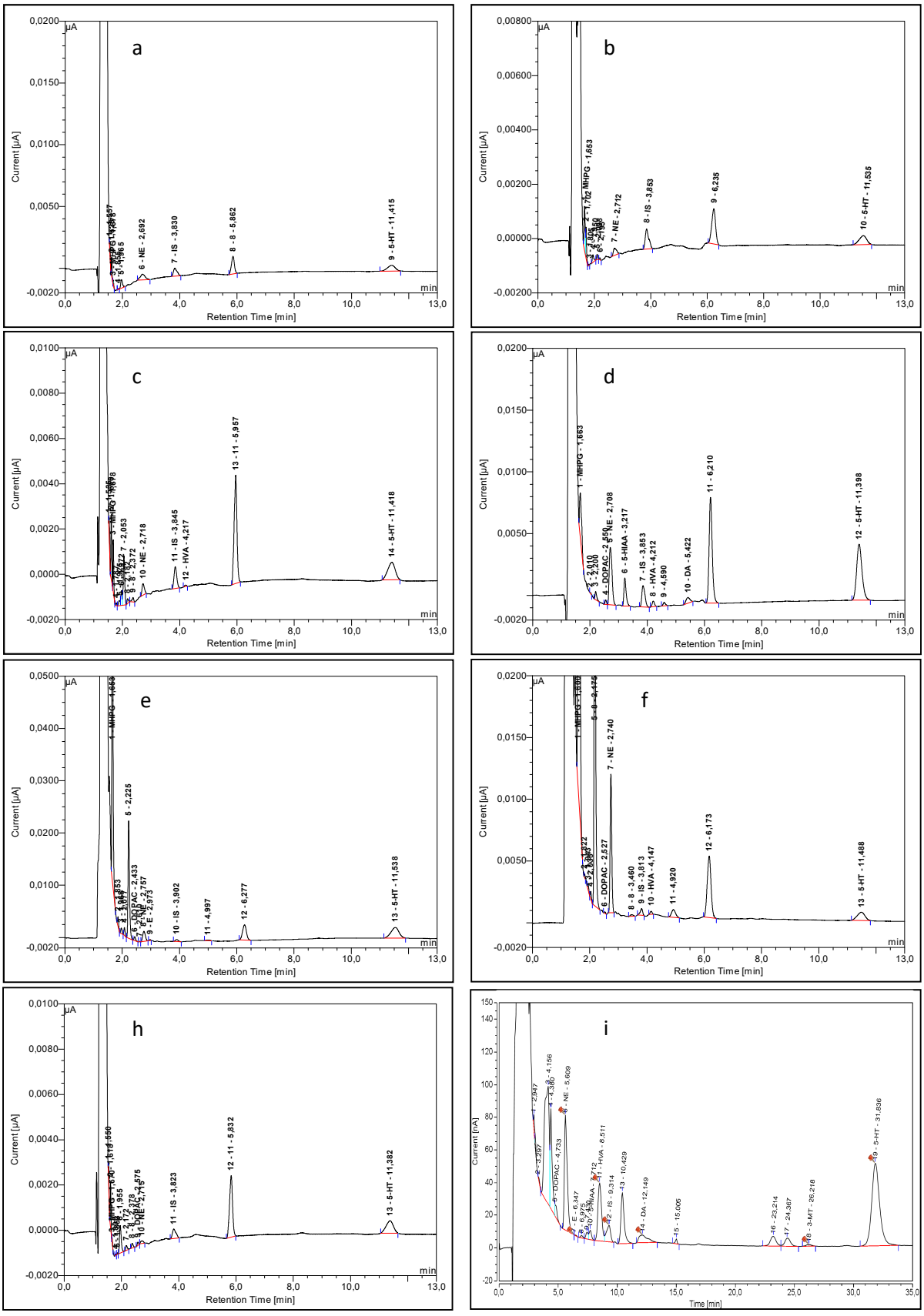

Figure 26: Chromatograms of biological samples; a: soleus; b: EDL; c: gastrocnemius; d: hypothalamus; e: liver; f: pancreas; g: eWAT (all analyzed on system II) i: BAT (analyzed on System III).

Figure 26 shows the chromatograms of MAs in the tested tissue regions. The analytes are present in sufficient concentration above the LOQ and can be quantified reliably. No other endogenous compounds overlap with the analytes of interest.

For the analysis of macrophage cell culture and supernatant, addition of perchloric acid was also tested. However, due to low amounts of protein no precipitation pellet was formed after ultrasonication and centrifugation. In order to prevent protein build up on the pre-column and rapid blocking, samples were subjected to a centrifugal filter unit, usually used for protein concentration up to 0.5 kDa, which was used in this case to trap proteins and clean up the samples. Due to the tight filter matrix, samples took 30 minutes at high centrifugal speed for full passage into the reservoir. MA standard solution and blank solution were subjected to the process to ensure full recovery and no contamination from the filter. Figure 27 shows the resulting chromatograms. In the case of supernatant it is also necessary to analyze the medium without addition of cells to ensure analytes of interest originate from the cells and not the medium (Appendix 7.8).

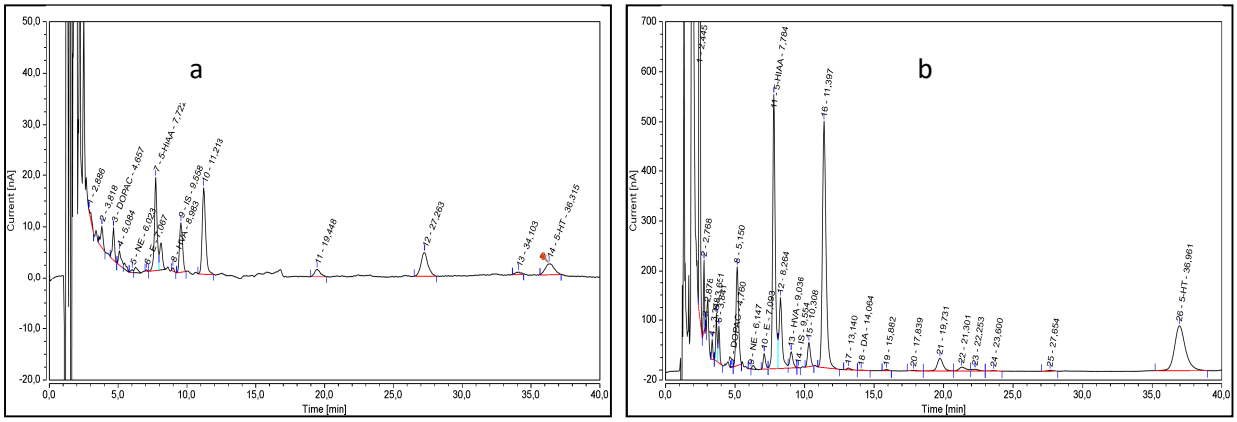

Figure 27: Chromatograms of macrophage cell pellet (a) and supernatant (b).

5.2.2. Validation

5.2.2.1. Sample validation: precision, accuracy, recovery

All tissues are comprised of the structural components protein and fat. Variable amounts of these could possibly affect analytes differently during and after the extraction. Therefore, the method also needed to be validated in tissue samples, to ensure that no matrix effects disturb the analysis and cause variable results. However, to reduce the number of necessary measurements, only three regions were used. Muscles consist mostly of protein, fat tissue consists mostly of lipids, while brain is mostly made up from lipids with a bit of structural protein content. Therefore, the gastrocnemius was chosen as an example for muscle tissue, eWAT was used for fat, and the hypothalamus for brain. These three tissue regions cover the array of possible macromolecule configuration and analyte concentration. An argument could be made that also enzyme content varies between further tissues and could cause variations in the analysis. However, addition of perchloric acid to the sample before

thawing and ultrasonication degrades the enzymes and ensures preservation of original neurotransmitter concentrations.

Table 8 shows the mean calculated amounts, the relative standard deviation (RSD), precision, and recovery. The precision and accuracy deviations were below 15 %, as recommended by the US Food and Drug Administration guidelines for bioanalytical methods. The exception was the metabolite MHPG; where the accuracy between the calculated and nominal values were well above 15 %. This is due to the fact that MHPG runs close to the solvent front and the peak area might be affected. However the compound was still included in the method to allow analysis in a semi-quantitative way. For DOPAC, the lowest spike in eWAT displayed an accuracy deviation of 17 %, which might be due to higher variations in the low amount of endogenous compound present, which was subtracted to achieve the calculated spiked amount. The recovery of the IS, which was used for the calculation of the analyte concentration was around 100 %, which was well above the general accepted value of 50 %.

For the complete validation it would be best to add the spiked components to the whole sample in perchloric acid before the homogenization, however, not enough mice were available to allow the analysis of one sample per data point. Therefore, the samples needed to be pooled, homogenized together, and then aliquoted to allow for sufficient number of measurements. However, the aliquotation of the sample between ultrasonication and centrifugation was not possible. Either pipettes were either blocked due to solid particles or the aliquots were not completely homogenous with differential liquid and solid content. It was necessary to first centrifuge the samples and then aliquot the supernatant, which were then used for different spike concentrations. This is a compromise, as the homogenization and centrifugation step was excluded from the spike. However, this procedure still shows that there are no disturbing compounds in the supernatant and no matrix effects are present from there. Additionally, a single spike experiment was conducted in eWAT and gastrocnemius, where the analytes were spiked before ultrasonication, to ensure that all analytes and the internal standard behave the same during this step and that no differential matrix effects are present, which was the case. This procedure still shows that the method works reliably not only in brain samples, but also peripheral tissues.

Table 8: Validation of MAs in hypothalamus, eWAT, and gastrocnemius; combined intraday means measured in triplicates over three days.

	Spiked Amount	Combined mean of calculated amount [pg]			Combined RSD [%]			Combined Accuracy [%]			Combined Recovery IS [%]		
		HYP	eWAT	GASTR	HYP	eWAT	GASTR	HYP	eWAT	GASTR	HYP	eWAT	GASTR
MHPG	500	505 ± 128	286 ± 120	410 ± 107	2.2 ± 1.4	4.1 ± 0.2	3.4 ± 2.3	101 ± 26	57 ± 24	82 ± 21	95 ± 2	97 ± 12	95 ± 10
	1000	886 ± 101	557 ± 135	691 ± 92	1.2 ± 0.5	1.5 ± 0.7	3.6 ± 1.6	92 ± 14	56 ± 13	69 ± 9	97 ± 11	95 ± 7	94 ± 5
	5000	4417 ± 827	3499 ± 705	3803 ± 1299	1.2 ± 0.3	1.9 ± 0.4	2.9 ± 1.9	88 ± 17	70 ± 14	76 ± 26	107 ± 3	105 ± 1	101 ± 6
DOPAC	500	509 ± 17	415 ± 10	429 ± 20	1 ± 0.3	1.3 ± 1	0.8 ± 0.2	102 ± 3	83 ± 2	86 ± 4			
	1000	969 ± 32	886 ± 29	897 ± 18	1.3 ± 1.4	2.5 ± 2.6	1.2 ± 0.8	100 ± 1	89 ± 3	90 ± 2			
	5000	4504 ± 39	4407 ± 56	4474 ± 492	0.6 ± 0.2	1.6 ± 1.4	2.2 ± 1.1	90 ± 1	88 ± 1	89 ± 10			
NE	500	535 ± 2	431 ± 13	495 ± 38	0.8 ± 0.2	1.2 ± 1.1	0.7 ± 0.4	107 ± 0	86 ± 3	99 ± 8			
	1000	1034 ± 82	933 ± 29	1024 ± 45	2 ± 0.9	2.3 ± 2	1.9 ± 2.1	106 ± 4	93 ± 3	102 ± 5			
	5000	4758 ± 270	4648 ± 90	4934 ± 226	0.4 ± 0.1	2 ± 1.4	1.3 ± 1.4	95 ± 5	93 ± 2	99 ± 5			
E	500	511 ± 23	469 ± 18	459 ± 22	1.1 ± 0.5	2 ± 1.7	0.5 ± 0.3	102 ± 5	94 ± 4	92 ± 4			
	1000	1032 ± 73	972 ± 29	990 ± 51	2.1 ± 0.7	2.4 ± 2.3	2 ± 1.8	106 ± 4	97 ± 3	99 ± 5			
	5000	4881 ± 275	4820 ± 95	4965 ± 247	1 ± 0.2	1.9 ± 1.4	1.5 ± 1	98 ± 6	96 ± 2	99 ± 5			
5-HIAA	500	520 ± 32	468 ± 56	500 ± 30	1.4 ± 0.7	2.6 ± 0.5	1.7 ± 0.2	104 ± 6	94 ± 11	100 ± 6			
	1000	1068 ± 106	990 ± 17	1067 ± 46	3.9 ± 1	2.9 ± 1.4	3.3 ± 1.8	110 ± 6	99 ± 2	107 ± 5			
	5000	4821 ± 398	5262 ± 381	5325 ± 308	1.4 ± 1.1	2.9 ± 1.3	1.7 ± 0.6	96 ± 8	105 ± 8	107 ± 6			
HVA	500	521 ± 42	482 ± 53	455 ± 50	1.3 ± 0.4	1.6 ± 0.8	1.9 ± 0.2	104 ± 8	96 ± 11	91 ± 10			
	1000	948 ± 62	927 ± 101	844 ± 46	1 ± 0.2	2.8 ± 2.1	2.3 ± 1.9	98 ± 5	93 ± 10	84 ± 5			
	5000	4444 ± 348	4311 ± 392	4165 ± 840	0.4 ± 0.3	1.2 ± 0.7	1.9 ± 1.3	89 ± 7	86 ± 8	83 ± 17			
DA	500	493 ± 50	456 ± 11	502 ± 32	1.5 ± 1.1	2.2 ± 0.7	0.9 ± 0.5	99 ± 10	91 ± 2	100 ± 6			
	1000	988 ± 80	921 ± 26	1022 ± 59	1.8 ± 1.5	4.6 ± 1.7	2.6 ± 2.4	102 ± 4	92 ± 3	102 ± 6			
	5000	4687 ± 230	4656 ± 100	4830 ± 297	0.5 ± 0.3	2.5 ± 1.2	1.6 ± 1.3	94 ± 5	93 ± 2	97 ± 6			
3-MT	500	515 ± 22	493 ± 18	481 ± 39	1.5 ± 0.4	2.5 ± 1.5	2 ± 2.2	103 ± 4	99 ± 4	96 ± 8			
	1000	1007 ± 53	978 ± 40	1005 ± 12	2.3 ± 1	2.6 ± 2.5	2 ± 1.2	104 ± 2	98 ± 4	101 ± 1			
	5000	5143 ± 175	5105 ± 50	5310 ± 381	0.5 ± 0.1	2 ± 1	1.8 ± 1.3	103 ± 3	102 ± 1	106 ± 8			
5-HT	500	529 ± 22	498 ± 41	532 ± 16	1.3 ± 0.2	2.6 ± 1	2.2 ± 1.4	106 ± 4	100 ± 8	106 ± 3			
	1000	1022 ± 85	977 ± 64	1007 ± 19	2.1 ± 0.9	2.8 ± 1.2	4.4 ± 4.6	105 ± 5	98 ± 6	101 ± 2			
	5000	4977 ± 99	5025 ± 59	5112 ± 520	1.4 ± 0.5	2.3 ± 1.1	1.7 ± 1.1	100 ± 2	100 ± 1	102 ± 10			

5.2.2.2. Stability tests

The stability of both standard solution and extracted samples was also part of the validation procedure, to ensure good quality control in calibration standards and possible re-analysis of samples.

At first, working standard solutions at a concentration of 1 ng 40 μL^{-1} were produced from the standard stock solutions at a concentration of 1 ng μL^{-1}. MA and internal standard were combined in amber 4 mL vials, which could then be taken directly and be injected into system I at the correct concentration for daily calibration. Three of those working standards were produced and stored under different conditions. One was stored in the fridge at 4 °C. One was stored at -80 °C and only thawed at the selected time points. One was stored at -80 °C and thawed at room temperature for daily use. Figure 28 shows that the analytes are each affected differently by the storage conditions. 5-HT and its metabolite 5-HIAA are the least stable compounds and degrade very fast under all conditions and are below 40 % after two months. The other compounds are in the same range between 60 and 80 % after two months. Generally, except for 5-HT, permanent storage at -80 °C was the best option. At this condition after a month, the analytes except 5-HT and 5-HIAA, show a higher concentration than the beginning. As synthesis of new compounds is not possible, it is most likely that the solution was not completely thawed and a concentration gradient existed due to that. Further, for most compounds, storage at -80 °C and daily thawing caused the most degradation.

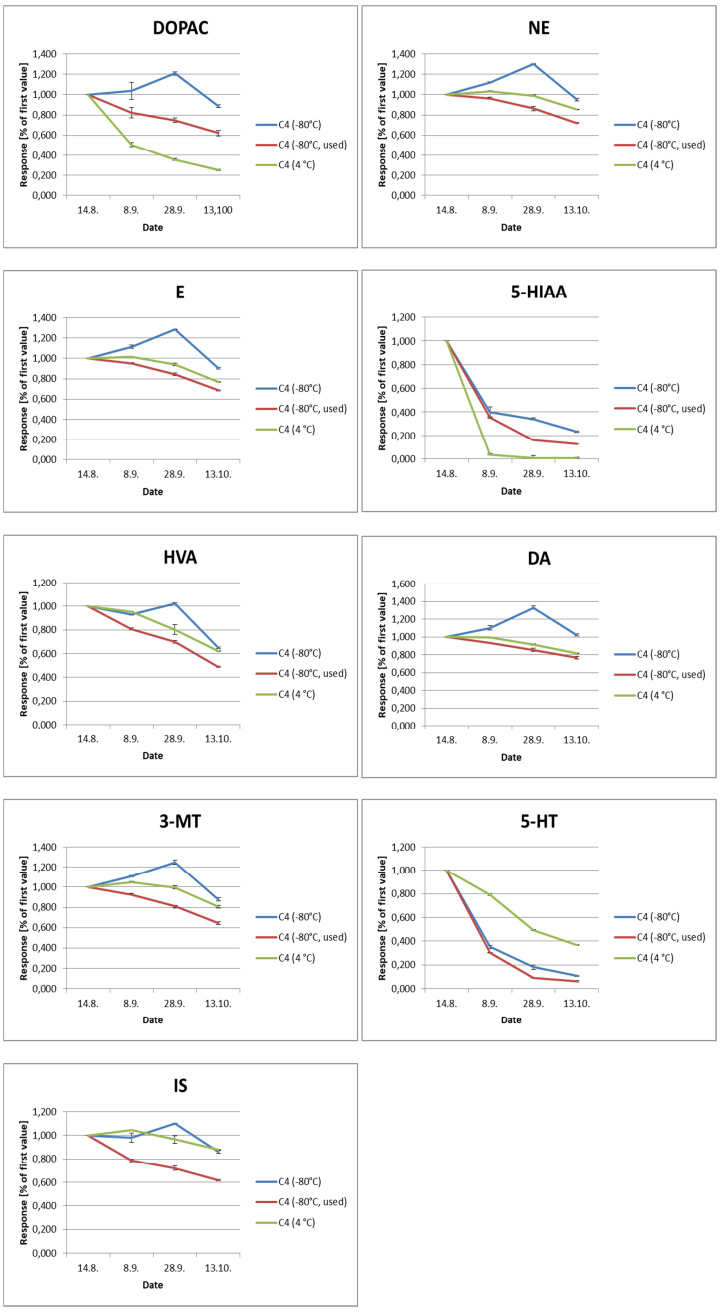

Figure 28: Degradation of prepared calibration standard at concentration of 1 ng 40 μL^{-1}; stored at 4°C, -80 °C, and -80°C with daily thawing; means of n=3.

This could be an effect of the thawing itself or an indication of the time spent at room temperature. Possibly, thawing of the standard in the fridge would yield different results. Permanent storage at 4 °C was in most cases in between, except for DOPAC and 5-HIAA. The latter was even degraded completely under this condition. Altogether, this experiment indicates that none of the variants were usable for prolonged measurement campaigns, where a daily standard solutions need to be injected at a constant concentration to give consistent results.

Therefore, it was also tested how the standard stock solutions at a concentration of 1 ng μL^{-1} degrade in storage at 4 °C. Here, calibration solutions were produced daily at a concentration of 1 ng 20 μL^{-1} from the standard stock solution, injected into system II, and plotted over half a year (see Figure 29). The standard solutions show no significant degradation over this time period. HVA shows a greater variation in the middle time period, however, at the end it is shown that it is not degraded and still present in the standard stock solutions at the starting concentration. The variation seen between the measurements is most likely caused by the preparation of the calibration solution. Possibly small impurities on the detector, present only for a short period of time before being oxidized and flushed away by the mobile phase, also caused a variation in response to the analytes.

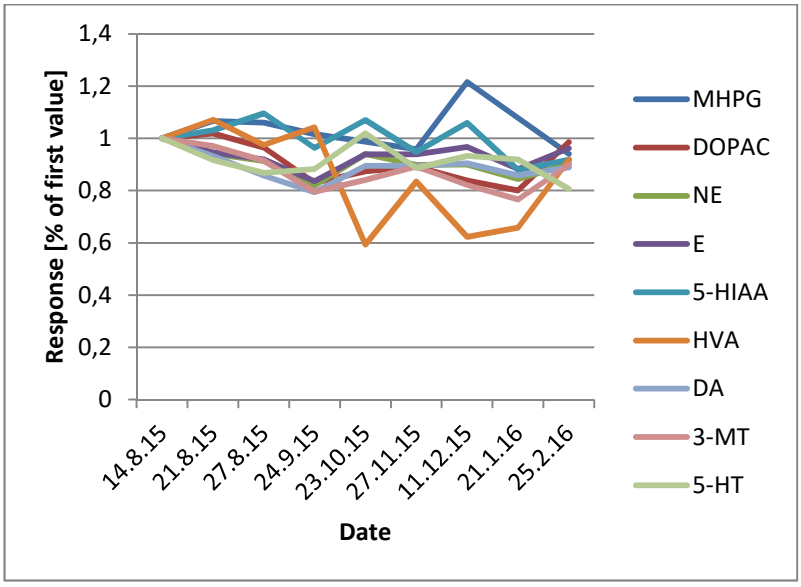

Figure 29: Degradation of standard solution [1 ng μL^{-1}] stored at 4 °C wrapped in alumina foil over 6 months.

This procedure of daily preparation of calibration solution is applicable to prolonged campaigns. The calibration has to be monitored, until a degradation of compounds becomes apparent and a new standard stock solution has to be produced.

Also of interest is the stability of extracted samples. After the extraction, an aliquot was taken for the measurements and the remaining samples were stored in 2 mL plastic tubes at – 80°C. In order to test the degradation of compounds under these conditions, one set of striatum samples was analyzed over one month and after one year to check the degradation of the compounds (see Figure 30). For the first four time points, the same three samples were used. However, for the last point, not enough material was available, so three other samples were compared to their initial analysis.

The plot indicates that the samples degrade slowly over time and are present at concentration of about 80 % after one month. All compounds behave the same and show the same pattern. However, after one year the analytes show a wide degradation pattern between 20 and 60%. Interestingly, 5-HIAA is the most stable compound during this experiment, in contrast to the storage in standard solution. This experiment shows that samples can be reanalyzed for up to one month with an expected variation of 20 %. However, it seems best to check samples for inconsistencies as soon as possible and re-measure immediately when necessary.

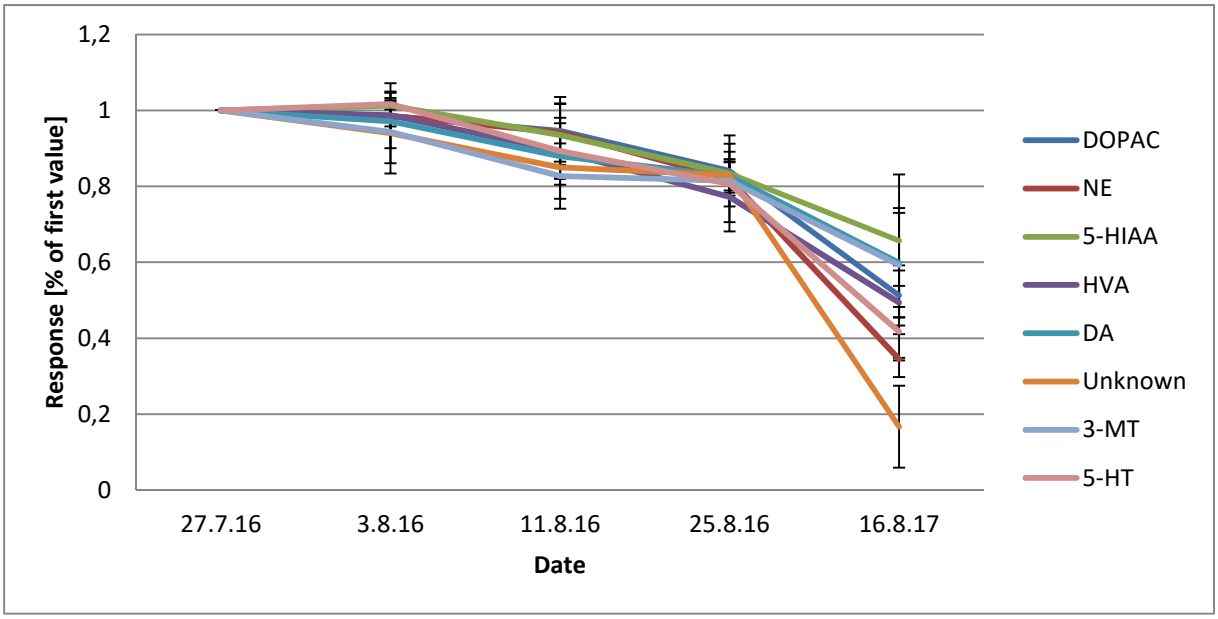

Figure 30: Degradation of extracted STR samples stored at -80°C; until 25.8.16 the same samples were analyzed; for 16.8.17 due to insufficient material other samples were tested; 3.8 n = 3; 11.8 n = 2; 25.8. n = 2; 16.8. n = 2.

Other tissue regions were not tested, however, most likely behave similarly. During the extraction procedure with addition of perchloric acid and ultrasonication, all enzymes and other macromolecules should be precipitated, so that conditions in various samples are consistent at the storage point. The stability of compounds in tissues before the extraction was not tested. However, to reduce enzymatic activity and degradation, all tissues were stored at -80 °C until extraction. As the focus of the method was on the comparison WT mice with KO or treated mice, this possible degradation was not a concern, as comparable samples are affected the same and are extracted and analyzed at the same time. However, to prevent possible loss of analytes causing a concentration below the LOD, dissected tissues should be analyzed as soon as possible.

5.2.3. Method application

So far, MAs have been routinely analyzed in clinical diagnostics in human blood, plasma, and urine. In research settings, focus has been mostly on animal brain tissues. However, despite wide ranging neuronal and hormonal effects in peripheral tissues, few methods exist for their analysis using electrochemical detection. A method for measuring NE, E, DA, and 5-HT along with several metabolites with ECD in rat heart muscles was developed by Mano et *al*, using a gradient HPLC system equipped with 16 ECD sensors. [111] As normal ECD detectors have only one or two ECD cells, the method appears difficult to apply in most laboratory settings. Eldrup et *al.* employed an SPE alumina extraction method, which limited analysis to catecholamines, in rat tissues including muscles, liver, and pancreas. [112] Analysis of the pancreas was also done in the solid tissue as well as isolated perfusated and islets. [113-117] NE, E, and 5-HIAA were analyzed in solid pancreas of rats, while CAs and 5-HT were measured in rabbits. An alumina SPE was employed for the analysis of perfusate and islets, which restricts analytes to CA as well. Garofalo et *al.* also used an alumina based method for MA detection in WAT of rats. [118] UV detection after derivatization has been reported for the analysis of CAs in murine liver.[66] A new methodology for the analysis of seven MAs was reported in peripheral tissues, however only data about striatum of mice was shown. [119] Another method could analyze 11 MAs, but was only used in rat hippocampus and cortex. [89] Therefore, in practice, the simultaneous measurement of monoamines in peripheral tissues with ECD was limited in number of compounds detectable and also mostly employed in rat tissues. The method reported in this work was the first that showed a validated method for the analysis of nine active MA neurotransmitters and metabolites in peripheral murine tissues and closes an analytical gap in the research of diseases.

Within this work, it was already applied in a couple of cooperations with the Institute for Diabetes and Obesity (IDO) from the Helmholtz Center Munich, where it provided valuable insights and support in the specific projects.

5.2.3.1. Monoamines in alternatively activated macrophages

The nervous system of mammals tries to keep the body in homeostasis. In order to hold the core temperature within tight bounds in a cold environment, thermogenesis is activated. This process can include voluntary movement, muscle shivering, but also uncoupled respiration in BAT. This respiration might also be a valuable pharmacological target for energy homeostasis in the world wide obesity epidemic. It is activated by CAs of the sympathetic nervous system [120]. Recently, evidence occurred that besides sympathetic postganglionic neurons and adrenal medulla, also alternatively activated macrophages (M2 macrophages) are a source of CAs and thereby promote thermogenesis in BAT. [121] However, these experiments were done in mice with a lifelong deficiency in macrophage signaling, which occurs also in the CNS and might cause altered sympathetic regulation

during development. In order to control for this, mice, where the gene for the expression of tyrosine hydroxylase can be deleted selectively in hematopoietic cells, including macrophages, after administration of tamoxifen were produced. These macrophages can no longer produce catecholamines, yet energy expenditure and core body temperature of KO mice were not changed at room temperature and after cold exposure, compared to WT mice. [122] For further clarification, monoamines were analyzed to elucidate the role of macrophages. Interleukin 4 (IL-4) is one of the key messengers that activate M2 macrophages. WT mice were treated chronically with IL-4 and then exposed to a cold environment. If macrophages indeed activate thermogenesis via catecholamines, the treated mice should have higher levels due to the higher activation after IL-4 treatment. However, neither active neurotransmitters nor metabolites were altered in BAT in comparison to mice treated with saline (Figure 31). Also analysis of detectable unknown peaks showed no variation between the groups. Here, only the peak area was compared, as no comparison with standards could be made to indicate concentration. No internal standard correction was used as well. The major unknown at retention time 10.5 min possibly represents tryptophan. No comparison with a tryptophan standard injection was made at the time point of the campaign, however, the differential response in the two detector channels is consistent with the experiments in section 5.2.3.2.

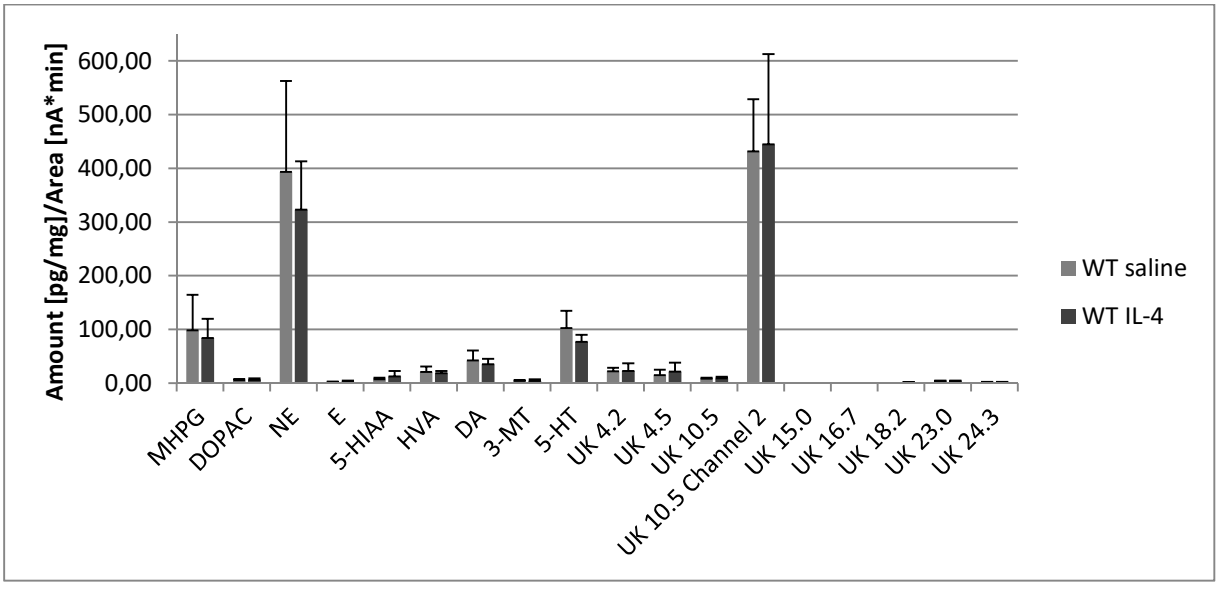

Figure 31: BAT of WT mice (4 months old) treated with saline (0.9%) (mean of n=7) and IL-4 (50µg/kg) (mean of n=7) for 12 days, exposed to cold environment (30°C during treatment, then 24h at 20 °C, 10 °C, and 5°C) before sacrification and analysis; known compounds are presented in concentration [pg/mg], UK = unknowns (number indicates retention time) in peak area per injection [nA*min]; analyzed on system III.

Further, the group found that there was no effect of bone marrow derived macrophages after activation with differential doses of IL-4 on differentiation of primary iWAT cells, browning of adipocytes, or on thermogenesis in BAT primary cells. Isolated macrophages as well as their medium supernatant were analyzed for the presence of CAs. Figure 32 shows the peak area per sample

injection of the analytes, to allow comparison with unknown compounds. Calculated concentrations for known analytes can be found in Appendix 7.7.

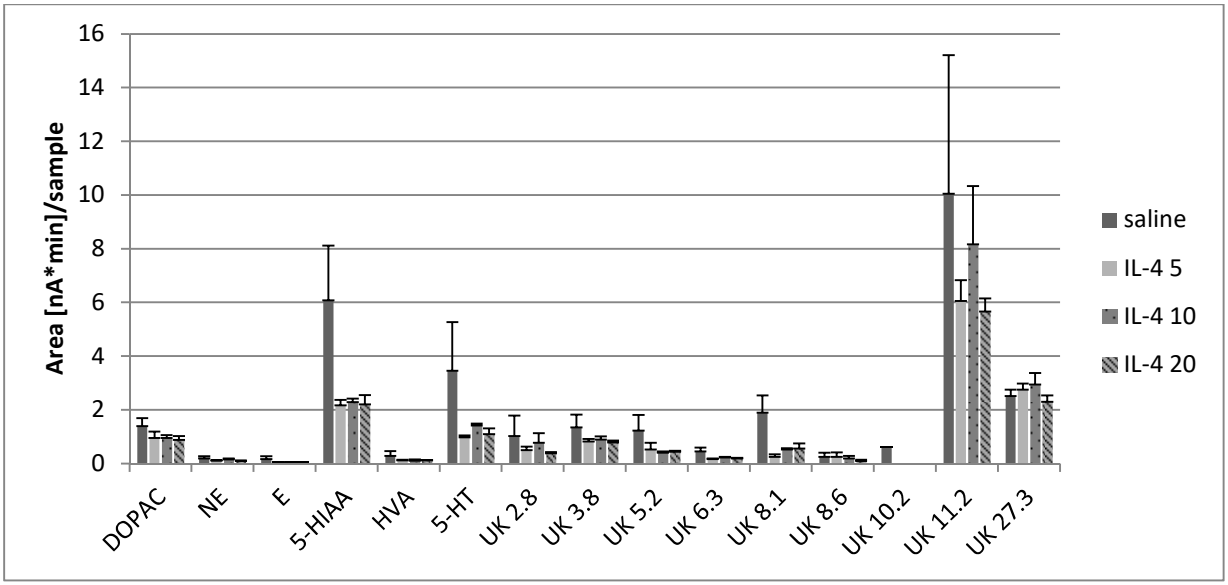

Figure 32: Monoamines in bone marrow derived macrophages treated with IL 4 (saline n=2; IL-4 5 ng mL^{-1}, 10 ng mL^{-1}, 20 ng mL^{-1} n=3); unknown numbers indicate retention time; analyzed on system III.

ANOVA analysis of groups showed no differential production of CAs after polarization of macrophages with IL-4. Differences were shown between 5-HIAA ($p = 0.02$), unknown 6.3 ($p= 0.02$) and unknown 8.1 ($p = 0.01$). However, pairwise t-tests between groups showed no significant differences. These results likely present no effect of IL-4 treatment, but rather an effect of the high variance of the control group. Interestingly, this variance seems to affect the tryptophan pathway more, as 5-HT is also close to significance in ANOVA analysis ($p = 0.1$). Therefore, taking an α of 0.15, the unknowns at 5.2 min, 6.3 min and 8.1 min might indicate precursors or metabolites of 5-HT.

The macrophage medium supernatant also indicated no increase of adrenergic compounds upon stimulation with IL-4. Figure 33 shows the peak area per sample injection to allow comparison with unknowns. However, E, HVA, 5-HT, 5-HIAA and some unknown substances showed a decrease in the treated groups. Pairwise t-tests showed the statistical significance was present only in comparison to the control group and no IL-4 concentration dependence could be observed. The decrease in neurotransmitters and metabolites indicates an increased turnover and activation of the macrophages. This increased turnover does not show in the cells themselves, but only in exchange with the medium, possibly due to polarization of the macrophages upon stimulation. However, no increased production of NE that could lead to stimulation of adipocyte browning or thermogenesis was observed.

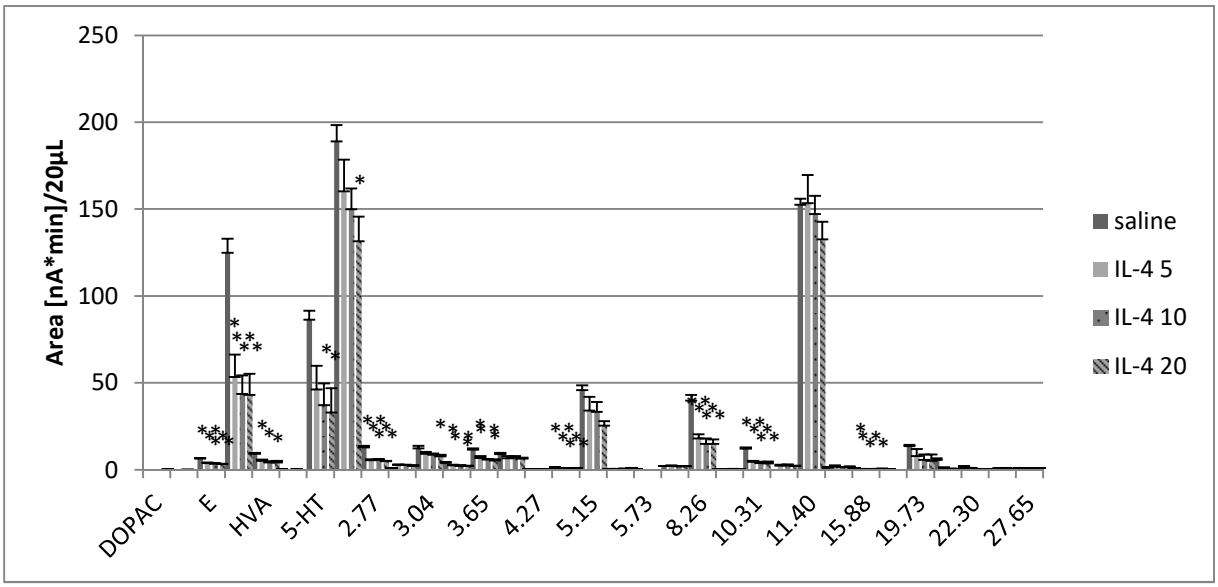

Figure 33: Monoamines in medium supernatant of bone marrow derived macrophages treated with IL-4 (saline n=2; IL-4 5 ng, 10 ng, 20 ng mL^{-1} n=3); unknown numbers indicate retention time; analyzed on system III.

Further, monoamines were also analyzed in mice kept at 4 °C for 6 h compared to mice kept at 22 °C (Figure 34). DOPAC, HVA, DA, 3-MT, and 5-HT showed a significant increase in the mice kept at 4°C. NE and E levels were significantly lower in mice kept at cold temperature. This indicates an increased turnover of these compounds and likely signifies an increased sympathetic activity.

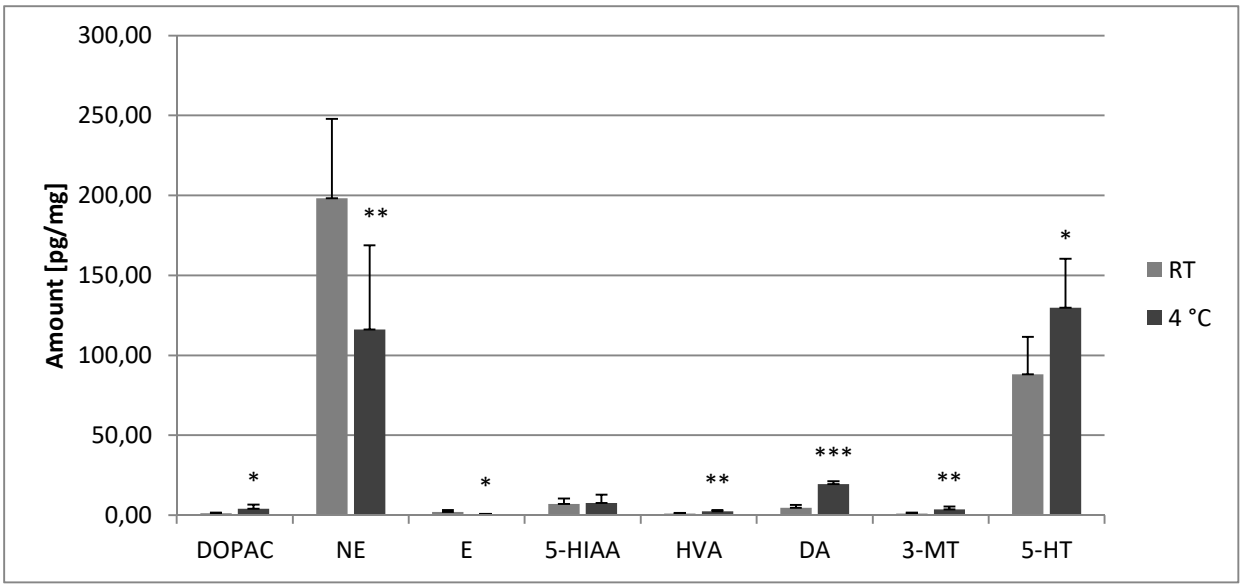

Figure 34: Comparison of monoamines in BAT of mice kept at room temperature or 4 °C for 6 h (each n = 8)

Taken together, these results show that the sympathetic nervous system is linked to thermogenesis in BAT of cold exposed mice. However, contrary to recent reports, macrophages do not seem to possess the ability to produce sufficient amounts of CAs to promote thermogenesis or browning of adipocytes. [122] The developed method for the analysis of monoamines in BAT and cell culture

proved to be a valuable tool and helped to produce evidence of the hypothesis not on the level of genetic markers, but the neurotransmitters themselves.

5.2.3.2. Monoamines in Dusp8 KO mice

Obesity, which is one of the primary risk factors in the development of type II diabetes, raises circulating free fatty acids (FFA) and inflammatory adipocytokines that are both known to activate c-Jun amino-terminal kinases (JNKs), which are part of the mitogen activated protein kinases (MAPK) signal cascade. [123] Once active, these kinases phosphorylate and thereby activate transcription factors which are transported into the cell nucleus and can activate a number of genes. Short and transient activation may be part of the normal stress response and promote cell survival, however, chronic activation may cause insulin resistance, which is the hallmark of diabetes. Four distinct pathways are potentially involved in this effect. On insulin target sites JNK inhibits the response to the docking of the insulin molecule onto the receptor site. In macrophages of adipose tissue they raise the activity and promote metabolic inflammation which can act directly on insulin target sites or promote release of FFAs, further promoting the cascade. JNK may also inhibit the pituitary-thyroid axis and lower circulating thyroid hormones, thereby increasing metabolic efficiency and adipose tissue. Finally, in hepatocytes of the liver, JNK may inhibit fatty acid oxidation and ketogenesis and further increase circulating free fatty acids. [124]

Global ablation of JNK protects from hyperglycemia and insulin resistance. [125] Additionally, inhibition of JNK restores the insulin signal pathways in the hypothalamus. [126] However, due to different forms and global expression of JNK, using it as a pharmacological target has proven difficult as no specific effects could be produced. [127] In contrast, another approach might be to target regulatory proteins of JNK. Among these inhibitors are dual-specifity phosphatases (Dusp). Dusp8 was shown to have greater activity towards JNK than to other members of the MAPK family. It is mostly expressed in the brain and not the heart or skeletal muscles. Genome wide association studies have shown Dusp8 to be a paternally inherited type II diabetes risk gene. [128]

Dusp8 KO mice of the IDO were shown to have similar bodyweight and glucose and insulin tolerance compared to WT mice when fed a standard chow diet. When fed a high fat diet, they still showed comparable bodyweight and composition. However, male Dusk8 KO mice showed an impaired glucose tolerance, which was not present in females. After overexpressing Dusp8 with adeno-associated virus in the hypothalamus, the glucose levels were normalized again. Also JNK1 co-deletion to Dusp8 normalized the insulin sensitivity.

The group also wanted to check the effect of Dusp8 ablation on sympathetic tone in these mice. As NE is a marker of sympathetic innervation, an experiment was designed to test the kinetics of NE turnover in peripheral murine regions. WT and Dusp8 KO mice were injected with

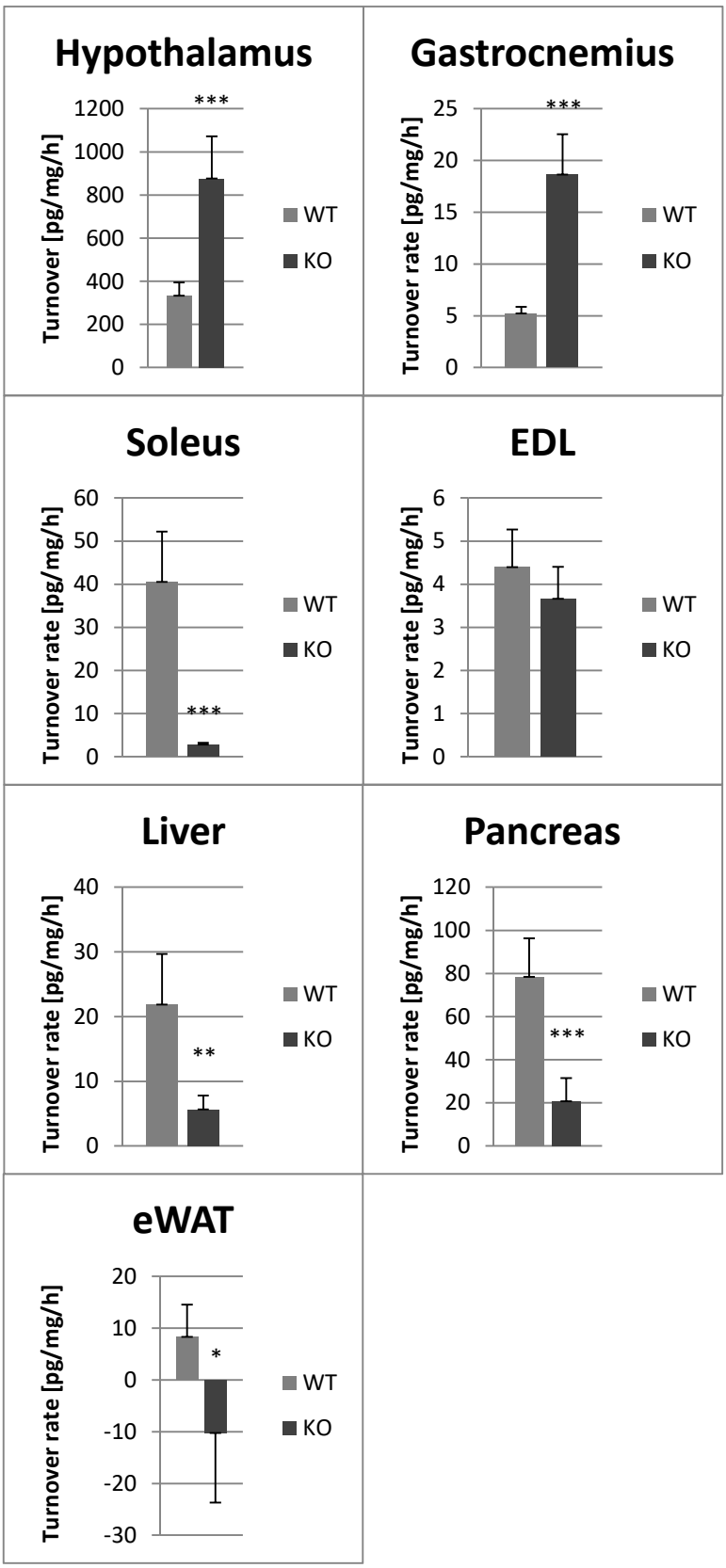

Figure 35: NE turnover in tissues of WT and Dusp8 KO mice, n = 6; liver analyzed on system I, remaining tissues analyzed on system II.

α -methyl-p-tyrosine (α-MPT). This molecule acts as a tyrosine hydroxylase enzyme inhibitor, which blocks the first step in the production of the catecholamines from tyrosine. Therefore, no more NE can be produced and the difference in NE levels between mice injected with saline and α-MPT can be used to determine the turnover of NE, as the formation and metabolization of NE is normally constant, but in case of α-MPT injection no more NE can be formed. This can be used as an indirect readout for NE outflow and therefore sympathetic innervation. For the calculation of the turnover, the method developed by Brodie et *al.* was used. [129] Here, the natural logarithms of the NE concentrations were calculated. The slope of the linear regression analysis between the different time points was used as the rate constant k_{NE}. The turnover rate was found by multiplying the rate constant with the initial concentration $[NE]_0$.

Figure 35 shows that the resulting NE turnover is not uniform across the tissues. The soleus, liver, and pancreas showed a significant decrease, while it was increased in the hypothalamus and the gastrocnemius. In the EDL, a trend toward a decrease of turnover was

visible, but did not reach statistical significance. In the eWAT, not only was there a decrease in NE turnover but further more NE was present after α-MPT treatment. This effect could also be based in the low concentration levels of NE in this tissue with the according higher variances in analysis. A comparison between the NE tissue concentrations of saline treated WT and KO mice showed no statistical differences in any tissue, though in the liver and soleus the p-value was below 0.1. Calculated concentrations for known analytes can be found in Appendix 7.9.

It has been shown that IL-1 administration increases NE metabolism in the hypothalamus while also increasing corticosterone in plasma. [130] As IL-1 can activate JNK, removal of its inhibitor Dusp8 could explain the increased NE turnover in the hypothalamus. This in turn possibly activates the hypothalamic-pituitary-adrenal (HPA) axis, which is responsible for stress response and increases glucocorticoid levels in the body. [131] Indeed, the Dusp8 KO mice displayed chronically elevated corticosterone levels, which were causally linked to the observed glucose intolerance. Glucocorticoids have been shown to inhibit catecholamine synthesis and release in rats and humans [132, 133], which could explains the observed lower NE turnover in the peripheral tissues of Dusp8 KO mice. The reduced sympathetic activity could be one of the mechanism through which glucocorticoids influence glucose homeostasis. [134] The sympathetic nervous system has been shown to increase glucagon secretion in the pancreas. [135] A decrease in NE outflow could therefore explain the observed increased storage of glycogen in liver and skeletal muscles. However, even though the sympathetic nervous system is thought to decrease lipid metabolism in the liver [136], a decrease of sympathetic tone in the Dusp8 KO mice does not alter plasma lipid levels. On the other hand, NE increases lipolysis in white adipose tissue [137], where a decrease in sympathetic tone might counterbalance the effect in the liver. Further, the sympathetic nervous system seems upregulate glucose uptake in skeletal muscles. [138] A decrease in NE turnover might contribute this way to glucose resistance in Dusp8 KO mice. However, there seems to be a differential effect among different types of muscles, as in the gastrocnemius the turnover was increased, while the EDL was not statistically affected. Possibly, the different composition of muscly fiber types or sympathetic innervation plays a role here. [139, 140]. Altogether, it appears that Dusp8 has a multifactorial effect on glucose homeostasis.

The experiment with α-MTP also offered interesting possibilities for unknown identification. As the treatment blocks a known metabolic pathway, unknown peaks of the resulting chromatograms were also checked for an according concentration change to maybe help in the discovery of their identity. Figure 36 shows the response of the detector for each analyte and unknown peak occurring in the chromatograms of the separate tissues. Even though the structures of the foreign peaks are completely unknown, the IS used for the monoamines was used to adjust for the recovery of all

peaks, to possibly reduce the occurring variance. Afterwards, the results were normalized to mg of tissue to adjust for weight differences between individuals.

On clear difference is the peak at around 2.25 min in all analyzed tissues. It only appears in the α-MPT treated groups in WT and KO mice. A first thought was that it could be α-MPT itself, as the structure should be detectable by the ECD. It could be indeed oxidized by the detector, however, the retention time did not fit, as it elutes closer to the eluent front at 1.5 min. The next candidates were the compounds in the metabolic pathway before the blocked reaction, tyrosine and phenylalanine. Tyrosine was not the compound only visible in the treated groups, but is possible the peak present at 1.89 min in some of the tissues. Phenylalanine, however, was not detectable with the ECD. The unknown at 2.45 min was possibly 5-hydroxy-L-tryptophan, a precursor in the 5-HT pathway, which was identified by spiking experiments. Looking at the KEGG pathway of tyrosine, which represents genetic information of possible pathways to and from the original compound, further possible candidates were kynurenine, which possibly was the unknown at 3.12 min. Other tested compounds tyramine, hordenine, and normetanephrine of the tyrosine pathway could not be linked to unknowns present in the sample.

All these identifications are to be treated cautiously, as the campaign and the spiking experiments for the identification of unknowns were done with different chromatographic methods due to temperature differences in the laboratory as described in the method development (see section 5.2.1.1). A comparison was made according to the retention time shifts of known compounds and peak order, however, some compounds may respond differently than others to changes in the mobile phase. However, the result that none of the tested compounds represents the peak at 2.25 min is certain, as this peak could be clearly identified with the new method due to its lack of presence in the saline groups.

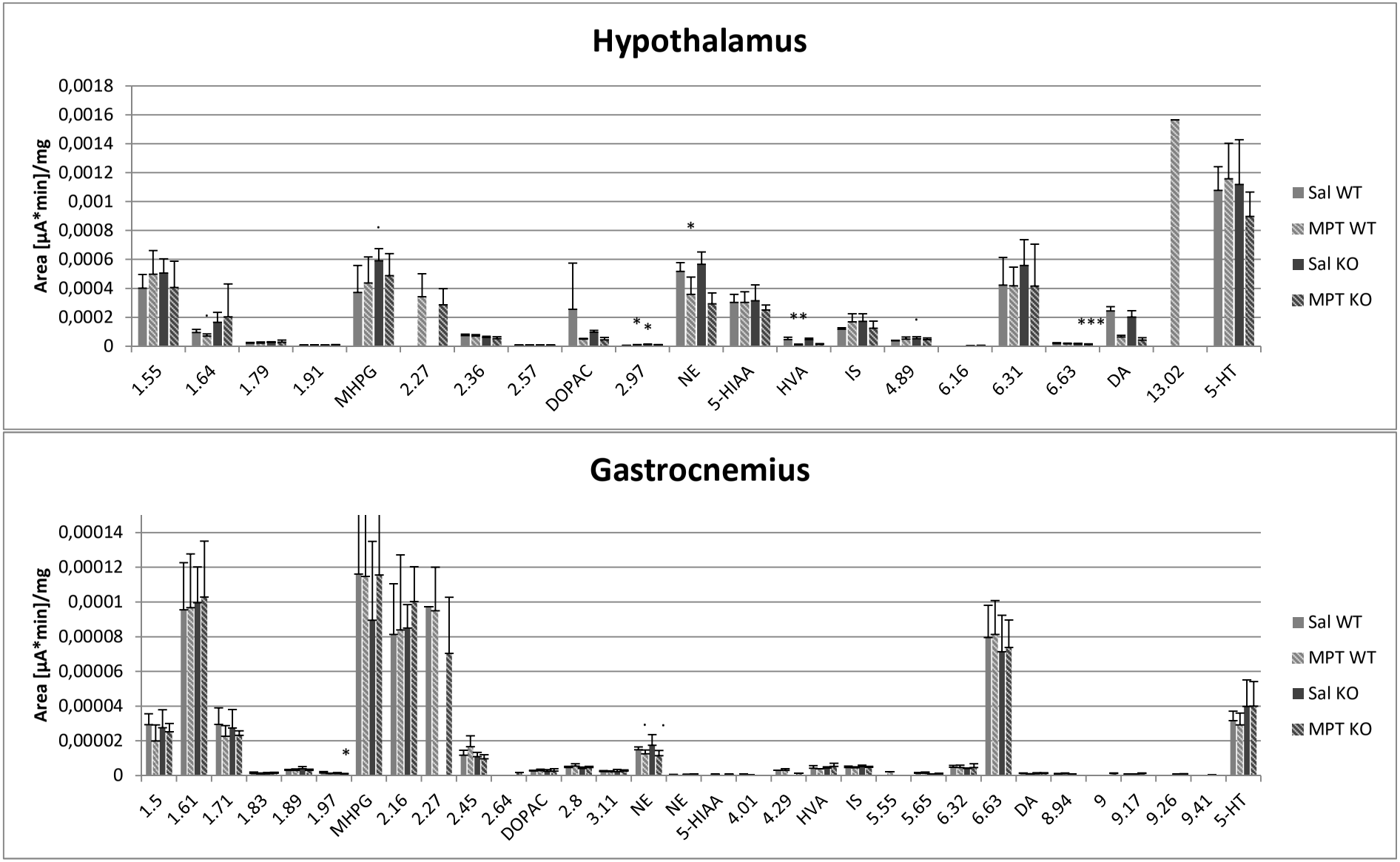
Hypothalamus
Area [µA*min]/mg
0,0018
0,0016
0,0014
0,0012
0,001
0,0008
0,0006
0,0004
0,0002
0
1.55
1.64
1.79
1.91
MHPG
2.27
2.36
2.57
DOPAC
2.97
NE
5-HIAA
HVA
IS
4.89
6.16
6.31
6.63
DA
13.02
5-HT
Sal WT
MPT WT
Sal KO
MPT KO
Gastrocnemius
Area [µA*min]/mg
0,00014
0,00012
0,0001
0,00008
0,00006
0,00004
0,00002
0
1.5
1.61
1.71
1.83
1.89
1.97
MHPG
2.16
2.27
2.45
2.64
DOPAC
2.8
3.11
NE
NE
5-HIAA
4.01
4.29
HVA
IS
5.55
5.65
6.32
6.63
DA
8.94
9
9.17
9.26
9.41
5-HT
Sal WT
MPT WT
Sal KO
MPT KO

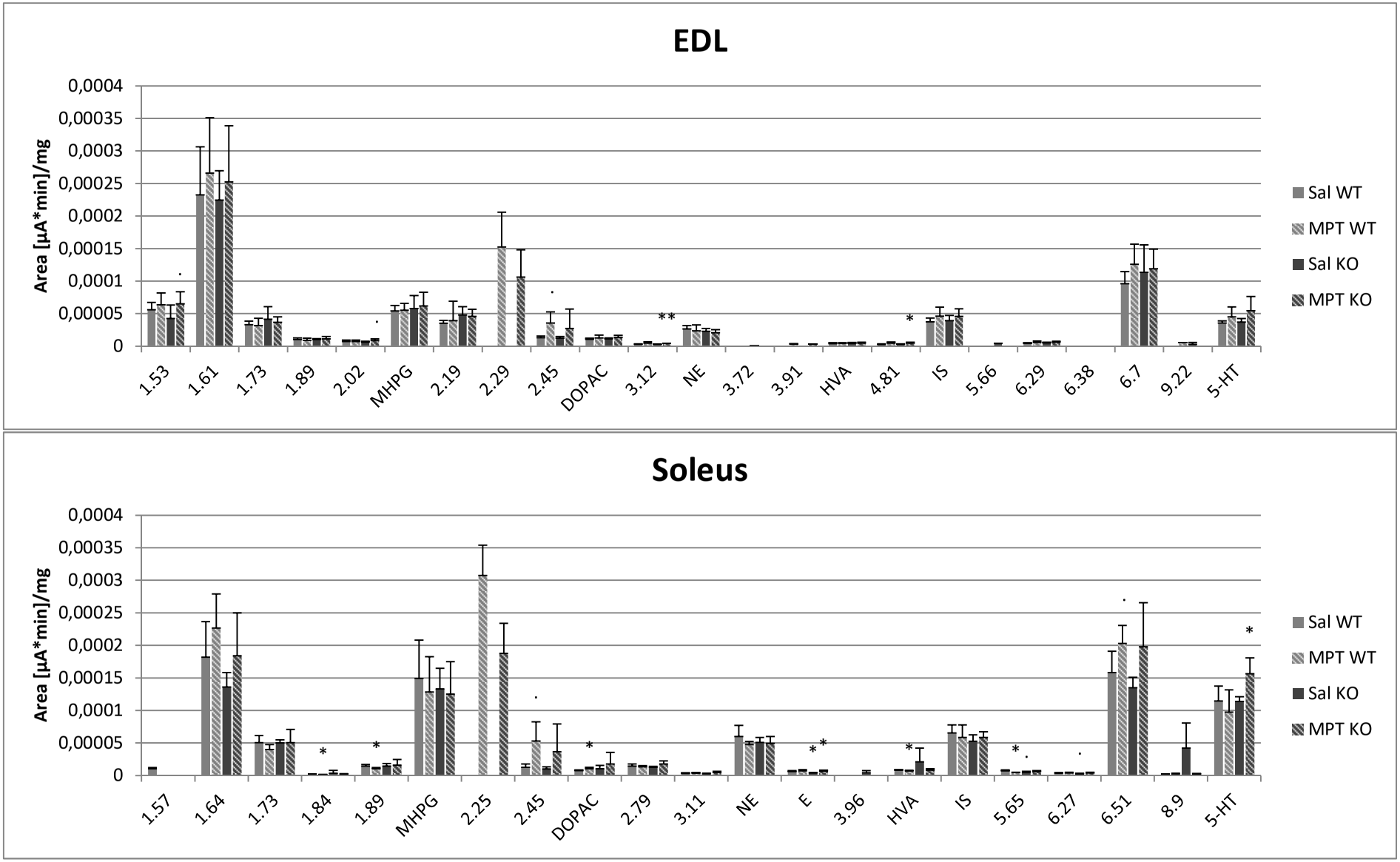
EDL
Area [µA*min]/mg
0,0004
0,00035
0,0003
0,00025
0,0002
0,00015
0,0001
0,00005
0
1.53
1.61
1.73
1.89
2.02
MHPG
2.19
2.29
2.45
DOPAC
3.12
NE
3.72
3.91
HVA
4.81
IS
5.66
6.29
6.38
6.7
9.22
5-HT
Sal WT
MPT WT
Sal KO
MPT KO
Soleus
Area [µA*min]/mg
0,0004
0,00035
0,0003
0,00025
0,0002
0,00015
0,0001
0,00005
0
1.57
1.64
1.73
1.84
1.89
MHPG
2.25
2.45
DOPAC
2.79
3.11
NE
E
3.96
HVA
IS
5.65
6.27
6.51
8.9
5-HT
Sal WT
MPT WT
Sal KO
MPT KO

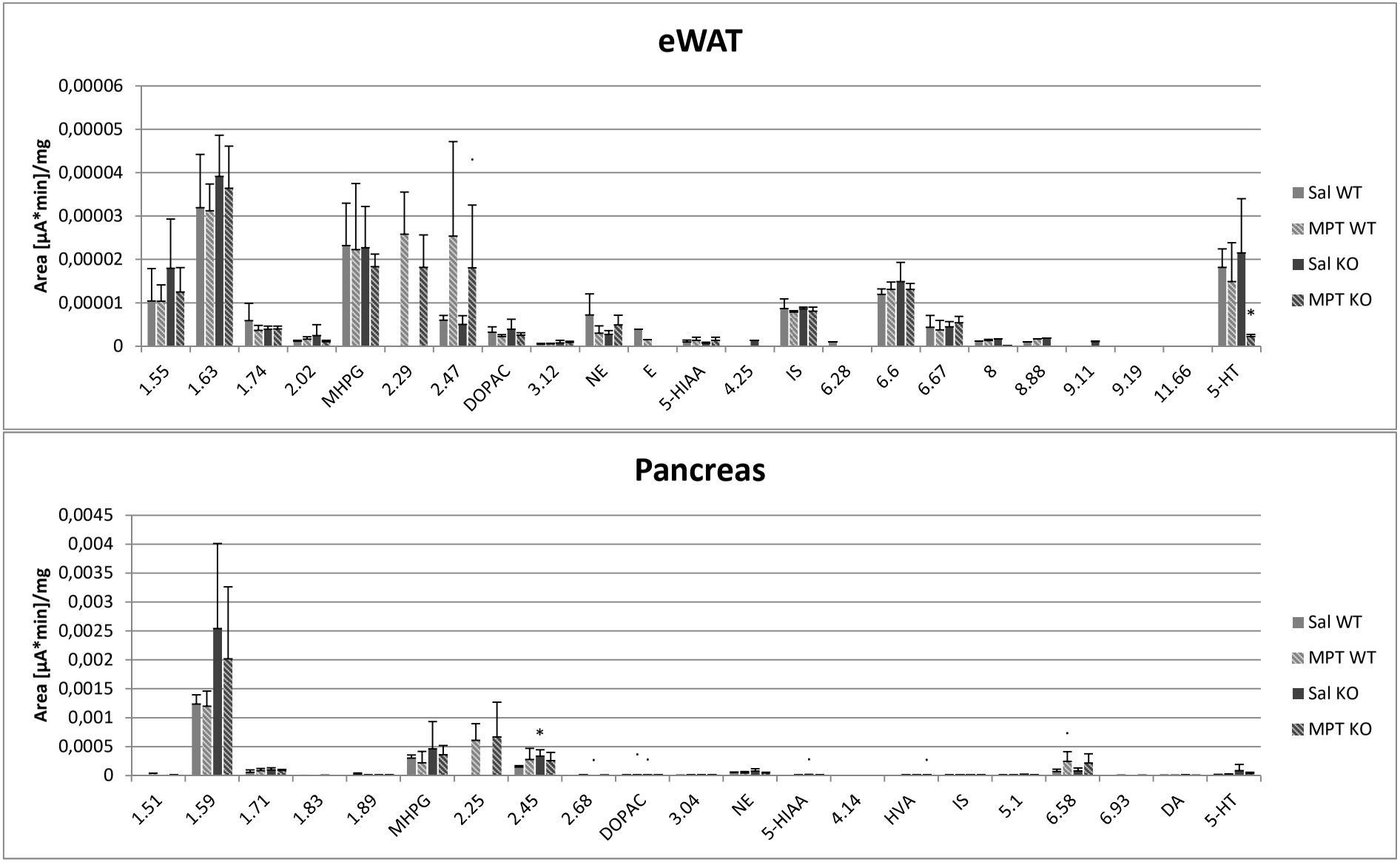

Figure 36: Response [µA*min] of analytes and unknowns per mg tissue material in WT and KO mice, treated with saline or α-MPT; n = 6; unknown numbers indicate retention time, analyzed on system II.

Another compound that could be clearly connected between new and old method is the unknown at 6.65 min, as it is the highest later eluting unknown peak and runs alone without interfering compounds. L-tryptophan, the direct precursor of 5-HT, showed the same retention time and heightened only this peak without shouldering during spiking experiments of remaining gastrocnemius sample. Additionally, in system III with the two coulometric channels, an L-tryptophan standard showed a much higher response in channel 2 at higher voltage. This effect also occurred in a tested soleus sample for the corresponding unknown peak. Therefore, this peak could be identified with relative certainty as L-tryptophan.

Several candidates from the KEGG pathway remain for the differential unknown peak at 2.25 min. Dopaquinone should not be detectable with ECD at a positive potential as it has no groups that can be oxidized. The direct product 4-hydroxyphenylpyruvate has a logP of 0.9 that indicates a later elution time. This is also the case for 4-coumarate (log P 1.5) and phenol (logP 1.46). Another direct product is 3-amino-3-(4-hydroxyphenyl)-propanoate, that has a possible fitting logP of -0.23. Should the opportunity arise again in a future cooperation with an α-MPT treatment experiment, this compound should be tested as a likely candidate. However, it is also possible that the pathway is affected further downstream, which would make identification of the unknown quite difficult. Further, in a future campaign, the opportunity should be taken to confirm the identity of L-tyrosine, 5-hydroxy-L-tryptophan, and kynurenine.

5.3. MS identification

These considerations about the identification of unknowns relied solely on comparison of the retention times and could be prone to errors, when other compounds are eluted at the same time. Therefore, for a definite confirmation of the unknown peaks, MS experiments were attempted. As the catecholamines are generally not volatile enough, a chemical tag is added to increase the sensitivity at the detector. Here, we used a nucleophilic reaction under basic conditions with benzoyl chloride, which reacts with the hydroxy groups and makes the compound more hydrophobic (Figure 37). [75] This increases retention of polar compounds on RP HPLC columns and also decreases ion suppression, which increases sensitivity on MS instruments. All the available hydroxy groups of the compounds react with the benzoyl chloride tag.

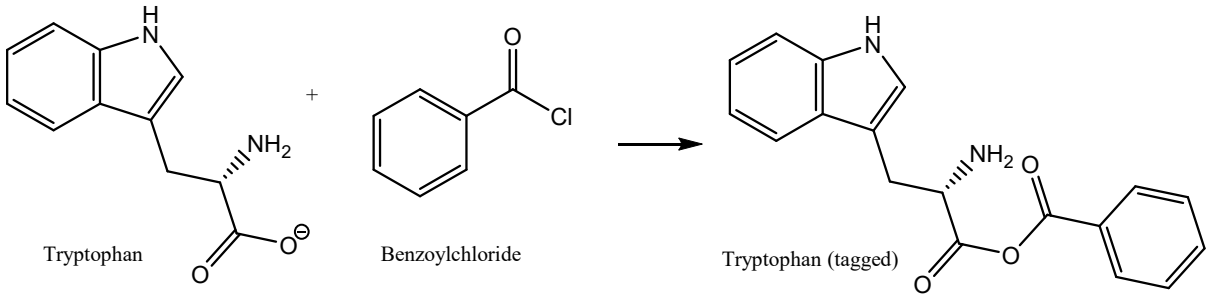

Figure 37: Tagging reaction of tryptophan with benzoylchloride.

At first, the tagging reaction was done with standard solutions under the relative conditions used by Wong et *al*. [75] 10 µL of 100 mM Na_2CO_3 and 10 µL Benzoylchloride (2 % (v/v) in ACN) were added after another to separate standards of NE, DA, 5-HT and TRP (20 µL, [1 ng μL^{-1}] in 0.3 M $HClO_4$). The mixture was vortexed briefly and then subjected to MS analysis. In order to confirm the reaction was complete, a DA aliquot was analyzed with ECD before and after the tagging. No more electrochemical signal was detectable, as all the hydroxy groups normally oxidized were occupied by the benzoyl tag. The m/z ratios of the single ion tagged compounds in positive ionization mode were calculated with the MassLynx software. Table 9 gives the resulting retention times as well as the total ion count (TIC) for the initial test conditions with a capillary voltage of 4 kV, a cone voltage of 30 V, a collision energy of 4 eV, and a scan time of 1.5 s.

Table 9: $[M-H]^+$, retention time, and TIC of tagged MA compounds.

Compound	tagged	$[M-H]^+$	Retention time [min]	TIC (initial)	TIC (optimized)
TRP	mono	309.1239	10.7	128	687
5-HT	bi	385.1474	17.0	1.1×10^3	4.22×10^3
NE	tri	482.1604	17.4	718	3.01×10^3
DA	tri	466.1654	18.2	947	-

The sensitivity of the instrument to TRP is much lower compared to the other MA analytes and no real peak could be detected in the chromatogram. A test in negative ion mode resulted in an even lower ion count. Therefore, positive ionization mode was chosen. Additionally, a higher amount of 30 µL of standard solution (1 ng μL^{-1}) was used for the next optimization trials. Raising the collision energy to 10 eV, cone voltage to 35 V, scan time to 2.5 s and lowering capillary voltage to 2.5 kV, raised the TIC for tagged tryptophan to a TIC of 687. Higher collision energy resulted in fragmentation and a low intensity at the detector. Two of the other standards were tested again to

check the improvements for other MAs, which were also intensified. As the extraction from the HPLC would be in RECIPE mobile phase, a standard was produced in this solvent and subjected to the tagging reaction to confirm that it was still functional. As the mobile phase contains buffers, a higher amount of Na_2CO_3 was needed to achieve a basic pH necessary for the reaction. 50 µL of 1 M Na_2CO_3 and 10 µL of benzoyl chloride (2 % in ACN) were added to 30 µL TRP in RECIPE (1 ng μL^{-1}). The resulting intensity in the MS instrument was reduced to a TIC of 198.

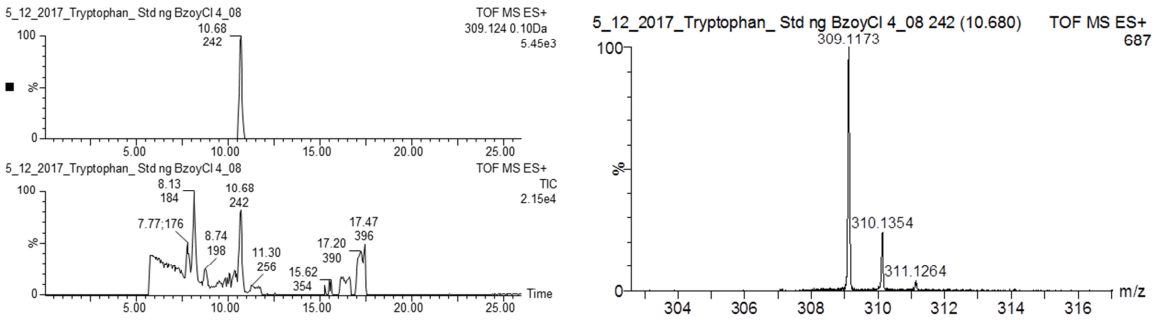

Figure 38: MS Chromatogram of tagged TRP; 30 µL standard (1ng μL^{-1}) + 10 µL of 100 mM Na_2CO_3 + 10 µL Benzoylchloride (2 % (v/v) in ACN); capillary voltage 2.5 kV, cone voltage 35 V, collision energy 10 eV, scan time 2.5 s.

As the sensitivity of TRP in the MS was not sufficient, a negative result in an extraction sample of the unknown compound would not necessarily be a disproval of its identity. Therefore, it was first checked whether the extraction procedure would result in a positive confirmation of one of the known peaks with a higher sensitivity in the MS detector. 5-HT was chosen as it was present in higher concentration than other compounds in brain samples and also elutes separately from other peaks so no interferences occur. It was extracted from a STR sample by HPLC and 100 µL of the extract subjected to 160 µL of 1 M Na_2CO_3 and 20 µL of benzoylchloride (1 % in ACN). The MS chromatogram showed no peak of the tagged compound. Another 5-HT cut from STR was evaporated in a rotary centrifuge for 2 h, before adding 50 µL 1 M Na_2CO_3 and 10 µL benzoylchloride (2 % in ACN) to 30 µL of the concentrate. ECD measurements confirmed present of 5-HT in the original extracted, a concentration of the compound after evaporation, but also degradation indicated by the appearance of a separate peak. Injection of the tagged analyte to the MS did not show the compound.

Concentration of the extract under nitrogen was also likely to result in the degradation of analyte. Freeze drying was tested, however the precipitated buffer salts prevented a reconstitution in a low amount of solvent. Therefore, an identification of unknown peaks from the HPLC/ECD instrument was not possible with the tested procedure as no sufficient concentration for our MS could be reached. Further experiments could try to develop a method for the use of a mobile phase without

addition of buffers and then freeze drying after the extraction to allow reconstitution in a small amount of solvent. Another alternative would be the employment of a modern triple QQQ MS instrument capable of achieving a much higher sensitivity.

5.4. Norlaudanosoline and morphine analysis

5.4.1. Implications of MO/NL and review of previous analyses

The MA neurotransmitters analyzed so far fall into the category of hydrophilic compounds. Due to their small molecule structure and multiple hydroxy groups, they are highly polar and very soluble in water. However, also hydrophobic molecules such as steroids function as neurotransmitters and hormones and might present interesting targets in the development of analytical methods for biomarkers. As the ECD is not suitable for an untargeted approach and identification of unknowns after ECD assay was not likely with the available instrumentation, a target molecule had to be chosen as model for the analysis of lipophilic compounds.

The focus was put to the development of a method for the analysis of norlaudanosoline, which has a logP between 1.34 (calculated with ALOGPS) and 1.84 (calculated with ChemAxon). This compound is a metabolite of the tyrosine pathway as a product of DA and L-DOPAL and also an intermediate of the endogenous morphine production in mammals. [141, 142] As one of the hallmarks of Parkinson's disease is a reduction of dopaminergic neurons and therefore dopamine [143], a link to the morphinergic pathway via NL might be possible, making it an interesting analytical target.

One of the major treatments for the symptoms of Parkinson's disease is administration of L-DOPA. [144] As a precursor it is used to increase DA levels and improve symptoms. In urine of patients treated with L-DOPA, increased levels of codeine and NL, precursors to MO, as well as MO itself in some cases, were found. [45] This suggests that some of the supplied L-DOPA is converted to MO via the NL pathway. Further, an increase of endogenous morphine like compounds immunoreactivity was found in human PD patients, showing a dysregulation of MO independent from L-DOPA treatment. [145] However, this increase runs contrary to other findings were dopamine is necessary for the formation of MO and loss of dopamine would mean loss of MO as well. [146]

Whether this change in MO levels is responsible for motor symptoms or one of the compensation mechanisms of the body for the loss of DA is still unclear. On one hand, it has been shown that acute treatment with MO alleviates tremor symptoms in PD monkeys. [147] As L-DOPA improves bradykinesia but not tremors, different pathways seem to be at play. Further, low doses of exogenous MO seem to have a neuroprotective effect by reducing reactive oxygen species and lowering endoplasmic reticulum stress. [148] However, chronic use of MO seems to cause cell

apoptosis and cerebral dysfunction. [149] As supra physiological doses were given, this might indicate dose dependent effects of endogenous and exogenous MO. Additionally, experiments indicate that MO can affect the expression of PARK2 and PINK1, two important genes, implicated in the onset of PD. [150] Also here the question of a pathological or compensatory effect remains.

Another symptom of Parkinson's disease is pain, classified into several categories. [151] As exogenous MO is commonly used as an analgesic to treat pain symptoms [152], endogenous MO might also be involved in nociception. The fact that treatment with L-DOPA, which normalizes MO levels, also alleviates pain symptoms [153], further indicates that a change of MO in PD patients might contribute to pain symptoms.

Furthermore, NL also appears to have a direct effect on brain and behavior. After ethanol administration, its levels were increased in the midbrain and striatum of rats. [154] On the other hand, alcohol consumption also increased after NL administration in rats. [41, 155] This compound and possibly the MO pathway might be involved in addiction disorders. There is also evidence that NL might inhibit dopamine synthesis via tyrosine hydroxylase [156], might inhibit dopamine uptake [157], and generally have a neurotoxic effect. [158] However, these studies were all done with supra physiological levels of NL. Whether or not endogenous levels have the same effect remains unclear.

Much of the role of MO and NL, especially in context of Parkinson's disease and its treatment is still unresolved. It is therefore necessary to have fast and comprehensive analytical methods to get a clearer sense of the involvement of these compounds.

In literature, MO has been detected in human plasma [159, 160], serum [161], and brain tissue [162]. Electrochemical detection was used in all cases, except for one of the plasma analysis, where UV detection was employed. For the extraction out of serum, multiple liquid liquid extraction steps were performed, with the first being multiple equivalents of 10 % isobutanol in chloroform out of serum and borate buffer. One of the plasma analyses used LLE as well, with multiples of 10 % isopropanol in chloroform out of borate buffer dilution and hydrochloric acid, respectively. The other plasma analysis used C-18 SPE cartridges for the extraction of MO. For the analysis of the compound in brain, a radioimmunoassay coupled to electrochemical detection was used. The homogenization was performed in hydrochloric acid, which was then extracted with multiples 10 % isopropanol in chloroform, which were subjected to a C18 SPE. In all but the brain study, pharmacological levels after administration were analyzed. Endogenous MO was also found in primate brain tissue. [163] Here, GC-MS was used as the mode of detection, however the samples had to be derivatized to raise the volatility and make the analyte accessible by the detector. For the extraction, SPE with C-8 and a cation exchanger was used. In rats, MO was found in the adrenal

gland [164], in the whole brain [165] as well as the amygdala [166]. All of the tissues were first homogenized in hydrochloric acid, extracted with 10% isopropanol in chloroform, and subjected to C-18 SPE cartridges before analysis with electrochemical detection. GC-MS with derivatization was also used in these studies for the identification of MO.

In mice, MO could be detected in urine samples after administration of NL by using High Resolution-LC-MS after purification with C-18 SPE. [141] Furthermore, it could be detected in the whole brain [167, 168], the cerebrum, cerebellum, and the hippocampus [169] after drug administration. One whole brain study employed extraction with butanol out of hydrochloric acid after homogenization, which was then re-extracted into hydrochloric acid after addition of heptane and could therefore be classified as an early variant of the later popularized dispersive liquid liquid microextraction. The other used extraction with a chloroform/isopropanol mixture and subjected the extractant to microchip electrophoresis with electrochemical detection. For the analysis of the smaller brain region, UPLC-MS analysis was performed after purification with hydrophilic-lipophilic balanced SPE. Furthermore, ELISA was used to detect morphine in cerebrum, cerebellum, and brainstem, but HPLC-MS experiments were only conducted for the complete brain. [170] Samples were extracted with methanol and then purified before analysis with a separate HPLC system. Endogenous MO and MO like compounds could also be identified with immunoreactivity in single small brain regions of rats. [145] The same study also used HPLC-MS to analyze endogenous morphine in the whole brain of WT and α-MPT treated mice after purification in hydrophilic-lipophilic balanced well plates, but was not able to detect it in the striatum.

NL has never been analyzed in mice brain tissue. It has previously been detected in whole rat brains after L-DOPA treatment or ethanol consumption. [154, 171] There, electrochemical detection was used after purification and concentration on a C-18 SPE cartridge, an ion exchange column, another C-18 cartridge, and an alumina SPE cartridge. The same procedure was used to detect NL in human urine after L-DOPA medication. [172] Further, GC-MS was used to detect NL in rat brain after L-DOPA treatment after homogenization with perchloric acid and concentration with alumina SPE. [173] Additionally, endogenous NL was found in human grey matter of the frontal cortex. [174] There, also electrochemical detection was used. After homogenization with semicarbazide and perchloric acid, purification was performed on a combined primary-secondary amine and phenyl boric acid cartridge. Another approach was the direct injection of the supernatant after rat brain tissue homogenization and centrifugation, coupled to electrochemical detection. [175] There, however, no NL was found after chronic ethanol consumption in contrast to other studies, so the procedure might not be sufficient enough. The same study also analyzed urine after purification with alumina SPE. Here, NL could be detected with ECD after treatment with L-DOPA.

Despite the clear connection between NL and MO in the same metabolic pathway, few applications analyzed both compounds together. In human urine, both MO and NL could be found. [45] However, two liters of urine had to be extracted with 5 volumes of 10% butanol in chloroform and submitted to a C-18 SPE cartridge after evaporation and resuspension. The extract was then derivatized before injection into a GC-MS system. For the analysis of both NL and MO, human cells were homogenized with perchloric acid, extracted with 10 % isopropanol in chloroform and subjected to C-18 SPE. [142] After elution in two different fractions from the cartridge and derivatization they were analyzed with GC-MS. NL could only be found in one specific cell type, while MO was more abundant.

This review shows that ECD is a popular and reliable method for the analysis of both MO and NL. MS was also increasingly used as the mode of detection. However, the MS system available for this work had previously shown low sensitivity in the analysis of CAs in groundwater amphipods. [176] As the concentration of MO and NL was expected to be similarly low and system III was equipped with a modern coulometric detector cell capable of achieving high sensitivity, it was decided to employ the ECD for method development.

The matrices varied from liquids such as urine and plasma to solids such as cells and brain tissue. However, only MO was previously analyzed endogenously in whole murine brain tissue with means other than immunoreactivity. While this is an easy and generally accepted method, there might be issues with cross reactivity that might make other methods necessary for a reliable quantitative analysis. However, ECD and MS were only used in whole mice brain. NL was never analyzed in mice brain tissue. As mice are the most abundant laboratory animal [2] and both compounds are implicated in Parkinson's disease, this seems to be an analytical gap. Therefore, the goal was to achieve the analysis of MO and NL in single murine brain regions to help researchers get a clearer picture of the DA-NL-MO axis at a higher resolution than previously available. MO with its lower lipophilicity (logP 0.99 calculated with ALOGPS and 0.90 calculated with ChemAxon) was included into the method development, even though the focus at first was on lipophilic compounds.

5.4.2. Dispersive liquid liquid microextraction method development

First, the mobile phase was adjusted with an organic content of 30 % MeOH to achieve a sufficient separation and elution on HPLC system III, resulting in suitable retention times of MO at 3.3 min and NL at 4.9 min. Nalorphine was chosen as the IS for MO, while higenamine was the IS for NL. They eluted between the two analytes without overlapping.

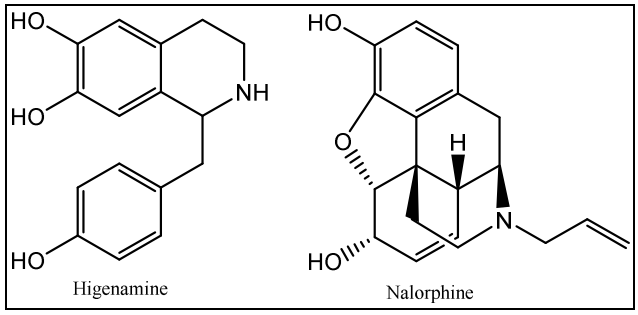

Figure 39: Structure of HG and NP, used as internal standards for NL and MO, respectively.

In literature, for the extraction of NL, mostly alumina SPE cartridges were used for the purification and concentration of the compound. In the case of C-18 cartridges, it eluted in a different fraction than MO. For the latter analyte, mostly a mixture of LLE and C-18 SPE were used for the extraction. RECIPE cartridges for concentration of CAs, based on alumina, were tested for NL. In our case, they were not suitable to trap the compound with a recovery of 14 %, even though the molecule has two catechol structures. C-18 columns were not tested, as two elution fractions would be necessary for both compounds [142], which would make the already laborious SPE method even more time consuming. As a high throughput is of great importance in modern analytical methods, this is a major disadvantage. Further, green chemistry is another aspect that is gaining more attention. SPE methods generally consume lots of solvents during the washing steps and also waste in form of the high cost disposable columns. Therefore, the intention was to find another method that allows a fast extraction of both MO and NL at the same time and improves on the green chemistry aspect.

Therefore, the attention was turned to the relatively novel method of dispersive liquid liquid microextraction. Developed in 2006 [99], it has become increasingly popular, with hundreds of new publications per year. Briefly, the aqueous sample containing the analytes is injected with a mixture of an extractant and a disperser. The extractant is not miscible with the sample phase, while the disperser is miscible with both. The result is a fine dispersion of small droplets of extractant in the aqueous phase, causing a very fast equilibrium state and extraction of the analytes into the extractant. Depending on its density, the extractant can either be found at the bottom or the top of the aqueous phase after centrifugation and can either be taken by syringe or other means. [102]

A few DLLME methods exist for the analysis of MO. All of them focus on the human abuse of drugs and analyze it in plasma [177, 178], urine [179, 180], and blood [181], while none was found for the analysis in solid tissues. Mostly, chloroform was used as the extractant, except in one plasma analysis, where undecanol was applied. As disperser, the typical candidates acetone, acetonitrile,

and methanol were used among the studies. Some of the publications used NaCl as a salting out agent to assist in the extraction, while one chose $ZnSO_4$. At lower pH, MO is not neutral, but ionic due to protonation at the amine group and therefore favors the aqueous phase, preventing extraction. Thus, all methods raised the pH of the aqueous phase before the adding the extractant. No DLLME method has been developed for the extraction of NL.

As one of the most important aspects in the development of a DLLME method is choosing the right extraction agent, various organic solvents were tested for their ability to capture both NL and MO. In a simple preliminary trial, 200 µL of H_2O were spiked separately with MO and NL. Then, 100 µL of organic solvent was added and the mixture vortexed for 1 min. Afterwards, the aqueous phase was subjected to HPLC analysis, to approximately judge the potential of the organic solvent to extract the compounds. As Table 10 shows, none of the typical extraction solvents used in DLLME work for the target compounds.

Table 10: Results of partition experiments between spiked water and organic solvent, given as percentage of compound remaining in the aqueous phase.

Solvent	DCM	$CHCl_3$	TCE	Butanol	Hexanol	Undecanol	TBP
MO	× (100 %)	× (100 %)	× (100 %)	✓ (77 %)	× (100 %)	× (100 %)	× (100 %)
NL	× (91 %)	× (91 %)	✓ (42 %)	✓ (64 %)	× (98 %)	× (84 %)	✓ (0 %)

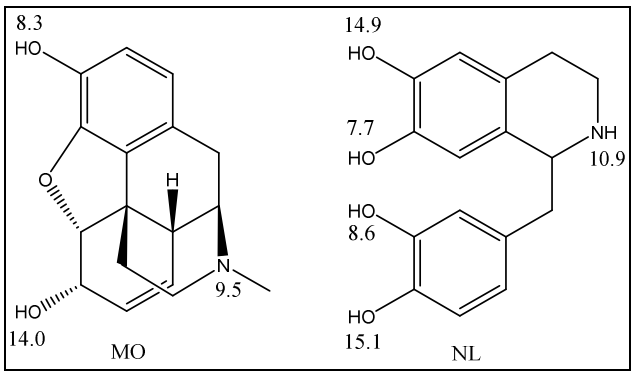

Figure 40: pKa of MO and NL as calculated with ChemDraw 3D.

MO could not be extracted, as no pH adjustment was made. Even though the analyte was spiked as the free base, the neutral pH of water is enough to protonate the amine groups, which has a pKa value of 9.5 (Figure 40), and ionize the molecule. NL was added in perchloric acid and is therefore also fully protonated. However, raising the pH here lowers extraction efficiency into organic solvents as the molecule becomes deprotonated and therefore ionized. Additionally, it also lowers sensitivity at the ECD, as deprotonated hydroxy groups cannot be oxidized by the applied current.

The common extractants DCM and $CHCl_3$ could not recover NL. Even though it has a higher logP than MO, the hydroxy groups favor the hydrogen bonding in the aqueous phase. TCE achieved a higher

extraction at 40 % analyte remaining due to its increased polarity with more halogen atoms. Out of the alkanols, only butanol achieved somewhat of an extraction. With the higher order chains, the polarity is decreased and the hydroxy groups of NL again prevent extraction. However, TBP achieved a full recovery of NL. This organic solvent is commonly used in a LLE method for the recovery of uranium out spent nuclear fuel rods, with which it builds metal complexes. [182] Furthermore, it has been previously used in DLLME methods for the extraction of phenols and nicotinic acid. [103, 183, 184] Two of those studies used MeOH as disperser, while one application favored acetonitrile. None of the methods made any further adjustments with pH, but one used NaCl as a salting out agent.

The proposed mechanism of extraction is the formation of molecular complexes based on hydrogen bonding (Figure 41). The phosphate group can act as a hydrogen bond acceptor, while the hydroxy groups of NL can act as hydrogen bond donors. While some experiments and calculations might suggest that TBP-phenol complexes from stronger hydrogen bonds than phenol-water complexes [185, 186], the comparability of these among each other and with NL might not be high. Still, the complete extraction of NL with TBP suggests that the TBP-NL complex is stronger than the H_2O-NL complex. Further, the aliphatic chains might also stabilize the remaining NL molecule in the organic phase, compared to the polar aqueous phase.

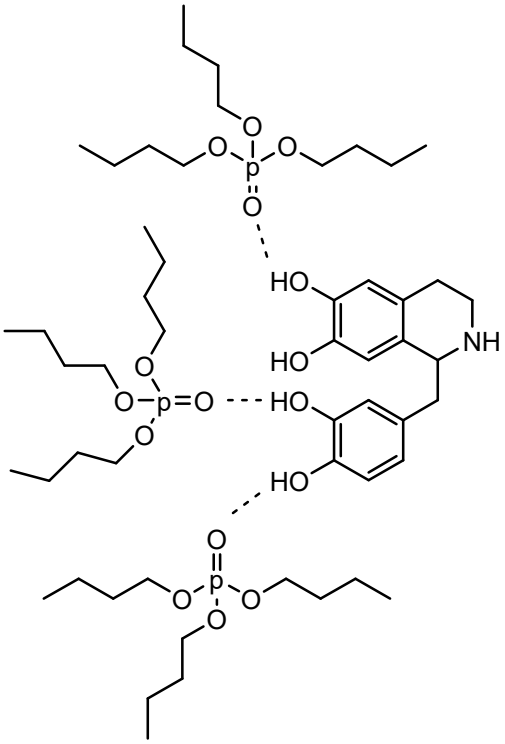

Figure 41: Schematic extraction mechanism of NL with TBP based on hydrogen bond molecular complexes.

The aliphatic chains of TBP are also responsible for the immiscibility with water. However, in comparison with other DLLME extractants, TBP has a lower density than water and is therefore found at the top of the two immiscible phases after centrifugation. In this case, special means are usually employed to take the organic phase. One of the DLLME studies using TBP employed an automatic syringe device, where the aqueous phase can be discarded automatically. Another used a handmade centrifugation tube with a narrow neck, which allows easier taking of the extractant. The last study preferred conventional polypropylene pipettes turned upside down. The reservoir functions as the container, while the shaft contained the organic phase after centrifugation. Here, this method was tested, however, during the experiments, even with various sized pipettes, the volume of the reservoir was either to small and caused spilling during centrifugation or too large and the extractant could not be brought into the narrow shaft. At last, as previously shown [187], the water phase was treated as a high density extractant in conventional DLLME and taken with a syringe until only the TBP phase remained, which could then be further used.

To check whether adjusting the pH could aid in the extraction of MO with TBP another experiment was performed. MO was spiked in 100 µL H_2O, the pH was adjusted with a fixed volume of base but varying molarity of NaOH, and mixed with 100 µL TBP. After centrifugation, the aqueous phase was analyzed for residues of MO (Table 11). The ability of TBP to extract MO out of the aqueous phase is dependent on the pH level. At pH above 9.5, the amine group is deprotonated and the molecule becomes neutral, reducing the strong ionic interaction with water and making extraction with TBP possible. However, raising the pH further, the aromatic hydroxy group is deprotonated, generating another ion and removing one hydrogen bond donor, thus lowering extraction efficiency again.

Table 11: Percentage of MO left in the aqueous phase after mixing with TBP at various pH levels.

pH	10.4	10.7	10.9	11
MO	18 %	14 %	74 %	86 %

Possibly more of the previously tested solvents would be able to extract MO after adjustment of pH. However, as TBP showed the best ability to extract NL and also has the potential to extract both compounds, it was chosen as the extractant going forward with the DLLME procedure. One big disadvantage of this solvent is, however, that it cannot be evaporated due to its low vapor pressure. Direct injection of TBP extract into the HPLC system showed the NL peak, but at a reduced intensity. Most likely, the TBP caused dispersion upon injection and reduced the access of the detector to the analytes. This meant that moving forward with the method development, first, a modification to enable the full extraction of MO had to be found and, second, an additional step for the re-

extraction of the analytes into a suitable solvent had to be introduced. Still, TBP looked very promising, as it might also enable extraction of analytes across a wider range of lipophilicity and might be especially suitable for all analytes containing hydroxy groups necessary for detection with ECD.

The proper disperser for the extraction of NL and MO was tested separately. In first trials for the extraction of NL, TBP was varied from 0 to 200 µL, while MeOH was constant at 500 µL. The sample volume was 4 mL H_2O with 40 ng NL added. 130 µL TBP was found as the optimum. Afterwards, THF, ACN, and acetone were tested as disperser at a volume of 500 µL. With MeOH as disperser, double the amount could be extracted than with acetone. With ACN, 80% of the amount with acetone was extracted, while with THF no NL could be extracted. To test dispersers for MO, 10 ng were added to 100 µL of H_2O at pH 10.7, while 50 µL TBP were used. Adding 150 µL of disperser, ACN showed the best ability to aid extraction of MO. Acetone was 20 % worse than ACN. However, as MeOH was only 10 % worse than ACN, but seemed to function much better for NL, it was chosen as the disperser for the DLLME procedure.

Oftentimes, salts are used in DLLME to aid in the extraction of analytes, based on the so called salting out effect. Here, the solubility of a non-electrolyte molecule in the aqueous phase is decreased as the salt concentration increases. The Hofmeister series, which ranks salts on their ability to precipitate proteins, has been found to correlate with this partitioning effect for anions, while the cations might behave differently. [188] As the latter are also more susceptible to the structure of the solutes, these variabilities cannot be quantified and have to be judged on a case by case basis. However, the anions have a much more pronounced effect than the cations, which might therefore be negligible.

$CO_3^{2-} > SO_4^{2-} > S_2O_3^{2-} > H_2PO_4^- > F^- > Cl^- > Br^- \approx NO_3^- > I^- > ClO_4^- > SCN^-$ (Anion Hofmeister series)

$(CH_3)_4N^+ > Cs^+ > Rb^+ > NH_4^+ > K^+ > Na^+ > Li^+ > Mg^{2+} > Ca^{2+}$ (Cation Hofmeister series)

Ions on the left side are called kosmotropes (order making), and cause a salting out effect. The ions on the right side are chaotropes (chaos making) and have the opposite effect, meaning they can salt in molecules. While the exact mechanism remains unclear, the high charge density kosmotropes are thought to cause electronic repulsion of solutes and also enhance the hydrophobic effect [188], where theses ions are solvated by water molecules, thereby reducing the solvation shell of the solutes, which then aggregate and partition into the organic phase.

The kosmotropic anions sulfate, dihydrogen phosphate, and chloride were tested for their ability to salt out MO and NL. 10 ng NL (1 ng μL^{-1} in 0.3 M $HClO_4$) was spiked to 100 µL H_2O. 20 µL TBP was added, shaken until dispersion, and the aqueous phase analyzed after centrifugation. In separate

trials 30 mg NaCl, $MgSO_4$, and NaH_2PO_4 were added and compared. The same experiment was repeated with MO.

Table 12: Effect of salting out agents on the extraction of MO and NL; given as percentage of analyte remaining in the aqueous phase.

Salt	None	$MgSO_4$	NaH_2PO_4	NaCl
MO	100 %	52 %	60 %	54 %
NL	7 %	4 %	4.4 %	4.3 %

Clearly, the addition of salt has a higher effect for MO than NL. As no prior pH adjustment was made, MO was present in ionic form and therefore influenced more by the electronic repulsion and enhanced hydrophobic interaction. The Hofmeister series does not hold true for the sodium salts, however the sulfate ion seems to have the largest effect. $MgSO_4$ however, might possibly result in formation of magnesium perchlorate, when combined with perchloric acid that was planned for use in the first homogenization step of the solid tissue samples. This results in a flame promoting, strong oxidizing agent, and might form explosive mixtures. Even though the chance of it happening during the extraction procedure and disposal of the remains was judged to be low, the use of this salt was rejected. As there was almost no difference to $MgSO_4$, NaCl this was the salt chosen for the method development.

5.4.3. DLLME method optimization

5.4.3.1. Extraction

Taking the results together, multiple factors have to be optimized in the method. The volumes of the extractant TBP and the disperser MeOH, as well as pH level and amount of salt added seem to have an effect on the extraction efficiency of MO and NL. A DoE approach was taken to optimize the multiple factors affecting the extraction to reduce the number of experiments and also to find interactions between factors. Here, the factors are organized within in desired ranges and the software combines the factors together in a suitable way. Once the measurements are done, a polynomial regression analysis is performed. The resulting model statistically analyses the results and gives the optimal combination of all factors within the applied ranges, typically presented in a graphical way in 3D or contour plots.

It is apparent that a higher pH is necessary to neutralize MO and achieve full extraction. However, at those pH levels NL becomes ionized and partitioning in the organic phase is reduced. In order to prevent this, it was planned to perform a gradient DLLME procedure, where in a first step NL is extracted. Afterwards, the pH level is adjusted and MO removed from the sample with additional

added extractant. Therefore, separate DoEs were done for both analytes with different factors. For NL, extractant, disperser, and salt concentration were optimized, while for MO the pH was added.

As the solid sample had to be first homogenized and proteins precipitated just as in the MA extraction method, 0.3 M $HClO_4$ was chosen as the aqueous sample base. The amount could be chosen freely, however, small murine brain regions did not require much solvent. In order to reduce the total amount of solvents necessary, a lower amount of 100 µL was chosen. 10 µL of MO or NL (1 ng μL^{-1}) were added as standards before the DLLME procedure. The remaining water phase was analyzed for residues of the compounds and the total extraction calculated from there.

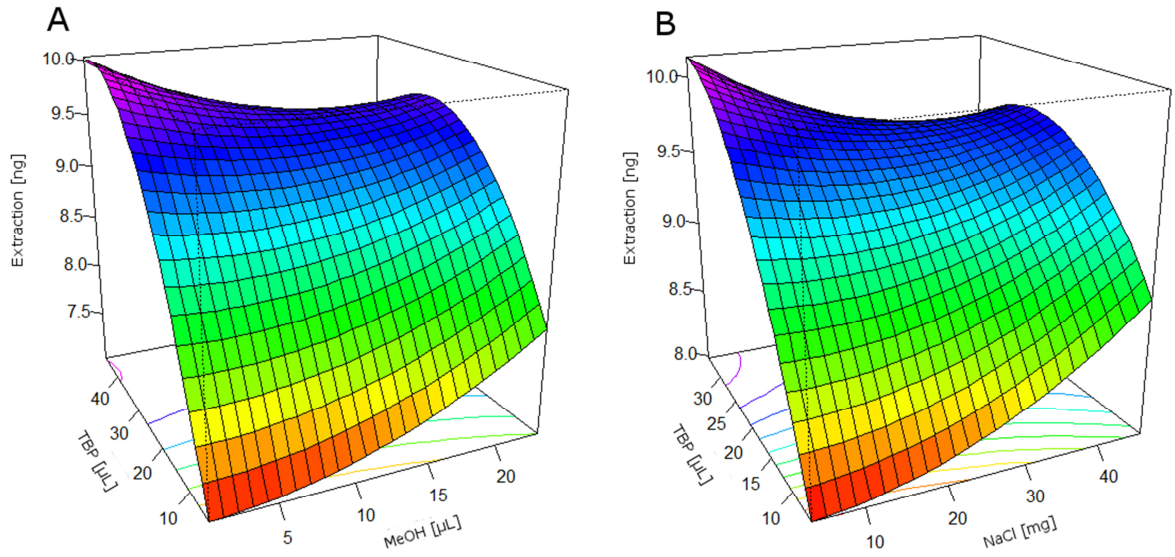

Figure 42: RSP of NL Extraction; A: Factors TBP (4 - 46 µL) and MeOH (1 - 23µL), factor TBP (p = 0.0007) and second order factor TBP (p = 0.01) significant, R^2 = 0.81; B Factors TBP (6 - 34µL) and NaCl (4 - 46 mg), factor TBP (p = 0.00009), two factor interaction (p = 0.02), second order factor TBP (p = 0.0009) significant, R^2 = 0.96.

At first, just TBP and MeOH were tested as the factors in the extraction of NL (Figure 42 A). The resulting model showed that at lower levels of TBP, MeOH had a positive effect. However, at higher levels of TBP necessary for the complete extraction, the disperser had a negative effect. Interestingly, also without added disperser TBP could achieve a stable dispersion of fine droplets in the aqueous phase, due to its phosphate group capable of building hydrogen bonds but the aliphatic chains preventing miscibility. Lower amounts of TBP were probably not enough for a sufficient dispersion, so MeOH helped achieving it. At higher amounts, MeOH possibly caused a shift in phase separation between TBP and the aqueous phase and prevented full extraction.

After discarding the use of a disperser, another experiment with NaCl as the second factor was run (Figure 42 B). The same trend occurred, as NaCl also showed a slight positive effect at lower TBP levels. Here, it enhanced the hydrophobic effect and prevented hydrogen bonds between the

analyte and water molecules. But again, at higher levels of extractant, it seemed to reduce the extraction efficiency slightly, possibly preventing hydrogen bonds between the extractant and the aqueous phase, thereby reducing the dispersion and phase partitioning. It was confirmed in experiments without the addition of salt and disperser that 20 µL TBP extracted 90 % of NL, 30 µL extracted 93 %, while with 35 and 40 µL the amount was raised to 97 %.

In a separate DoE (Figure 43 A), the extraction of MO out of water was tested. At first, the three factors TBP, MeOH, and pH were tested together. Even though no statistical significance of the factors was discovered, the model showed that higher TBP levels achieve a better extraction. Displaying the other two factors in a response surface plot at a slice with the highest TBP levels, indicated that either a pH of 8 and no MeOH or a pH of 12 and higher levels of MeOH caused a better extraction of MO. At pH 8 most of the aromatic hydroxy groups as well as the amino group are still protonated, giving the molecule a positive charge. At pH 12, the amino group and the hydroxy group are deprotonated, making it negatively charged. Apparently, the positively charged compound is affected more by MeOH. Possibly, the negative charge prevents hydrogen bonding in the water phase and raises the hydrophobic effect, even though the charge should reduce extraction into non-polar TBP. The protonated form however, is capable of building full hydrogen bonding, and is therefore susceptible to MeOH effects, just like the fully protonated NL. As MeOH lowered the extraction of NL, it was decided that going forward no disperser should be used, as MO recovery seemed possible without it.

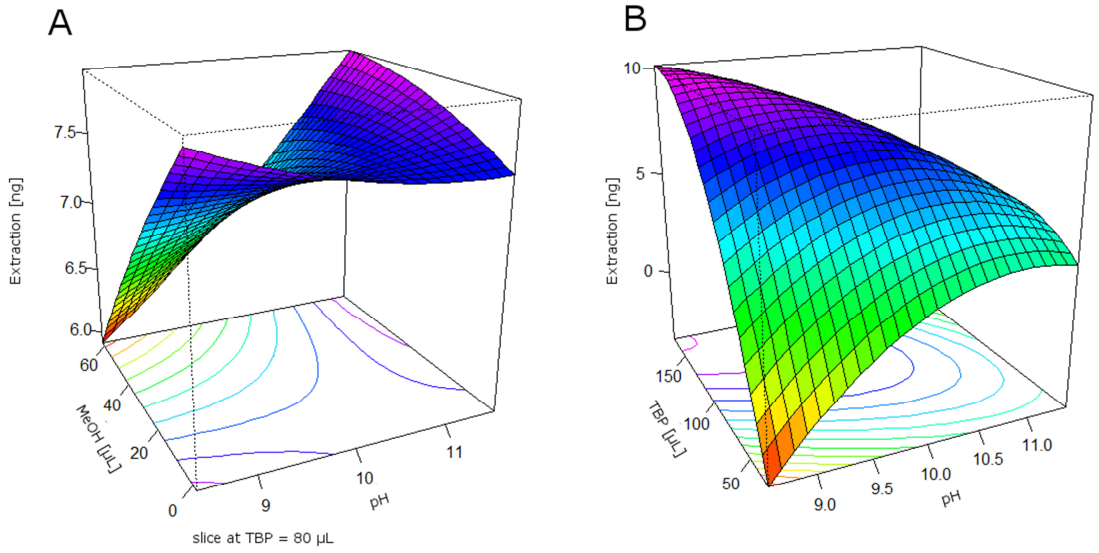

Figure 43: RSP of MO extraction; A: Factors TBP (8 - 72 µL), MeOH (0 - 61 µL), and pH (8 – 12), single factors not statistical significant, total model significant (P=0.04), R^2 = 0.78; B: DoE with TBP and pH, no statistical significance, R^2 = 0.64.

An experiment (Figure 43 B) with only two factors TBP and pH, were no disperser was added, showed that at pH 8 a full extraction of MO could be achieved with 150 % TBP of the original sample volume. At higher pH, the efficiency dropped off to zero. Interestingly, at lower levels of TBP, a better extraction was achieved at pH 11, though nowhere near complete. This goes contrary to the previous experiment, where a higher extraction was achieved at pH 11. However, for this model no statistical significance was found. Further, the coefficient of determination was low at around 60 % and the model therefore deemed not reliable.

Another DoE was performed (Figure 44) with NaCl introduced as an additional factor as well as an increased pH range, to get a complete picture of the correlations. The first two graphs compare the pH and salt at high (A) and low (B) levels of TBP. At high levels of extractant full recovery was achieved at low pH, while at low levels of extractant a higher pH was necessary. Addition of salt was necessary at 150 µL TBP to achieve full extraction, while at lower levels there was a reduced effect. Graph C and D show the statistical effect between TBP and pH more clearly, at low and high levels of salt, respectively. At low pH, MO is fully protonated and carries a positive charge at the amine group. The model shows that an extraction into TBP is possible despite this charge. However, high levels are necessary, possibly as more phosphate groups are necessary to stabilize the charge in the organic phase. At a pH of 8 – 9, the amino group becomes slowly deprotonated while at the same time the hydroxy group at the aromatic ring becomes deprotonated and negatively charged. Higher levels of TBP now have a negative effect, conceivably due to repelling with the phosphate group. At lower amounts, however, there appears to be a stronger repulsion from the aqueous phase, causing distribution into the organic phase. Further, the salting out agent seems to cause a stronger repulsion of the positively charged MO species, making less TBP necessary for a full extraction at lower pH levels. It also enables full extraction at lower volumes of TBP at pH 8 and above, while also reducing the negative effect of high TBP at the same pH.

In comparison with the NL extraction models, adopting a higher pH value would either lower the extraction of NL or make the two steps necessary, where first a lower amount of TBP would be used to extract NL. Then the pH would have to be adjusted and in a second step MO would be extracted. Confirming the model at lower TBP with high pH and higher TBP with low pH and varying salt content, it was found that with 150 µL TBP and addition of 35 mg NaCl, an extraction of 95 % was achieved. However, with 150 µL TBP, 40 mg NaCl, and pH 10, a complete extraction was achieved. The latter was therefore chosen as the conditions for the gradient extraction of MO.

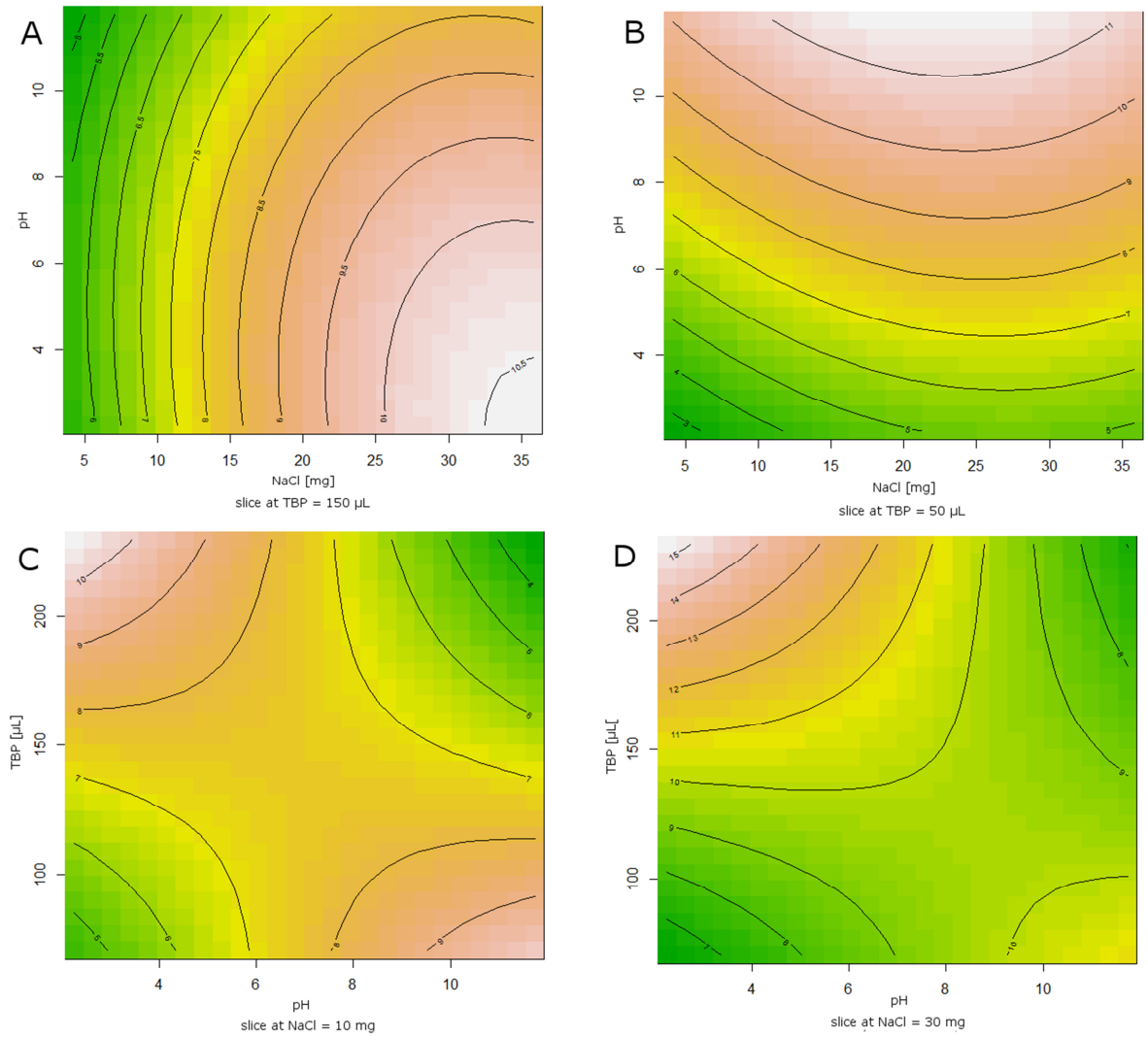

Figure 44: RSP MO Extraction; factors TBP (70 – 230 µL), pH (2 - 12), and NaCl (4 – 36 mg); factors pH (p = 0.048) and NaCl (p = 0.0002), two factor interaction TBP/pH (p = 0.003), and second order interaction NaCl (p = 0.006) statistical significant, R^2 = 0.93.

5.4.3.2. Re-extraction

At first, the re-extraction of both analytes was tested separately as well. Due to the high affinity of NL to the TBP phase, re-extraction seemed to be difficult. However, it was theorized that addition of a large alkyl alcohol to the organic phase could displace the analyte and cause distribution in the aqueous phase. Test trials were performed with 100 µL water/ 50 µL TBP. As already shown in Table 10, NL was found completely in the organic phase. Addition of 100 µL octanol caused a re-extraction into water at 70 %. No difference was observed between hexanol, octanol, and undecanol. Therefore, a DoE was done with the factors H_2O and octanol (Figure 45 A). The optimal amount of TBP (40 µL) for the extraction of NL, with 10 ng of analyte added, was used as the starting point for the experiments. Even though the addition of octanol was not statistically significant, it had a clear effect. However, according to the response surface model, at lower levels of H_2O it had a negative

effect and while with a higher volume a full re-extraction was possible, no pre-concentration could be achieved, as the end volume of aqueous phase was close to the starting volume.

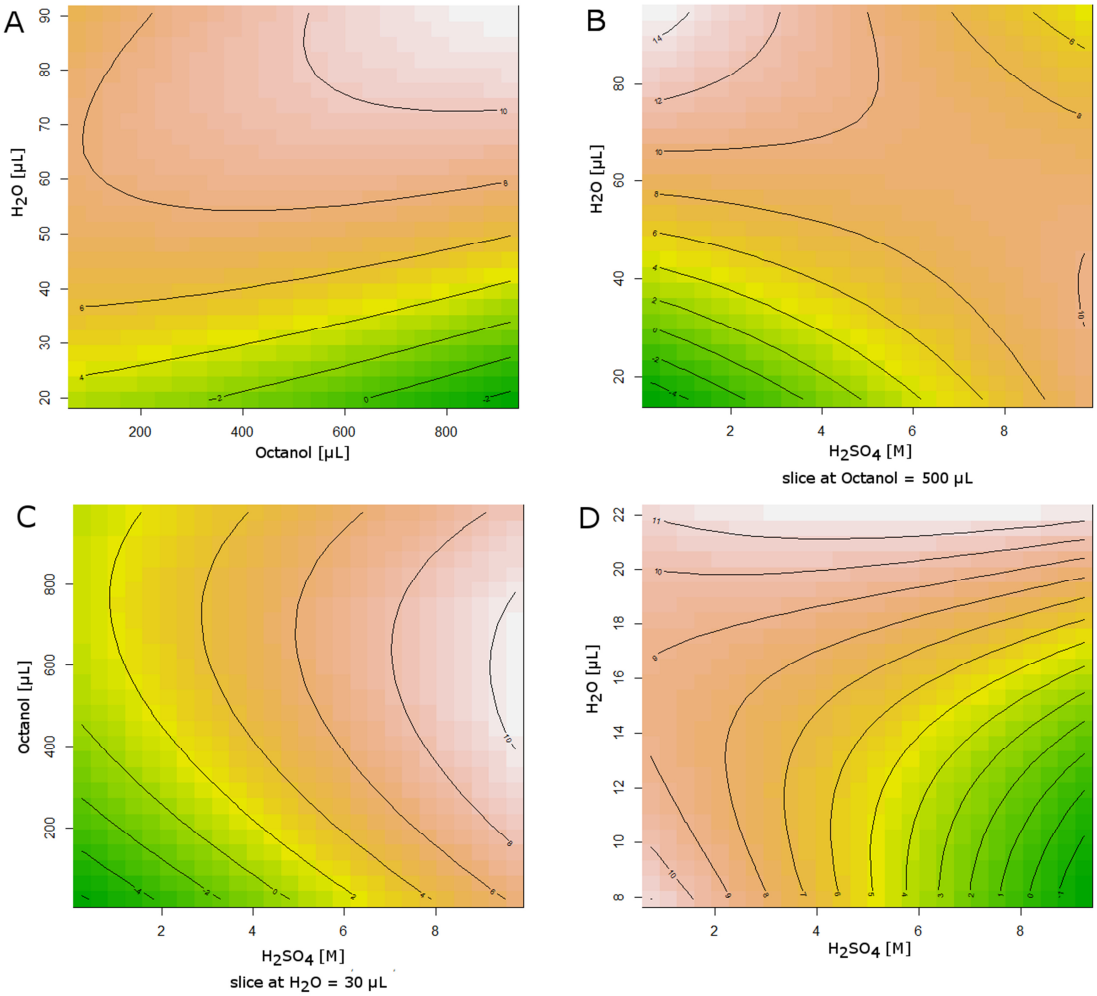

Figure 45: RSP of re-extraction of NL and MO out of TBP; A: Sample 40 µL TBP + 10ng NL, factors H_2O (20 – 90 µL) and octanol (76 – 924 µL), factor H_2O (p = 0.0003) and second order interaction H_2O (p = 0.028) significant, R^2 = 0.89; B & C: Sample 40 µL TBP + 10ng NL, factors H_2O (15- 95 µL), octanol (26 – 974 µL), and H_2SO_4 (5 µL 0- 10 M), factors H_2O (0.0004), octanol (0.001), and second order interaction H_2O (0.004), octanol (0.002) significant; R_2 = 0.95; D: Sample 150 µL TBP +10 µL MO, factors H_2O (8 – 22 µL) and H_2SO_4 (5 µL 0 – 9 M), factors H_2O (p = 0.03) and H_2SO_4 (p = 0.04) significant, R^2 = 0.72.

As in the extraction DoE it was apparent that a higher amount of ionic NaCl prevented full extraction, it was tested whether this effect could also aid the re-extraction. For this, sulfuric acid was chosen, as its anion is a stronger kosmotrope and had already shown a slightly higher effect (Table 12). Addition of this factor to the DoE (Figure 45 B/C) showed that, indeed, it had a positive effect. Figure B shows with no addition of H_2SO_4, full re-extraction can be achieved with 500 µL octanol and around 70 µL of H_2O. Adding 5 µL of 9 M H_2SO_4, however, lowered the amount of necessary water to 30 µL, which was confirmed by another perspective of the model (Figure C).

Another DoE (Figure 45 D) was used to check the amount of H_2O and the effect of sulfuric acid on the re-extraction of MO. The sample was prepared as 150 µL TBP with the addition of 10 ng MO. Here, at lower amounts of H_2O, the acid had a strong negative effect. At 20 µL H_2O the effect was almost completely nullified and full re-extraction of MO was achieved. The ratio between water and TBP was considerably lower, as it has a lower affinity for TBP. This presented a further problem. When a gradient step extraction of NL and MO was employed, the two extractant phases could not be combined to be extracted in one single step, as the higher amount of TBP would prevent using 30 µL of H_2O for the re-extraction of NL. Each phase would have to be back extracted separately, which would be possible but adds another step. It also increases the total amount of aqueous final sample, so that two measurements would have to be performed, to retain the concentration factor for each re-extraction. Altogether, this prevents a high throughput of samples. While the approach works in general and could be used for the analysis of one of the compounds, it was abandoned for the analysis of both analytes.

Next, various acids and bases were tested as addition to the water extractant. Among them were also organic acids and bases that should be able to distribute into non-polar organic solvents and cause a reaction there, in case the pH adjusted water phase does not reach the analytes in the TBP phase. For MO re-extraction, NaOH, ammoniac, ethyl acetate, formic acid, phosphoric acid, and perchloric acid at varied concentrations were tested. Further, p-toluenesulfonic acid, 1,5,7-triazabicyclo[4.4.0]dec-5-en, tributylamine, NaOH solved in MeOH, and trimethylamine were added to the organic phase before water extraction. For NL, ammoniac, NaOH, tetrabutylammonium hydroxide were applied. Here, samples were acidified again after extraction to adjust for the pH dependent response of the ECD. However, none of these test trials achieved a meaningful re-extraction of the analytes into the aqueous phase, which lead to abandoning of this approach

One variant of DLLME that has been previously developed for polar compounds is reversed phase DLLME. [189, 190] Here, the analytes were extracted with water out of cyclohexane with ethyl acetate as disperser, meaning that the polarities of conventional DLLME were switched. This procedure was also used for other polar compounds and even elements with mixtures of water/acetone/toluene and nitric acid/isopropanol/biodiesel, respectively. [191, 192] The idea was to replicate this procedure for the re-extraction of MO and NL into an HPLC suitable phase.

The extracted TBP was supposed to be the disperser and an added organic solvent should function as the sample phase. Therefore, water could not be used as an extractant in this case, as TBP is only soluble in the organic phase and cannot aid in a fine dispersion. However, methanol is also non miscible with higher order non-polar alkanes, such as cyclohexane, and could be used as an extractant. TBP is miscible with both and could function as the disperser. To the best of the author's

knowledge, this variant with MeOH used as an extractant instead of a disperser, has not been done before and was pursued as the method for the re-extraction of the analytes.

Test runs confirmed that this mode of operation was functional for the purpose. 5 mL of cyclohexane were added to 250 µL of TBP, spiked with 10 ng NL and MO, while 400 µL of MeOH were added. After evaporation of most of the extractant, 84 % and 72 % were found in this phase, respectively. Nonane, and dodecane were also tested, but were not superior to cyclohexane, which was therefore further used as the non-polar solvent phase. However, it was observed that when temperatures in the laboratory were higher, no dispersion was achieved between cyclohexane, TBP, and MeOH. Cooling cyclohexane and MeOH in the fridge at 4 °C before use remedied this problem and enabled a stable dispersion. If cyclohexane was left in the fridge for longer periods, it solidified and first had to be thawed before use.

Further, it was found that once all MeOH was evaporated, a small amount of TBP (3 - 5 µL) and H_2O (20 µL) remained. Some of the water of the aqueous samples was most likely distributed into the TBP extractant and then moved together with some of the TBP into the MeOH phase. This mixture could then not be reconstituted with the mobile phase, as it caused extraction of analytes again and reduced sensitivity in the instrument. This effect also occurred when MeOH was not evaporated completely, however, a higher MeOH content resulted in higher recovery. Washing the extractant with organic solvents such as cyclohexane, hexane, or dodecane to remove excess TBP, did improve response of the extractant without evaporation, but not of the concentrated extractant. Finally, this reduction in sensitivity upon the injection of the MeOH extractant could be prevented by reducing the injection speed of the sample into the HPLC system. The slow syringe speed probably prevented the formation of a dispersion in the mobile phase and therefore enabled access of the detector to the analytes.

It was also found that when performing the whole procedure from the beginning, addition of NaCl for the extraction of MO also caused a lower recovery of this compound in the second extraction step. Therefore, another DoE was performed for the first extraction step. It was checked, whether a higher amount of TBP was able to extract both compounds at the same time. The volume did now not matter as much as before, as the extractant of the second step was now easily evaporated and the method scalable. With water as extractant, this was not possible, so the amount of TBP had to be controlled before. Thus, no pH adjustment or addition of salt was made. The model (Figure 46) showed that at 350 µL TBP an optimum for the extraction of both MO and NL was achieved. Even though the model only showed an efficiency of 80 % for MO, separate confirmation trials showed full extraction for both compounds at 300 µL. As in the previous models, addition of MeOH caused a

drop in extraction efficiency. Technically, this step can now no longer be called DLLME, as no disperser was added and multiples of sample volume was used for the extractant.

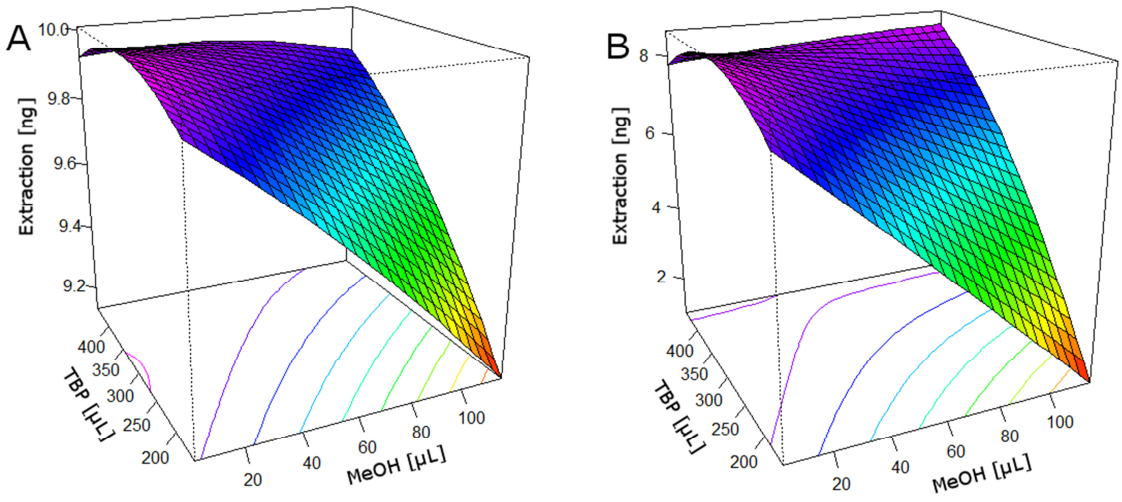

Figure 46: RSP Extraction of NL and MO, factors TBP (160 – 440 µL) and MeOH (3 – 117 µL); A: Extraction of NL, factors TBP (p = 0.00005), MeOH (p = 0.00002), two factor interaction (p = 0.003), and second order factor TBP (p = 0.002) significant, R^2 = 0.97; B: Extraction of MO, factors same as A, factors TBP (p = 0.0006), MeOH (p = 0.002), and two factor interaction (p = 0.02) significant, R^2 = 0.91.

Figure 47 shows the RSP for the second extraction step. The first extraction step was also performed for every sample, to reduce the effect of the addition of standards to the TBP phase. Beforehand, it was also checked whether the centrifugation time had an effect on the extraction. As longer centrifugation had a slight negative effect, it was kept at the minimum of 1 min at 4 °C in the centrifuge. The factors analyzed were the volume of cyclohexane as organic sample phase and MeOH as extractant. For NL (A), a clear optimum could be identified in the model. The model for MO (B) showed potential for further improvement, but was also sufficient at the same point as NL. The two internal standards HG (C) and NP (D) matched their respective analytical counterparts and were extracted at the same rate. Measurements with 5 mL cyclohexane and 60 µL MeOH confirmed the extraction efficiency of around 80 % for all analytes.

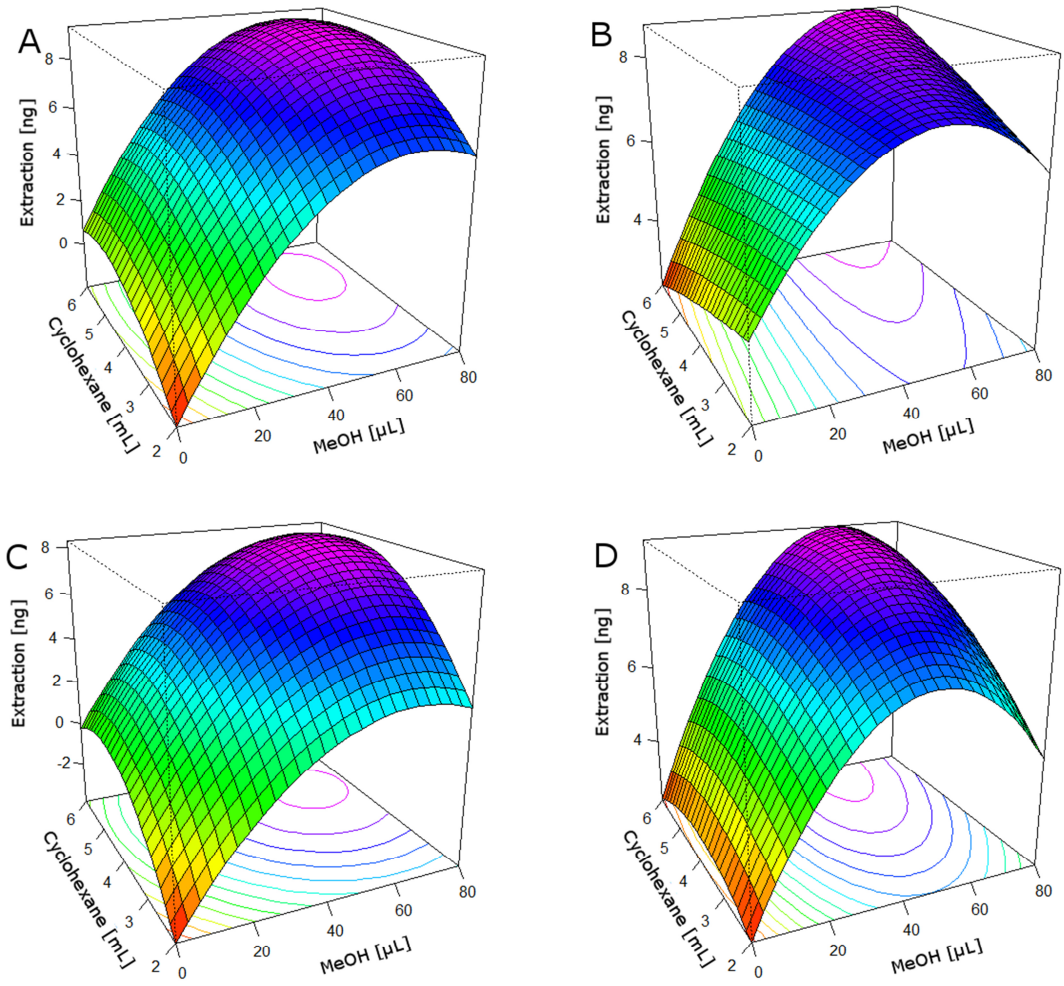

Figure 47: RSP of NL, MO, HG, NP full extraction, factors cyclohexane (2 -6 mL) and MeOH (0 – 80 µL); A: NL extraction, factors cyclohexane (p = 0.01), MeOH (p = 0.0002), and second order factor MeOH (p = 0.02) significant, R^2 = 0.98; B: MO extraction, factor MeOH (p = 0.001) and second order factor MeOH (p = 0.03) significant, R^2 = 0.97; C: HG extraction, factors cyclohexane (p = 0.0002), MeOH (p = 0.00002), second order factor cyclohexane (p = 0.006), and second order factor MeOH (0.003) significant, R^2 = 1.00; D: NP extraction, factor MeOH (p = 0.01) significant, R^2 = 0.90.

The small TBP residue in the extractant caused problems on the column as well. After multiple injections, peak splitting and retention time shifts occurred. Most likely, TBP was retained on the C-18 column and was responsible for a differential elution of the analytes. This problem could be fixed by adding ACN to the mobile phase. Increasing the elution strength of the mobile phase prevented retention of TBP on the column and removed the issue of peak splitting and peak shifting. Using only ACN at the same concentration as MeOH resulted in a faster run time, yet, the analytes peaks overlapped with other endogenous compounds. A mobile phase composition of RECIPE with 15 % MeOH and 5 % ACN also prevented peak splitting and resulted in suitable analyte retention with separate peaks at the cost of longer run time of 30 min. Over time, retention times could still shifted towards longer retention times, however, intraday they remained stable.

A flow path for the final optimized full extraction of MO and NL out of brain tissues with the exact volumes used at the single steps is presented in Figure 48.

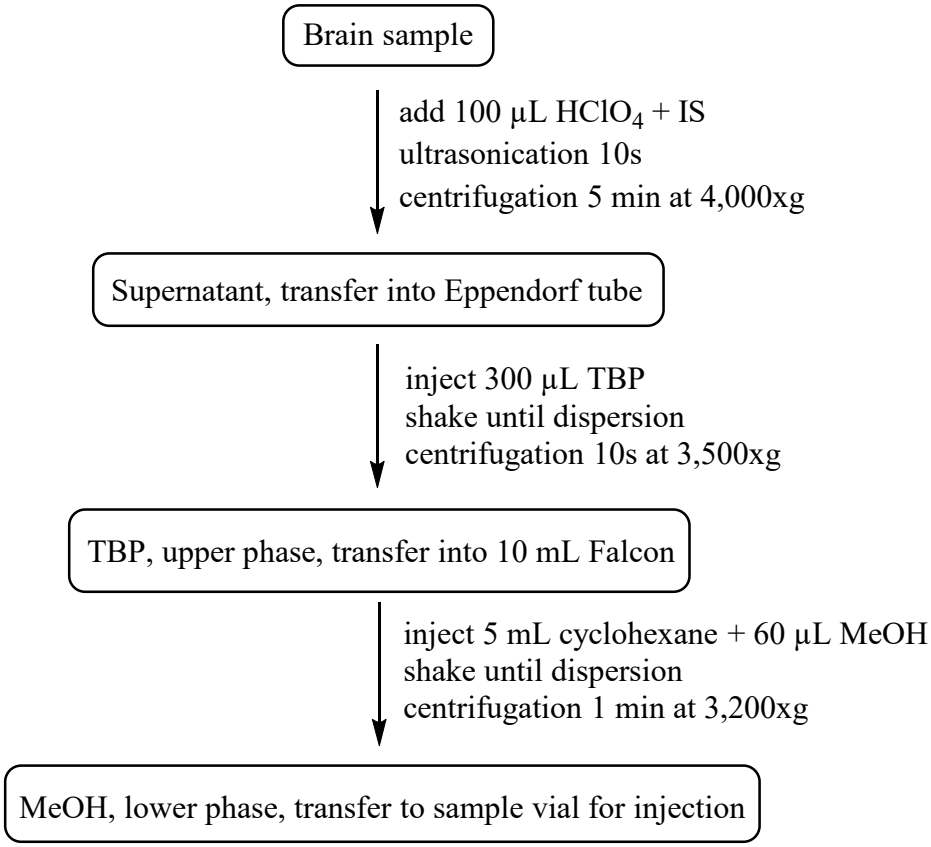

Figure 48: Flow path of the extraction of MO and NL out of brain tissue.

5.4.4. Validation: precision, accuracy, and recovery

The precision, accuracy, and recovery of MO and NL were determined by spiking thalamus samples of mice. Due to a shortage of WT mice available, different genotypes were used. As these samples were pooled each day, the possibility of a differential effect any genotype might have on the recovery of MO and NL should be greatly reduced. However, the validation (Table 13) showed that the method is well within acceptable parameters and it is highly unlikely that an effect on the analytes exists in WT mice, which does not exist in a mix of genotypes.

Table 13: Combined calculated intraday and inter-day mean, relative standard deviation, accuracy, and recovery of IS in spiked thalamus samples. Measurements were done in triplicates on three days.

Analyte	Spiked amount [ng]	Mean calculated amount [ng]	Combined RSD [%]	Combined Accuracy [%]	Combined Recovery IS [%]
MO	0.5	0.5 ± 0.05	3.6 ± 1.6	99.6 ± 10.4	81.9 ± 3.8
	1	1 ± 0.05	3.4 ± 2.1	100.4 ± 4.5	81.1 ± 1.9
	5	4.83 ± 0.28	3.1 ± 0.7	96.6 ± 5.6	80.4 ± 7.9
NL	0.5	0.54 ± 0.01	3.4 ± 1.1	108 ± 2.5	82.1 ± 1.8
	1	1.08 ± 0.03	2.2 ± 0.3	107.9 ± 4.5	77.6 ± 6.8
	5	5.19 ± 0.17	2.3 ± 1.1	103.9 ± 5.6	77.8 ± 5.1

The homogenate of the pooled thalamus samples could not be aliquoted equally as liquid and solid parts could not be separated homogenously. Therefore, spiking before the homogenization, as is usually done, was not possible as the results would be contorted due to the aliquotation. Also, spiking of single thalami was not possible due to the shortage of sample material. Thus, the spiking was done in the aliquots of the supernatant after centrifugation instead. Any effect of the solid particles of the pellet could not be tested with this validation. However, it was shown that no matrix effects of the supernatant exist. It was also tested that the ultrasonication during the homogenization did not reduce the concentration of analytes due to thermic effects.

The precision of the method was very good with deviations below 5 %. This reproducibility enables a reliable comparison between samples. The accuracy is presented as the percentage of the calculated amount of analyte to the expected amount and was close to a 100 %. Both parameters are below the 15 % deviation specified by the requirements of the US Food and Drug Administration for bioanalytical method validation. Here, recovery is presented as the percentage of detected internal standard to the amount spiked in the beginning of extraction. It represents loss of IS through the procedure and is used to correct for the loss of analytes as well. It also is above the 50 % recovery required by the FDA. Each day, a blank extraction without spiked analytes and IS was performed to confirm that no endogenous compounds are present under the analyte peaks.

Table 14: Percentage of analyte to according IS over 5 standard extractions.

Analyte/IS	1	2	3	4	5	Mean
MO/NP	98.1	100.7	98.4	100.6	103.4	100.2 ± 1.9
NL/HG	103.7	101.7	96.8	100.1	101.8	100.8 ± 2.3

Table 14 shows 5 extraction out of standard solution, where the percentage of analyte to its according IS calculated. The deviation of the pairs is between 96 and 104 %. Therefore, the analytes and their IS behave the same during the extraction procedure. The high calculated accuracy during the thalamus spiking experiments also confirms that in real sample matrix no differential effects between analytes and respective IS are present.

5.4.5. Method application

After the validation, the method was applied to the single brain regions thalamus, hypothalamus, hippocampus, striatum, olfactory bulb, and prefrontal cortex of C57Bl/6J mice (male, age 4-8 months).

For each brain region, one sample was analyzed without the addition of IS to ensure no endogenous compounds are causing underlying peaks and disturbing the calculations. Table 15 shows the results of the measurements with added IS. The recoveries of the IS are generally lower than during the validation. This is due to fact that here the IS was spiked into the sample before the homogenization. The centrifugation traps some of the analytes in the pellet. However, washing the pellet with either further perchloric acid or MeOH did not result in increased recovery of analytes. Therefore, some of the analytes must be bound irreversibly to precipitated proteins during ultrasonication and centrifugation. To still ensure the correct calculation of the analytes according to their IS, a separate thalamus sample was spiked with both analytes and IS before homogenization. There, they still showed the same behavior during the whole procedure and therefore have the same recovery.

In the analyzed brain region samples, both NL and MO were found in all of the thalamus samples. One of the hippocampus samples showed a MO peak, however, it was the one without addition of IS. Therefore, the mean recovery in the other hippocampus samples was taken for an estimation of the concentration. Further, also in one prefrontal cortex NL was found. In two of the striatum samples, MO was detected. The amounts of analytes were in the lower pg mg^{-1} range, close to the limit of detection, but still distinguishable from the baseline. The other regions hypothalamus and olfactory bulb showed no analyte peaks. Previously, MO was found with ELISA in mice at 0.4 pg mg^{-1} in the cortex, 0.6 pg mg^{-1} in the olfactory bulb, and 2.1 pg mg^{-1} in the hippocampus. [193] Our results match the amount found in the single hippocampus, however, in the smaller area of the prefrontal cortex and the olfactory bulb, our instrument might not be sensitive enough.

One of the thalamus samples was spiked with a standard solution of MO and NL (10 µL remaining sample + 20 µL 0.02 ng μL^{-1} MO/NL in 0.3 M $HClO_4$) (see Figure 49 B). Due to the limited amount of remaining sample, it was diluted through the spike. Nonetheless, all peaks from the original sample are still present and the analyte peaks show a higher area without any peak shoulders in the front or the back. While it is no definite proof, it is a strong indication towards the identity of the peaks emerging from the analytes. Due to insufficient remaining sample material after one injection, the other brain regions could not be spiked, however, the retention times of supposed analyte peaks match the standard injection at the beginning of the day.

Figure 49 shows chromatograms of the analyzed brain samples. MO and NL are close to the LOD, but still clearly distinguishable from the baseline. In the hippocampus sample where MO was found, in later parts of the chromatogram a strong baseline shift occurred that prevents analysis of NL. This change in current might due to impurities or a change at the electrode surface.

The unknown peaks present in the samples might represent MAs. They were not identified by spiking, however, chromatogram H shows the MA retention times in standard solution in relation to MO, NL, and their IS. It was further shown that the developed DLLME procedure was able to extract MAs out of standard solution, also pointing towards the unknown peaks present in brain region chromatograms as MAs. Most of the compounds showed a similar enrichment to MO and NL. However, MHPG, DOPAC, 5-HIAA, HVA, and 3-MT showed a lower pre-concentration, most likely due to a higher number of polar hydroxy groups in these compounds, preventing extraction in TBP (see Appendix 7.10). This offers the possibility of validating MAs in the application of DLLME to further increase the resolution of the morphinergic pathway. It further shows that the developed method is suitable for the extraction of both hydro- and lipophilic compounds.

Table 15: MO and NL in single brain regions; n=3; injection volume =20 µL; mean [pg/mg]; recovery IS [%], n.d. = non detectable.

	Thalamus		Hypothalamus		Hippocampus		Striatum		Olfactory Bulbus		Prefrontal Cortex	
	Mean	Recovery	Mean]	Recovery	Mean	Recovery	Mean	Recovery	Mean	Recovery	Mean	Recovery
MO	18.8 ± 3.9	69 ± 5	n.d.	75 ± 2	3.9	53 ± 7	25.6 ± 4.9	61 ± 2	n.d.	77 ± 4	n.d.	66 ± 10
NL	7.2 ± 2.3	61 ± 6	n.d.	63 ± 2	n.d.	47 ± 9	n.d.	56 ± 1	n.d.	56 ± 5	17.4	58 ± 6

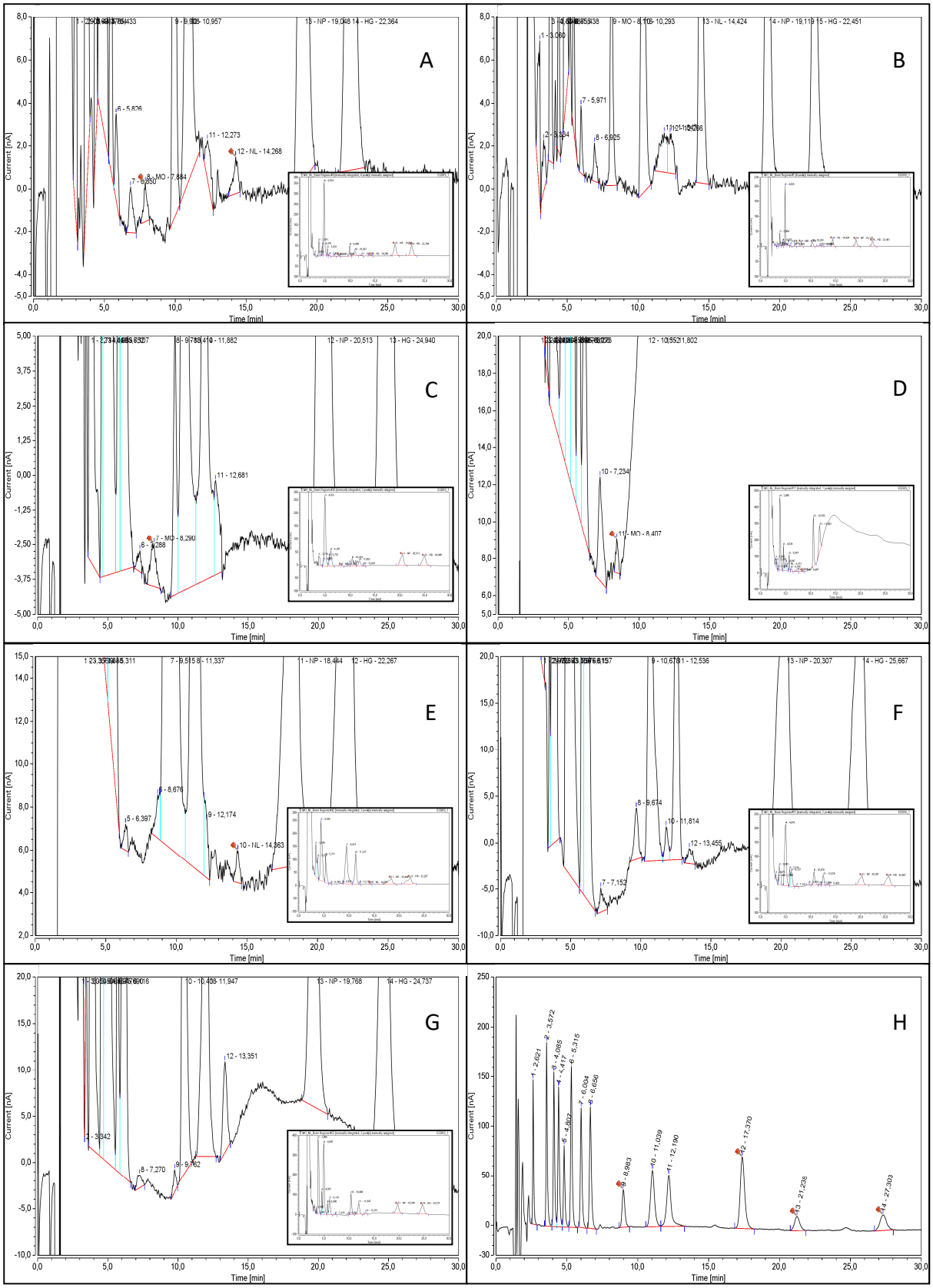

Figure 49: Chromatograms of brain region samples after DLLME; A: Thalamus; B: Thalamus spiked with MO and NL; C: Striatum; D: Hippocampus; E: Prefrontal Cortex; F: Olfactory bulb; G: Hypothalamus; H: Chromatogram of standard solution (1 ng per injection), 1 MPHG, 2 DOPAC, 3 NE; 4 E, 5 5-HIAA, 6 DHBA, 7 HVA, 8 DA, 9 MO, 10 3-MT, 11 5-HT, 12 NL, 13 NP, 14 HG.

Comparing the results in the brain regions with existing literature shows contrasting conclusions. It has been previously shown that DA is a necessary precursor for the formation of endogenous MO. [146] However, it has also been shown that cells other than dopaminergic neurons can form this compound. [142] Moreover, immunoreactivity of mice brains revealed that MO is not present in dopaminergic neurons, but in GABAergic and glutamatergic neurons, as well as astrocytes. [194] As these do not contain tyrosine hydroxylase necessary for the formation of DA, it is likely that these cells either take up MO from the extracellular space or form MO from uptaken precursors themselves. However, this method could not discriminate between MO, MO glucuronides, and codeine.

Our results partially support this. On one side, in the regions with high dopaminergic projections, the hypothalamus, prefrontal cortex, and olfactory bulb [195], no MO could be found. But, the NL found in one of the prefrontal cortex samples could also indicate that the pathway is in place and was just generally below the LOD. Further, in the thalamus, which contains almost no dopaminergic innervation, both MO and NL were found. However, in some of both the hippocampus and the striatum which are innervated by dopaminergic neurons, MO was found. This generally supports the hypothesis that MO precursors or finished product are transported to non-dopaminergic cell for further use.

Inconsistent with previous immunoreactivity experiments, are the results in the thalamus. In our analysis, this was the only region that consistently displayed both NL and MO, however, no immunoreactivity was shown in this region so far. [36] One possible explanation could be that MO is bound to proteins and cannot be detected with immunoreactivity, but is hydrolyzed and freed up during our acidic homogenization procedure. This might possibly indicate a specific function of MO within the thalamus. However, it could also be the case that other compounds than MO and NL are detected within the same retention time in this region, which could not be discerned by the ECD detector. Yet, our MS instrument did not have the necessary sensitivity for the detection of unknown peaks at lower concentrations, which made a conformation of these peaks impossible in our laboratory. Further, our sample size was comparatively low and the results might not reflect the norm, but rather present outliers of some sort. Altogether, these results should not be taken as a refutation or conformation of any previous results, but rather point towards the fact that the MO pathway in the brain is not yet fully understood and many functions remain a possibility, making further research necessary.

The developed method worked for the detection of MO and NL, and was used in murine brain regions within the conformation limits of the ECD. As it offers a fast extraction of both compounds, it can be used by other laboratories for the conformation of the findings with state-of-the-art sensitive

MS/MS instruments. The further possibility of the inclusion of MAs might make this a comprehensible tool for researchers, especially on Parkinson's disease, where higher concentrations of both analytes might be present and the ECD could be useful in routine analysis. Additionally, more compounds of the MO pathway could be included, as the method is suitable for both lipophilic and moderately hydrophilic compounds.

VI. Conclusion and Outlook

Lifestyle diseases such as obesity and diabetes are becoming more prevalent in industrialized western countries. Due to the increased suffering and societal cost, focused research is applied on the etiology, cure, and prevention. There, a central component is the involvement of the nervous system and neurotransmitters as one of its basic components. In order to achieve a full understanding of their mechanistic effects in these diseases, suitable and reliable analytical methods are necessary. As mice are often used as model organism, analytical methods have to be tailored for this application.

In the presented work, HPLC coupled to electrochemical detection was used for the development of a method for the detection of active neurotransmitter monoamines and metabolites in peripheral murine tissues. The analysis of neurotransmitter networks was extended from the brain to liver, pancreas, muscles, and brown and white adipose tissue as well as cell cultures with a simple extraction variant not reliant on high workload solid phase extraction. Further, a chromatographic method based on a solid core particle column was developed to reduce instrumental analysis time and enable high throughput applications. Altogether, nine compounds (dopamine, norepinephrine, epinephrine, and serotonin, 3,4-dihydroxyphenylglycol, 3,4-dihydroxyphenylacetic acid, 3-methoxytyramine, homovanillic acid, and 5-hydroxyindoleacetic) could be analyzed in a single run, which is the highest resolution of the monoamine neurotransmitter networks in peripheral murine tissues with ECD so far.

Further improvements to the method could be made by the inclusion of proposed compounds suitable for detection with electrochemical detection to raise the number of detected analytes and enable an even higher resolution of metabolic networks. Their presence and identity should be checked in all presented tissue regions and might solve some of the unknown peaks present in the samples. The developed workflow for the identification of unknown peaks present in electrochemical chromatograms was not successful due to sensitivity limitations of the available mass spectrometry instrumentation. In the future, analysis might be possible by using chromatographic conditions without addition of buffers in the extraction HPLC instrument to enable freeze drying of the extracted aliquots, without precipitation of buffers. This might possibly raise concentration enough to enable analysis of the extract with the available mass spectrometer and allow identification of compounds.

After development, the method was applied within research projects concerning diabetes which shows the usefulness and applicability of this bioanalytical assay. Through the application in brown adipose tissue and cell cultures of alternatively activated macrophages, it could help to show that

these cells do not produce catecholamines and do not contribute to the browning of white adipose tissue. Additionally, it could also help to determine mechanistic effect of an observed glucose intolerance in dual specifity phosphatase deficient mice through the application in analyzing sympathetic innervation.

As most electrochemical HPLC methods focus on the application on hydrophilic neurotransmitters, the extension to lipophilic compounds was investigated. Norlaudanosoline was chosen as a model compound, due to its importance in the endogenous formation of morphine, which has implications in Parkinson's disease. A sensitive method for the analysis of endogenous morphine and norlaudanosoline in single murine brain regions was developed. The employed extraction procedure featured a novel variant of dispersive liquid liquid microextraction where methanol was used as an extractant for the first time. Both compounds could be found in specific regions of wildtype mice brains. Further improvements of the method might be possible by the inclusion of further intermediates of the morphine pathway, suitable for the analysis with electrochemical detection, to raise the resolution of this pathway. Altogether, the method opens up the possible application to Parkinson's disease mouse models, where abnormalities of endogenous morphine production could be studied. Finally, the applicability of the novel dispersive liquid liquid microextraction procedure to other analytical fields such as environmental analytics could be considered.

VII. Appendix

7.1. List of figures

7.2. List of tables

7.3. List of equipment, consumables, and chemicals

Table 16: Equipment.

Article	Company	Model
Centrifuges: • Non-cooled • Cooled	 Eppendorf Thermo Scientific	 Centrifuge 5415 C Hereaus Multifgue 3 SR+
Nitrogen mortar	Belart	H-37260-0001
Rotary evaporator	Christ	RVC 2-18 CDplus
Turrrax	Janke & Kunkel	Ultraturrax T25
Ultrasonic bath	Bandelin	Sonorex RK156
Ultrasonication rod	Bandelin electronics	

Table 17: Consumables.

Article	Company	Article no.
Biopulverizer beads	Fisher Scientific	MP116750200
Centrifugal filter units, 0.5 mL, 3K	Amicon	10704645
Columns: • Atlantis T3 3µm, 3.0 x 150 mm • Atlantis T3 3µm, 4.6 x 150 mm • Accucore C18 2.6 µm, 2.1 x 100 mm • Accucore XL C18, 4 µm, 4.6 x 150 mm • ACQUITY UPLC M-Class HSS T3 1.8 µm, 300 µm x 150 mm	 • Waters • Waters • Thermo Scientific • Thermo Scientific • Waters	 • 186003723 • 186003729 • 74104-154630 • 17126-102130 • 186007472
Guard Columns: • Security Guard C18 • Security Guard Accucore XL C18	• Phenomenex • Thermo Scientific	• AJ0-4287 • 74104-014001
Glass snapring vials (use for MS)	Supelco	29132-U
Glass insert 250 µL (used for MS)	Supelco	27407
Snap Cap PTFE (used for MS)	Supelco	29306-U
Glassy carbon electrode	Thermo Scientifc	044113
Pippette tips: • 50-1000 µL • 10-200 µL • 0.5-20 µL	 • Eppendorf • Greiner bio-one • Greiner bio-one	 • 003000.919 • 739290 • 0030000.854
Polypropylene transfer pipette • 0.9 mL • 3.1 mL	 • Sigma Aldrich • Sigma Aldrich	 • Z350656-500EA • Z135011-500EA
Reference Electrode	Thermo Scientific	044198
Sample preparation kit for catecholamines in plasma:	RECIPE	• 1020

• SPE cartridge • Eluting reagent • Washing reagent		• 1022 • 1021
Snapring sample vials (used for ECD) Snap caps PTFE (used for ECD)	Supelco	29409-U 27427
Storage vials: • 15 mL • 5 mL • 2 mL • 1.5 mL	• Falcon • Sarstedt • Eppendorf • Sarstedt	• 352096 • 62.526.028 • 0030120.094 • 72.706
Syringe	Braun	9161465V
Syringe filter: • PTFE 0.2 µm, 4 mm • PTFE 0.45 µm, 13 mm • GHP 0.45 µm, 13 mm • RC 0.2 µm, 13 mm	• Whatman • Whatman • Life Sciences • Whatman	• 6784-0402 • 67841304 • 4556T • 10463040

Table 18: Chemicals.

Article	Company	Article no.
1,2-Propanediol	Sigma Aldrich	398039-25ML
1,5,7-Triazabicyclo[4.4.0]dec-5-ene	Sigma Aldrich	345571-5G
1-Butyl-3-Methylimidazolium hexafluorophosphate	Sigma Aldrich	70956-5G
1-Octanol	Merck	K27316991002
1-Pentanol	Sigma Aldrich	398268-500ML
1-Undecanol	Sigma Aldrich	U1001-100G
2,6-Dimethyl-4-Heptanone	Alfa Aesar	L16015
3,4-Dihydroxybenzylamine solution (IS)	Thermo Scientific	45-0137
3,4-Dihydroxyphenylacetic acid	Sigma Aldrich	11569-25MG
3-Methoxy-4-Hydroxyphenylglycol hemipiperazinium salt	Sigma Aldrich	H1377-50MG
3-Methoxytyramine hydrochloride	Sigma Aldrich	65390-250MG-F
5-Hydroxyindoleacetic acid	Sigma Aldrich	H8876-100MG
5-Hydroxy-L-Tryptophan	Sigma Aldrich	H9772-100MG
AccQ-Tag Ultra Derivatization Kit	Waters	176001235
Acetone	LGC Standards	SO-1142-B040
Acetonitrile	LGC Standards	SO-9640-B025
Acetylcholine chloride	Sigma Aldrich	A6625-25G
Ammonium sulfate	Merck	A166711042
Benzoy lchloride	Sigma Aldrich	259950-5ML

Benzyl chloride	Sigma Aldrich	185558-50G
Butyric acid	Sigma Aldrich	B103500-5ML
Calcium chloride	Sigma Aldrich	23922-4
Catecholamine standard solution (NE, E, DA)	Thermo Scientific	45-0206
Chlorobenzene	Sigma Aldrich	284513-100ML
Chloroform	LGC Standards	SO-1174-B025
Citric acid	Sigma Aldrich	251275-100G
Cyclohexane	LGC Standards	SO-1179-B025
D(+) Glucose	Merck	K32885137418
Dansyl chloride	Sigma Aldrich	03641-100MG
Dichloromethane	LGC Standards	SO-1185-B040
Dipotassium hydrogen phosphate	Roth	P749.2
Disodium hydrogen phosphate	Roth	T876.1
DL-Kynurenine	Sigma Aldrich	61250-250MG
DL-Normetanephrine hydrochloride	Sigma Aldrich	N7127-100MG
Estrone	Sigma Aldrich	E9750-500MG
Ethyl acetate	LGC Standards	SO-1191-B040
Hexane	LGC Standards	SO-1244-B040
Higenamine	LGC Standards	CDX-00008218-005
Homovanillic acid	Sigma Aldrich	69673-25MG
Hordenine	Sigma Aldrich	04476-100MG
Hydrochloric acid (37%)	Sigma Aldrich	30721-1L-GL
L-Glutamic acid	Sigma Aldrich	G1521-100G
L-Tryptophan	Sigma Aldrich	T0254-1G
L-Tyrosine	Merck	K32989871523
Magenesium phosphate hydrate	Sigma Aldrich	344702-500G
Magnesium sulfate heptahydrate	Roth	P027.1
Methanol	LGC Standards	SO-9658-B025
Mobile Phase	RECIPE	1210
Morphine	Sigma Aldrich	M-030-1ML
Nalorphine hydrochloride	Sigma Aldrich	N-924-1ML
n-Dodecane	Merck	S6240843114
Norlaudanosoline hydrobromide	Toronto Research Chemical	N661425
Octopamine hydrochloride	Sigma Aldrich	O025016

Perchloric acid 70 %	Sigma Aldirch	311421-250ML
Polyethylenglycol	Sigma Aldrich	84797-250G-F
Potassium phosphate tribasic	Sigma Aldrich	P5629-25
p-Toluenesulfonic acid monohydrate	Sigma Aldrich	402885-5G
Quercetin	Sigma Aldrich	Q4951-10G
Serotonin hydrochloride	Sigma Aldrich	H9523-100MG
Sodium ammonium hydrogen phosphate	Roth	T882.2
Sodium chloride	Roth	9265.1
Sodium dihydrogen phosphate dihydrate	Roth	2370.3
Sodium hydroxide	Merck	1.09136.1000
Sodium hydroxide pellets	Merck	K20266598
Sodium tetraborate	Sigma Aldrich	221732-100G
Sulfuric acid	Bernd Kraft	07060.3700
Tetrabutylammoniumhydroxide 1M in MeOH	Sigma Aldrich	230189-100ML
Tetrabutylammoniumhydroxide 1M in water	Sigma Aldrich	426326-25ML
Tetrachloroethylene	Sigma Aldirch	37696-100ML
Tetraethylmethylenediphosphate	Sigma Aldrich	359181-5ML
Tetrahydrofuran	Sigma Aldrich	401757-1L
Tributyl phosphate	Sigma Aldrich	240494-100ML
Triethylamine	Sigma Aldrich	471283-100ML
Tyramine hydrochloride	Sigma Aldrich	T2879-1G
Water (HPLC grade)	Merck	Z0483333802
β-Estradiol	Sigma Aldrich	E8875-250MG
γ-Aminobutyric acid	Sigma Aldrich	A2129-10G

7.4. Validation system I

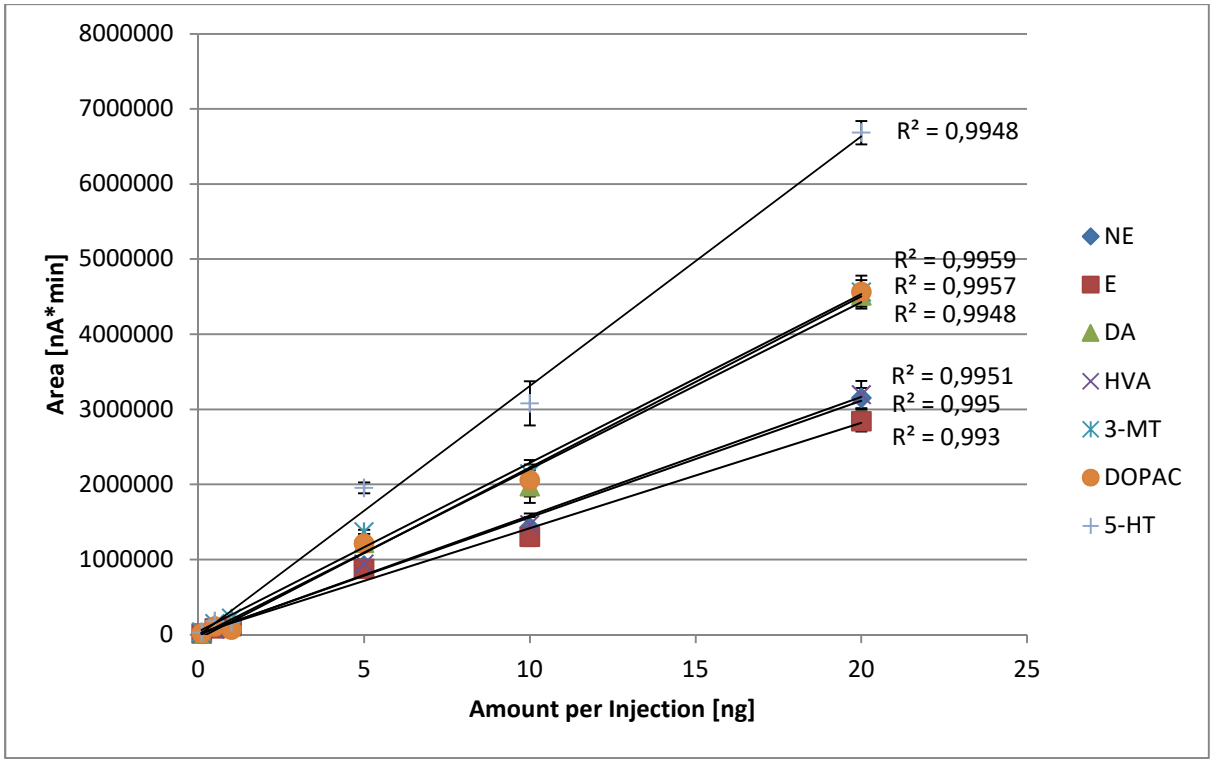

Figure 50: Linearity of MAs on system I, mean of n = 3.

Figure 51: LOD, LOQ, and RSD of system I; LOD/LOQ measured in diluted standard solution, RSD measured in aliquoted brain homogenate on five separate days.

	LOD [pg/µL]	LOQ [pg/µL]	RSD
NE	0.25	0.75	5.45
E	0.25	0.75	-
DA	0.25	0.75	9.15
HVA	0.25	0.75	6.71
3-MT	0.025	0.075	7.17
DOPAC	0.25	0.75	11.17
5-HT	0.625	1.875	23.00

7.5. Linearity graphs of MAs on system II and MA and MO/NL on system III

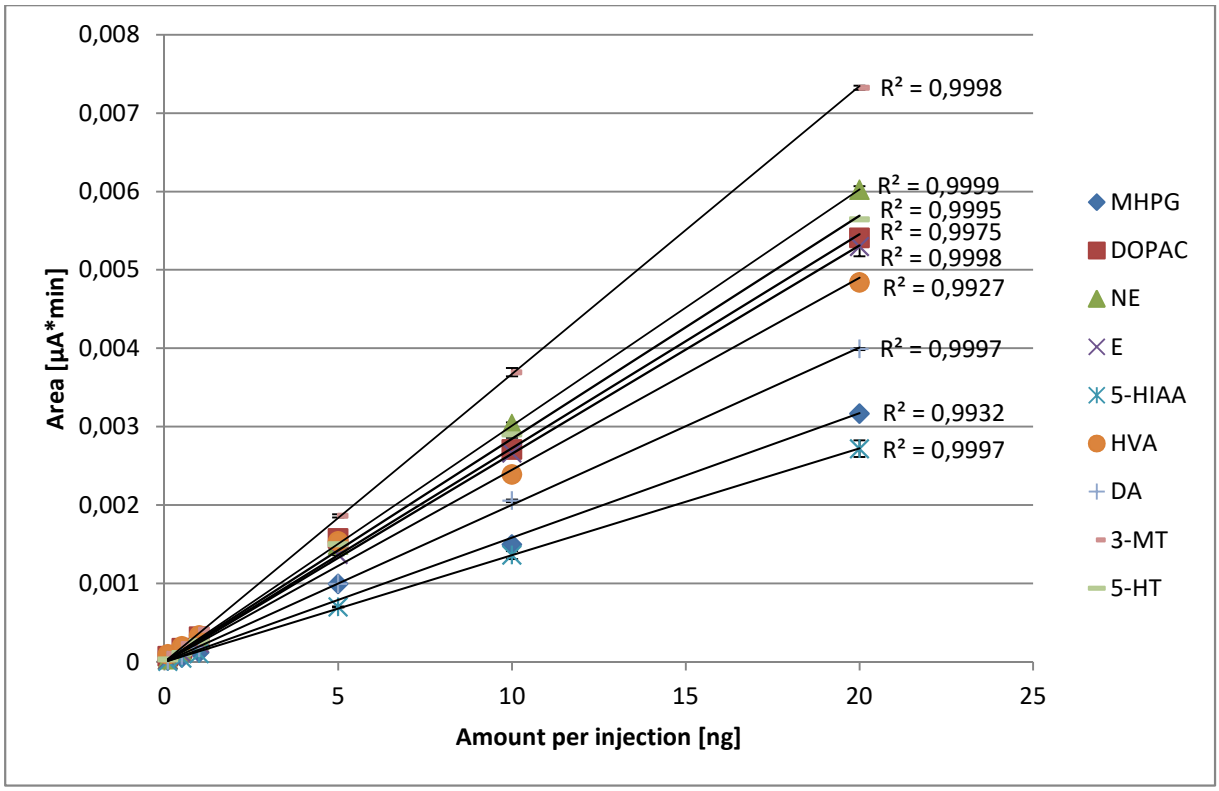

Figure 52: Linearity of MAs on system II; each point mean of n=3.

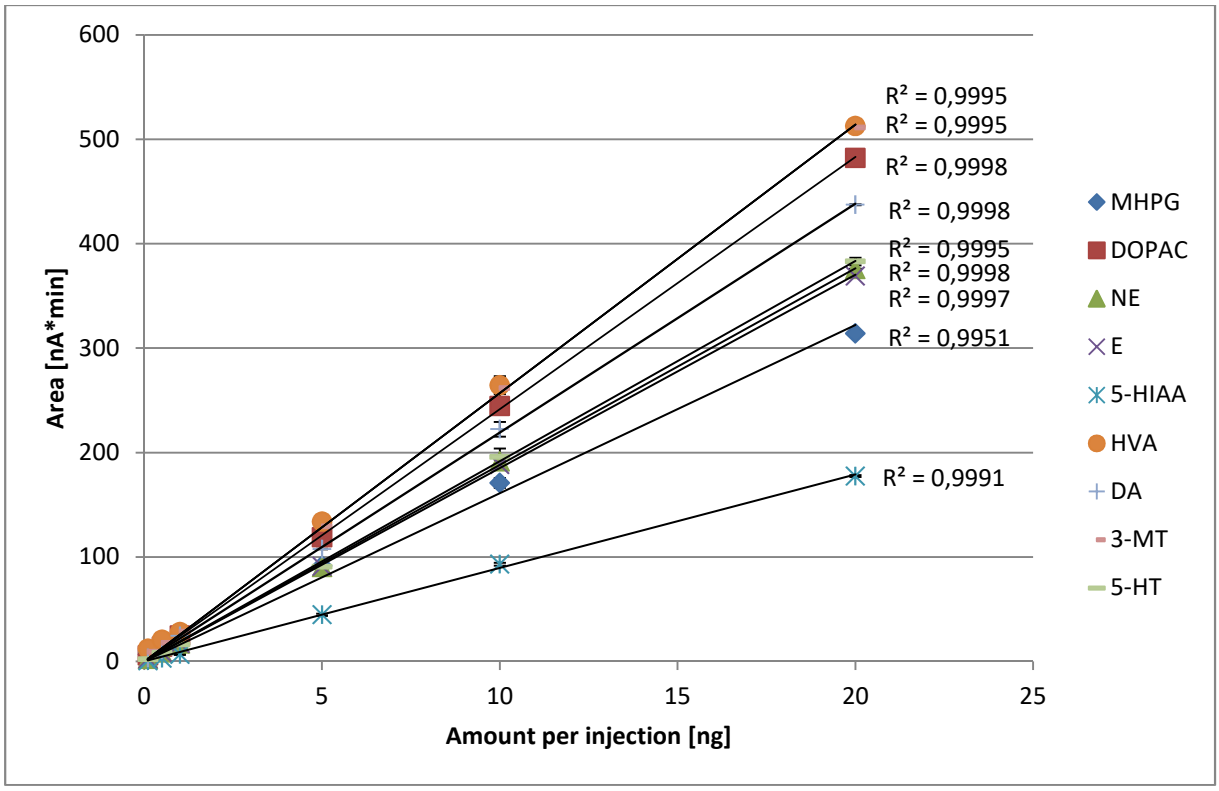

Figure 53: Linearity of MAs on System III with coulometric detector, mean of n=3.

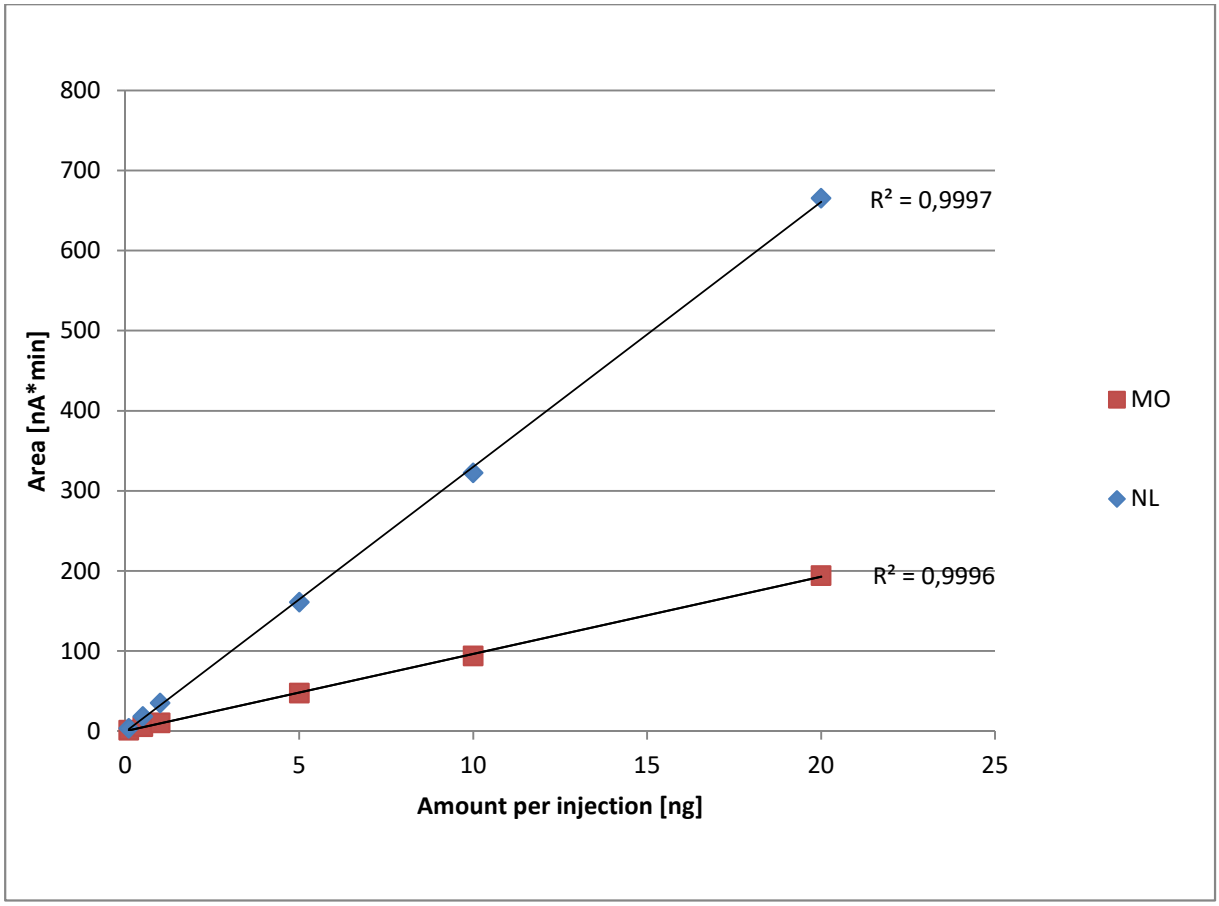

Figure 54: Linearity of MO and NL on system III with coulometric detector, mean of n=3.

7.6. Chromotagrams of MA standard on system II and III

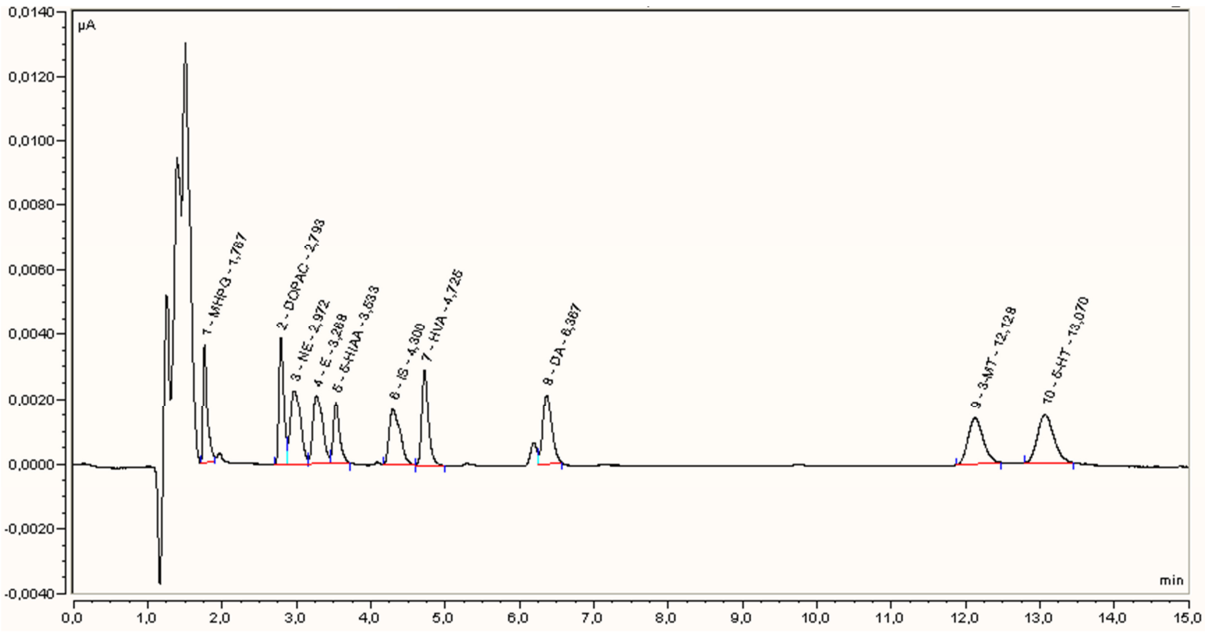

Figure 55: Chromatogram of MA standard solution (1 ng/injection) on system II.

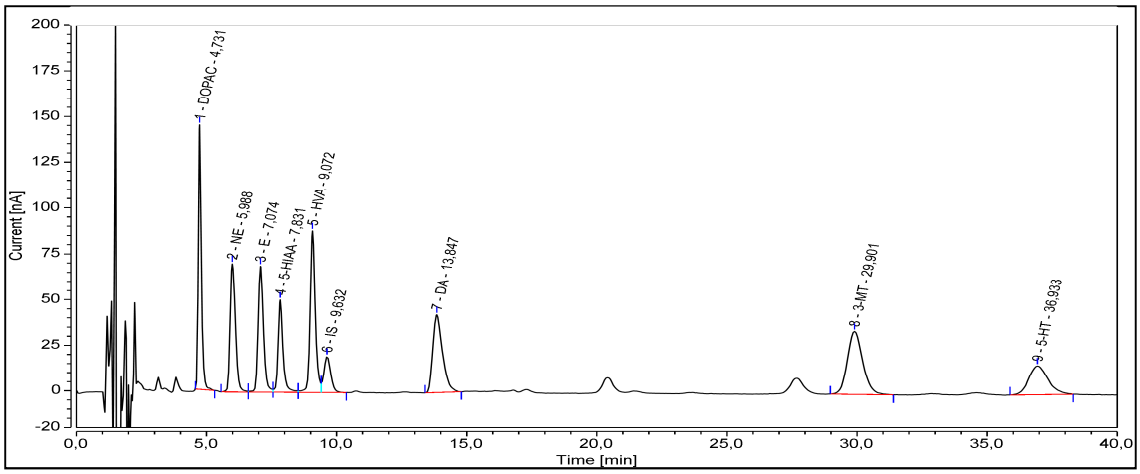

Figure 56: Chromatogram of MA standard solution (1 ng/injection) on system III.

7.7. Concentration values of MAs in BAT, macrophages, and supernatant

Table 19: Monoamines in bone marrow derived macrophages treated with IL 4 (saline n=2; IL-4 5 ng mL^{-1}, 10 ng mL^{-1}, 20 ng mL^{-1} n=3); n.d. = non detectable.

vhcl (pg/mg)	1	2	
MHPG	n.d.	20898.35	
DOPAC	551.6297	862.9202	
NE	66.49878	164.1944	
E	26.02444	166.054	
5-HIAA	3672.407	7410.068	
HVA	50.76345	229.9859	
DA	n.d.	n.d.	
3-MT	n.d.	n.d.	
5-HAT	1197.792	3826.131	
IL-4 5 [pg/mg]	**1**	**2**	**3**
MHPG	n.d.	7654.311	5695.244
DOPAC	448.6308	645.6192	365.6509
NE	49.7505	78.8116	58.84222
E	29.04319	33.89396	15.68755
5-HIAA	1755.417	1947.244	2215.523
HVA	74.83174	40.1602	50.85507
DA	n.d.	n.d.	n.d.
3-MT	n.d.	n.d.	n.d.
5-HAT	765.0559	804.6038	660.1558
IL-4 10 [pg/mg]	**1**	**2**	**3**
MHPG	n.d.	14743.06	n.d.
DOPAC	430.1611	559.1849	466.1247
NE	81.43835	118.1447	72.16328
E	20.13338	28.07358	37.01513
5-HIAA	2248.545	1969.004	2034.688
HVA	28.06372	59.28417	74.17133
DA	n.d.	n.d.	n.d.
3-MT	n.d.	n.d.	n.d.
5-HAT	1105.516	990.6929	988.1196
IL-4 20 (pg/mg]	**1**	**2**	**3**
MHPG	n.d.	n.d.	n.d.
DOPAC	441.493	544.9215	364.9369
NE	43.37821	60.00954	67.00836
E	23.79171	39.71914	22.76075
5-HIAA	1583.763	2138.428	2319.725
HVA	55.71935	63.53355	80.55529
DA	n.d.	n.d.	n.d.
3-MT	n.d.	n.d.	n.d.
5-HT	600.6486	957.9805	839.7325

Table 20: Monoamines in medium supernatant of bone marrow derived macrophages treated with IL-4 (saline n=2; IL-4 5 ng mL^{-1}, 10 ng mL^{-1}, 20 ng mL^{-1} n=3); n.d. = non detectable.

vhcl [pg µL^{-1}]	1	2	
Sample size (µL)	200.00	200.00	
MHPG	641.39	803.14	
DOPAC	0.44	0.32	
NE	0.21	0.27	
E	18.60	20.30	
5-HIAA	532.08	607.03	
HVA	21.00	23.82	
DA	0.73	0.67	
3-MT	n.d.	n.d.	
5-HT	294.58	333.00	
IL-4 5 [pg µL^{-1}]	**1**	**2**	**3**
Sample size (µL)	200.00	200.00	200.00
MHPG	453.08	602.95	548.73
DOPAC	0.66	0.50	0.34
NE	0.14	0.26	0.28
E	9.90	12.64	12.15
5-HIAA	232.31	320.95	177.31
HVA	11.08	15.26	10.92
DA	0.20	0.38	0.68
3-MT	n.d.	n.d.	n.d.
5-HT	173.54	225.70	103.85
IL-4 10 [pg µL^{-1}]	**1**	**2**	**3**
Sample size (µL)	200.00	200.00	200.00
MHPG	528.56	539.03	458.14
DOPAC	0.58	0.42	0.41
NE	0.17	0.22	0.15
E	11.37	11.39	9.42
5-HIAA	265.08	183.35	149.79
HVA	12.74	10.27	7.43
DA	0.38	0.54	0.78
3-MT	n.d.	n.d.	n.d.
5-HT	197.56	118.83	89.70
5-HT	192.19	86.44	79.90

IL-4 20 [pg(µL]	1	2	3
Sample size (µL)	200.00	200.00	200.00
MHPG	527.00	426.82	409.51
DOPAC	0.73	0.46	0.48
NE	0.24	0.24	0.23
E	11.11	8.93	9.20
5-HIAA	275.24	151.19	162.64
HVA	13.42	8.91	9.00
DA	0.43	0.46	0.42
3-MT	n.d.	n.d.	n.d.
5-HT	192.19	86.44	79.90
Medium	**1**	**2**	
Sample size (µL)	200.00	200.00	
MHPG	801.58	919.42	
DOPAC	n.d.	n.d.	
NE	n.d.	1.74	
E	41.42	43.09	
5-HIAA	332.95	334.92	
HVA	12.19	13.15	
DA	n.d.	n.d.	
3-MT	3.66	3.66	
5-HAT	346.44	432.64	

7.8. Chromatogram of macrophage medium without cells

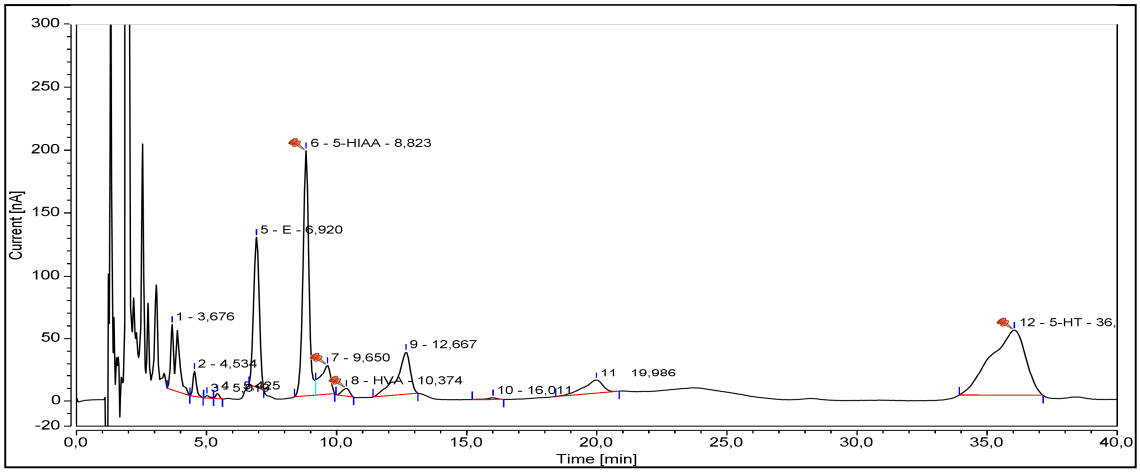

Figure 57: Chromatogram of macrophage medium without cells, subjected to same clean-up as macrophage supernatant.

7.9. Concentration of MAs in tissues of WT and Dusp8 KO mice

Table 21: Concentration of analytes [pg/mg] in WT and Dusp8 KO mice, treated with saline or α-MPT; n = 6; n.d. = non detectable.

HYP	Sal WT	MPT WT	Sal KO	MPT KO
DOPAC	311 ± 75	424 ± 395	282 ± 72	218 ± 57
NE	3026 ± 631	2170 ± 610	3653 ± 892	1884 ± 629
E	n.d.	n.d.	n.d.	n.d.
5-HIAA	987 ± 243	1042 ± 198	1005 ± 316	1021 ± 311
HVA	226 ± 106	47 ± 30	238 ± 80	60 ± 72
DA	1301 ± 313	434 ± 187	1041 ± 160	267 ± 71
3-MT	n.d.	n.d.	n.d.	n.d.
5-HT	2363 ± 451	2549 ± 403	2397 ± 548	2331 ± 452
Liver	**Sal WT**	**MPT WT**	**Sal KO**	**MPT KO**
DOPAC	5 ± 2	4 ± 4	3 ± 2	4 ± 1
NE	104 ± 37	55 ± 17	63 ± 24	48 ± 20
E	n.d.	n.d.	1 ± 1	0 ± 1
5-HIAA	16 ± 13	9 ± 2	8 ± 5	12 ± 7
HVA	1 ± 1	1 ± 2	0 ± 1	0 ± 1
DA	n.d.	n.d.	n.d.	n.d.
3-MT	101 ± 226	n.d.	28 ± 63	30 ± 66
5-HT	139 ± 57	136 ± 19	115 ± 33	133 ± 24
Pancreas	**Sal WT**	**MPT WT**	**Sal KO**	**MPT KO**
DOPAC	37 ± 6	55 ± 20	40 ± 5	47 ± 24
NE	436 ± 99	251 ± 81	337 ± 90	301 ± 58
E	n.d.	n.d.	n.d.	n.d.
5-HIAA	26 ± 4	36 ± 22	30 ± 8	34 ± 10
HVA	37 ± 9	32 ± 17	38 ± 19	42 ± 15
DA	29 ± 20	27 ± 19	33 ± 10	26 ± 10
3-MT	n.d.	n.d.	n.d.	n.d.
5-HT	46 ± 20	44 ± 16	42 ± 12	63 ± 21
Gastrocnemius	**Sal WT**	**MPT WT**	**Sal KO**	**MPT KO**
DOPAC	22 ± 4	21 ± 7	19 ± 3	22 ± 4
NE	118 ± 14	103 ± 21	129 ± 27	83 ± 17
E	3 ± 2	3 ± 3	6 ± 6	6 ± 3
5-HIAA	1 ± 2	3 ± 5	0 ± 0	1 ± 2
HVA	26 ± 11	12 ± 8	23 ± 2	31 ± 17
DA	6 ± 5	1 ± 3	8 ± 4	2 ± 3
3-MT	n.d.	n.d.	n.d.	n.d.
5-HT	87 ± 21	75 ± 21	110 ± 32	116 ± 37
EDL	**Sal WT**	**MPT WT**	**Sal KO**	**MPT KO**
DOPAC	24 ± 12	37 ± 16	21 ± 10	36 ± 18
NE	180 ± 36	167 ± 60	151 ± 31	141 ± 30
E	n.d.	n.d.	n.d.	n.d.
5-HIAA	n.d.	7 ± 7	1 ± 2	3 ± 6

HVA	18 ± 10	30 ± 9	24 ± 6	30 ± 9
DA	n.d.	n.d.	n.d.	n.d.
3-MT	n.d.	n.d.	n.d.	n.d.
5-HT	90 ± 9	110 ± 39	91 ± 15	136 ± 56
Soleus	**Sal WT**	**MPT WT**	**Sal KO**	**MPT KO**
DOPAC	56 ± 15	42 ± 9	51 ± 10	68 ± 22
NE	396 ± 73	283 ± 25	306 ± 52	298 ± 64
E	16 ± 3	22 ± 5	9 ± 5	19 ± 5
5-HIAA	n.d.	n.d.	n.d.	n.d.
HVA	42 ± 6	36 ± 3	39 ± 22	42 ± 11
DA	n.d.	n.d.	n.d.	n.d.
3-MT	n.d.	n.d.	n.d.	n.d.
5-HT	280 ± 71	262 ± 94	274 ± 35	369 ± 92
eWAT	**Sal WT**	**MPT WT**	**Sal KO**	**MPT KO**
DOPAC	11 ± 2	9 ± 2	16 ± 9	10 ± 2
NE	40 ± 30	21 ± 12	19 ± 6	34 ± 15
E	4 ± 9	2 ± 4	n.d.	n.d.
5-HIAA	3 ± 2	5 ± 2	3 ± 2	5 ± 2
HVA	n.d.	n.d.	n.d.	n.d.
DA	1 ± 3	n.d.	2 ± 4	n.d.
3-MT	n.d.	n.d.	n.d.	n.d.
5-HT	39 ± 16	38 ± 23	55 ± 32	57 ± 13

7.10. Concentration factors of MAs with DLLME

Table 22: Concentration factor of analytes after DLLME procedure out of a standard solution (10 ng per analyte in 110 µL 0.3 M $HClO_4$).

Analyte	Concentration factor after DLLME
MHPG	1.56
DOPAC	0.37
NE	2.24
E	2.3
5-HIAA	0.4
DHBA	2.17
HVA	0.27
DA	2.21
MO	2.66
3-MT	1.41
5-HT	2.76
NL	2.52
NP	2.68
HG	2.29

Bibliography

1. Miller, G., On the Origin of The Nervous System. Science, 2009. 325(5936): p. 24.
2. Johnson, M., Laboratory Mice and Rats. Materials and Methods, 2012. 2.
3. Zheng-Bradley, X., et al., Large scale comparison of global gene expression patterns in human and mouse. Genome Biology, 2010. 11(12): p. R124.
4. Herculano-Houzel, S., et al., Mammalian Brains Are Made of These: A Dataset of the Numbers and Densities of Neuronal and Nonneuronal Cells in the Brain of Glires, Primates, Scandentia, Eulipotyphlans, Afrotherians and Artiodactyls, and Their Relationship with Body Mass. Brain, Behavior and Evolution, 2015. 86(3-4): p. 145-163.
5. Snyder, J.M., et al., 20 - Nervous System, in Comparative Anatomy and Histology (Second Edition), P.M. Treuting, S.M. Dintzis, and K.S. Montine, Editors. 2018, Academic Press: San Diego. p. 403-444.
6. Ángeles Fernández-Gil, M., et al., Anatomy of the Brainstem: A Gaze Into the Stem of Life. Seminars in Ultrasound, CT and MRI, 2010. 31(3): p. 196-219.
7. Paulin, M.G., The Role of the Cerebellum in Motor Control and Perception. Brain, Behavior and Evolution, 1993. 41(1): p. 39-50.
8. Rhoton, A.L., Jr., THE CEREBRUM. Neurosurgery, 2007. 61(suppl_1): p. SHC-37-SHC-119.
9. Chayer, C. and M. Freedman, Frontal lobe functions. Current Neurology and Neuroscience Reports, 2001. 1(6): p. 547-552.
10. Berlucchi, G. and G. Vallar, Chapter 1 - The history of the neurophysiology and neurology of the parietal lobe, in Handbook of Clinical Neurology, G. Vallar and H.B. Coslett, Editors. 2018, Elsevier. p. 3-30.
11. Joseph, R., The Occipital Lobe, in Neuropsychology, Neuropsychiatry, and Behavioral Neurology, R. Joseph, Editor. 1990, Springer US: Boston, MA. p. 233-245.
12. Jackson, R.L., et al., An emergent functional parcellation of the temporal cortex. NeuroImage, 2018. 170: p. 385-399.
13. Nagayama, S., R. Homma, and F. Imamura, Neuronal organization of olfactory bulb circuits. Frontiers in neural circuits, 2014. 8: p. 98-98.
14. McGann, J.P., Poor human olfaction is a 19th-century myth. Science (New York, N.Y.), 2017. 356(6338): p. eaam7263.
15. Fama, R. and E.V. Sullivan, Thalamic structures and associated cognitive functions: Relations with age and aging. Neuroscience and biobehavioral reviews, 2015. 54: p. 29-37.
16. Pop, M., C. Crivii, and I. Opincariu, Anatomy and Function of the Hypothalamus. 2018.
17. Jarrard, L.E., On the role of the hippocampus in learning and memory in the rat. Behavioral and Neural Biology, 1993. 60(1): p. 9-26.
18. Rasia-Filho, A.A., R.G. Londero, and M. Achaval, Functional activities of the amygdala: an overview. Journal of psychiatry & neuroscience : JPN, 2000. 25(1): p. 14-23.
19. Lanciego, J.L., N. Luquin, and J.A. Obeso, Functional neuroanatomy of the basal ganglia. Cold Spring Harbor perspectives in medicine, 2012. 2(12): p. a009621-a009621.
20. Lodish H, B.A., Zipursky SL, et al. , Overview of Neuron Structure and Function. Available from: https://www.ncbi.nlm.nih.gov/books/NBK21535/, in Molecular Cell Biology. 2000, W. H. Freeman: New York.
21. Esplugues, J.V., NO as a signalling molecule in the nervous system. British journal of pharmacology, 2002. 135(5): p. 1079-1095.

22. Olff, M., et al., The role of oxytocin in social bonding, stress regulation and mental health: An update on the moderating effects of context and interindividual differences. Psychoneuroendocrinology, 2013. 38(9): p. 1883-1894.

23. Zhou, Y. and N.C. Danbolt, Glutamate as a neurotransmitter in the healthy brain. Journal of neural transmission (Vienna, Austria : 1996), 2014. 121(8): p. 799-817.

24. Ben-Ari, Y., The GABA excitatory/inhibitory developmental sequence: A personal journey. Neuroscience, 2014. 279: p. 187-219.

25. Purves D, A.G., Fitzpatrick D, et al., Neuroscience; Acetylcholine. Available from: https://www.ncbi.nlm.nih.gov/books/NBK11143/. 2nd edition ed. 2001, Sunderland (MA): Sinauer Associates.

26. Goldstein, D., Adrenaline and Noradrenaline. 2010.

27. O'Donnell, J., et al., Norepinephrine: a neuromodulator that boosts the function of multiple cell types to optimize CNS performance. Neurochemical research, 2012. 37(11): p. 2496-2512.

28. Mefford, I.N., Epinephrine in mammalian brain. Progress in Neuro-Psychopharmacology and Biological Psychiatry, 1988. 12(4): p. 365-388.

29. Klein, M.O., et al., Dopamine: Functions, Signaling, and Association with Neurological Diseases. Cellular and Molecular Neurobiology, 2019. 39(1): p. 31-59.

30. Berger, M., J.A. Gray, and B.L. Roth, The expanded biology of serotonin. Annual review of medicine, 2009. 60: p. 355-366.

31. Kostrzewa, R., The blood-brain barrier for catecholamines - Revisited. Neurotoxicity research, 2007. 11: p. 261-71.

32. Rios, M., et al., Catecholamine Synthesis is Mediated by Tyrosinase in the Absence of Tyrosine Hydroxylase. The Journal of Neuroscience, 1999. 19(9): p. 3519.

33. Eisenhofer, G., I.J. Kopin, and D.S. Goldstein, Catecholamine Metabolism: A Contemporary View with Implications for Physiology and Medicine. Pharmacological Reviews, 2004. 56(3): p. 331.

34. Tyce, G.M., Origin and Metabolism of Serotonin. Journal of Cardiovascular Pharmacology, 1990. 16: p. S1-S7.

35. Cockerham, R., et al., Subsecond Regulation of Synaptically Released Dopamine by COMT in the Olfactory Bulb. The Journal of Neuroscience, 2016. 36(29): p. 7779.

36. Laux-Biehlmann, A., et al., Endogenous morphine and its metabolites in mammals: History, synthesis, localization and perspectives. Neuroscience, 2013. 233: p. 95-117.

37. Homan, P., et al., Serotonin versus catecholamine deficiency: behavioral and neural effects of experimental depletion in remitted depression. Translational Psychiatry, 2015. 5: p. e532.

38. Meyer, J.H., et al., Elevated Monoamine Oxidase A Levels in the Brain: An Explanation for the Monoamine Imbalance of Major Depression. Archives of General Psychiatry, 2006. 63(11): p. 1209-1216.

39. Liu, B., et al., From Serotonin to Neuroplasticity: Evolvement of Theories for Major Depressive Disorder. Frontiers in cellular neuroscience, 2017. 11: p. 305-305.

40. Tomkins, D.M. and E.M. Sellers, Addiction and the brain: the role of neurotransmitters in the cause and treatment of drug dependence. CMAJ : Canadian Medical Association journal = journal de l'Association medicale canadienne, 2001. 164(6): p. 817-821.

41. Myers, R.D. and C.L. Melchior, Alcohol drinking: abnormal intake caused by tetrahydropapaveroline in brain. Science, 1977. 196(4289): p. 554.

42. Zhu, W., et al., Chronic alcohol exposure increases ganglia endogenous morphine levels. Archives of medical science : AMS, 2010. 6(3): p. 316-320.

43. Dexter, D.T. and P. Jenner, Parkinson disease: from pathology to molecular disease mechanisms. Free Radical Biology and Medicine, 2013. 62: p. 132-144.

44. Barone, P., Neurotransmission in Parkinson's disease: beyond dopamine. European Journal of Neurology, 2010. 17(3): p. 364-376.

45. Matsubara, K., et al., Increased urinary morphine, codeine and tetrahydropapaveroline in parkinsonian patient undergoing L-3,4-dihydroxyphenylalanine therapy: a possible biosynthetic pathway of morphine from L-3,4-dihydroxyphenylalanine in humans. Journal of Pharmacology and Experimental Therapeutics, 1992. 260(3): p. 974.

46. Bullard, K.M., et al., Prevalence of Diagnosed Diabetes in Adults by Diabetes Type - United States, 2016. MMWR. Morbidity and mortality weekly report, 2018. 67(12): p. 359-361.

47. Tamayo, T., et al., The Prevalence and Incidence of Diabetes in Germany. Deutsches Arzteblatt international, 2016. 113(11): p. 177-182.

48. Wu, Y., et al., Risk factors contributing to type 2 diabetes and recent advances in the treatment and prevention. International journal of medical sciences, 2014. 11(11): p. 1185-1200.

49. Kleinridders, A., et al., Insulin resistance in brain alters dopamine turnover and causes behavioral disorders. Proceedings of the National Academy of Sciences of the United States of America, 2015. 112(11): p. 3463-3468.

50. Ornstein, A.M., et al., Disruption of the Dopamine D2 Receptor Impairs Insulin Secretion and Causes Glucose Intolerance. Endocrinology, 2010. 151(4): p. 1441-1450.

51. Oh, C.M., S. Park, and H. Kim, Serotonin as a New Therapeutic Target for Diabetes Mellitus and Obesity. Diabetes & metabolism journal, 2016. 40(2): p. 89-98.

52. El-Merahbi, R., et al., The roles of peripheral serotonin in metabolic homeostasis. FEBS Letters, 2015. 589(15): p. 1728-1734.

53. Straznicky, N.E., et al., Neuroadrenergic dysfunction along the diabetes continuum: a comparative study in obese metabolic syndrome subjects. Diabetes, 2012. 61(10): p. 2506-2516.

54. Garris, D.R., Age- and diabetes-associated alterations in regional brain norepinephrine concentrations and adrenergic receptor populations in C57BL/KsJ mice. Developmental Brain Research, 1990. 51(2): p. 161-166.

55. Otto, M., Analytische Chemie. 3. Auflage ed. 2006, Weinheim: Wiley-VCH.

56. Ramis-Ramos, M.C.G.A.C.J.J.B.B.G., Reversed Phase Liquid Chromatography, in Analytical Separation Science. 2015. p. 159-198.

57. Hayes, R., et al., Core–shell particles: Preparation, fundamentals and applications in high performance liquid chromatography. Journal of Chromatography A, 2014. 1357: p. 36-52.

58. Robert J Flanagan, D.P., Robin Whelpton, Electrochemical Detection in HPLC: Analysis of Drugs and Poisons. 2005, Cambridge: The Royal Society of Chemistry.

59. Honeychurch, K., Review: The Application of Liquid Chromatography Electrochemical Detection for the Determination of Drugs of Abuse. Separations, 2016. 3(4): p. 28.

60. Finckh, B., et al., [31] High-performance liquid chromatography-coulometric electrochemical detection of ubiquinol 10, ubiquinone 10, carotenoids, and tocopherols in neonatal plasma, in Methods in Enzymology. 1999, Academic Press. p. 341-348.

61. Lin, Q., et al., Two-Electron, Two-Proton Oxidation of Catechol: Kinetics and Apparent Catalysis. The Journal of Physical Chemistry C, 2015. 119(3): p. 1489-1495.

62. Adenier, A., et al., Electrochemical Oxidation of Aliphatic Amines and Their Attachment to Carbon and Metal Surfaces. Langmuir, 2004. 20(19): p. 8243-8253.

63. Jayaraman, M., et al., Electrochemical detection of phenol in aqueous solutions. Vol. 11. 2004. 797-803.

64. Glish, G.L. and R.W. Vachet, The basics of mass spectrometry in the twenty-first century. Nature Reviews Drug Discovery, 2003. 2(2): p. 140-150.

65. De Benedetto, G.E., et al., A rapid and simple method for the determination of 3,4-dihydroxyphenylacetic acid, norepinephrine, dopamine, and serotonin in mouse brain homogenate by HPLC with fluorimetric detection. Journal of Pharmaceutical and Biomedical Analysis, 2014. 98: p. 266-270.

66. Huang, X., et al., Analysis of catecholamines and related compounds in one whole metabolic pathway with high performance liquid chromatography based on derivatization. Arabian Journal of Chemistry, 2014.

67. Liu, L., et al., Simultaneous determination of catecholamines and their metabolites related to Alzheimer's disease in human urine. Journal of Separation Science, 2011. 34(10): p. 1198-1204.

68. Kehr, J., et al., Microdialysis in freely moving mice: determination of acetylcholine, serotonin and noradrenaline release in galanin transgenic mice. Journal of Neuroscience Methods, 2001. 109(1): p. 71-80.

69. Tsunoda, M. and T. Funatsu, Catecholamine analysis with strong cation exchange column liquid chromatography–peroxyoxalate chemiluminescence reaction detection. Analytical and Bioanalytical Chemistry, 2012. 402(3): p. 1393-1397.

70. Baeyens, W.R.G., et al., Chemiluminescence-based detection: principles and analytical applications in flowing streams and in immunoassays. Journal of Pharmaceutical and Biomedical Analysis, 1998. 17(6): p. 941-953.

71. Thomas, J., R. Khanam, and D. Vohora, A validated HPLC-UV method and optimization of sample preparation technique for norepinephrine and serotonin in mouse brain. Pharmaceutical Biology, 2015. 53(10): p. 1539-1544.

72. Shi, T., et al., Advancing the sensitivity of selected reaction monitoring-based targeted quantitative proteomics. Proteomics, 2012. 12(8): p. 1074-1092.

73. Gustavsson, S.Å., et al., Studies of signal suppression in liquid chromatography–electrospray ionization mass spectrometry using volatile ion-pairing reagents. Journal of Chromatography A, 2001. 937(1): p. 41-47.

74. Deng, P., et al., Derivatization methods for quantitative bioanalysis by LC–MS/MS. Bioanalysis, 2011. 4(1): p. 49-69.

75. Wong, J.-M.T., et al., Benzoyl chloride derivatization with liquid chromatography–mass spectrometry for targeted metabolomics of neurochemicals in biological samples. Journal of Chromatography A, 2016. 1446: p. 78-90.

76. Van Eeckhaut, A., et al., Validation of bioanalytical LC–MS/MS assays: Evaluation of matrix effects. Journal of Chromatography B, 2009. 877(23): p. 2198-2207.

77. Johnsen, E., et al., Liquid chromatography-mass spectrometry platform for both small neurotransmitters and neuropeptides in blood, with automatic and robust solid phase extraction. Scientific Reports, 2015. 5: p. 9308.

78. Tufi, S., et al., Simultaneous analysis of multiple neurotransmitters by hydrophilic interaction liquid chromatography coupled to tandem mass spectrometry. Journal of Chromatography A, 2015. 1395: p. 79-87.

79. Yang, Z.-L., et al., An optimized method for neurotransmitters and their metabolites analysis in mouse hypothalamus by high performance liquid chromatography–Q Exactive hybrid quadrupole-

orbitrap high-resolution accurate mass spectrometry. Journal of Chromatography B, 2016. 1012-1013: p. 79-88.

80. Woo, H.I., et al., A simple and rapid analytical method based on solid-phase extraction and liquid chromatography–tandem mass spectrometry for the simultaneous determination of free catecholamines and metanephrines in urine and its application to routine clinical analysis. Clinical Biochemistry, 2016. 49(7): p. 573-579.

81. Sørensen, L.K. and M. Johannsen, Sensitive determination of monoamine neurotransmitters, their main metabolites and precursor amino acids in different mouse brain components by liquid chromatography–electrospray tandem mass spectrometry after selective sample clean-up. Biomedical Chromatography, 2019. 33(4): p. e4479.

82. Reinhoud, N.J., et al., Analysis of glutamate, GABA, noradrenaline, dopamine, serotonin, and metabolites using microbore UHPLC with electrochemical detection. ACS chemical neuroscience, 2013. 4(5): p. 888-894.

83. Bidel, F., et al., An HPLC-ECD method for monoamines and metabolites quantification in cuttlefish (cephalopod) brain tissue. Biomedical Chromatography, 2016. 30(8): p. 1175-1183.

84. Van Schoors, J., et al., An improved microbore UHPLC method with electrochemical detection for the simultaneous determination of low monoamine levels in in vivo brain microdialysis samples. Journal of Pharmaceutical and Biomedical Analysis, 2016. 127: p. 136-146.

85. Allen, S.A., et al., A simple and sensitive high-performance liquid chromatography–electrochemical detection assay for the quantitative determination of monoamines and respective metabolites in six discrete brain regions of mice. Biomedical Chromatography, 2017. 31(11): p. e3998.

86. Batllori, M., et al., Analysis of human cerebrospinal fluid monoamines and their cofactors by HPLC. Nature Protocols, 2017. 12(11): p. 2359-2375.

87. Du, T.T., et al., Simultaneous determination of tryptophan, kynurenine, kynurenic acid and two monoamines in rat plasma by HPLC-ECD/DAD. Journal of Pharmaceutical and Biomedical Analysis, 2018. 158: p. 8-14.

88. Nagler, J., et al., Comprehensive analysis of nine monoamines and metabolites in small amounts of peripheral murine (C57Bl/6 J) tissues. Biomedical Chromatography, 2018. 32(4): p. e4151.

89. Zhang, L., et al., Simultaneous determination of eleven compounds related to metabolism of bioamines in rat cortex and hippocampus by HPLC-ECD with boron-doped diamond working electrode. Journal of Pharmaceutical and Biomedical Analysis, 2016. 118: p. 41-51.

90. Chi, J.D., J. Odontiadis, and M. Franklin, Simultaneous determination of catecholamines in rat brain tissue by high-performance liquid chromatography. Journal of Chromatography B: Biomedical Sciences and Applications, 1999. 731(2): p. 361-367.

91. Parrot, S., P.-C. Neuzeret, and L. Denoroy, A rapid and sensitive method for the analysis of brain monoamine neurotransmitters using ultra-fast liquid chromatography coupled to electrochemical detection. Journal of Chromatography B, 2011. 879(32): p. 3871-3878.

92. Abo, R., N.-A. Kummer, and B. Merkel, Optimized photodegradation of Bisphenol A in water using ZnO, TiO₂ and SnO₂ photocatalysts under UV radiation as a decontamination procedure. Vol. 9. 2016. 27-35.

93. Ganhao, M.F., et al., Evaluation of a simple plasma catecholamine extraction procedure prior to high-performance liquid chromatography and electrochemical detection. Journal of Chromatography B: Biomedical Sciences and Applications, 1991. 564(1): p. 55-66.

94. Smith, E.A., A.L. Schwartz, and J.B. Lucot, Measurement of urinary catecholamines in small samples for mice. Journal of Pharmacological and Toxicological Methods, 2013. 67(1): p. 45-49.

95. Raggi, M.A., et al., Sensitive determination of 3-methoxy-4-hydroxyphenylglycol (MHPG) in human plasma by HPLC with electrochemical detection. Chromatographia, 2001. 53(7): p. 409-413.

96. Raggi, M.A., et al., Analysis of plasma catecholamines by liquid chromatography with amperometric detection using a novel SPE ion-exchange procedure. Journal of Separation Science, 2003. 26(12-13): p. 1141-1146.

97. Li, X., S. Li, and G. Kellermann, Simultaneous extraction and determination of monoamine neurotransmitters in human urine for clinical routine testing based on a dual functional solid phase extraction assisted by phenylboronic acid coupled with liquid chromatography-tandem mass spectrometry. Analytical and Bioanalytical Chemistry, 2017. 409(11): p. 2859-2871.

98. Hironori, T. and H. Tokishi, High-performance liquid chromatographie analysis of catecholamines in biological samples by liquid/liquid extraction prepurification. Journal of Pharmacological Methods, 1990. 23(1): p. 21-30.

99. Rezaee, M., et al., Determination of organic compounds in water using dispersive liquid–liquid microextraction. Journal of Chromatography A, 2006. 1116(1): p. 1-9.

100. Li, Y., et al., Development of a Efficient and Sensitive Dispersive Liquid–Liquid Microextraction Technique for Extraction and Preconcentration of 10 β2-Agonists in Animal Urine. PLOS ONE, 2015. 10(9): p. e0137194.

101. Saraji, M. and M.K. Boroujeni, Recent developments in dispersive liquid–liquid microextraction. Analytical and Bioanalytical Chemistry, 2014. 406(8): p. 2027-2066.

102. Kocúrová, L., et al., Recent advances in dispersive liquid–liquid microextraction using organic solvents lighter than water. A review. Microchemical Journal, 2012. 102: p. 11-17.

103. Hu, X.-Z., J.-H. Wu, and Y.-Q. Feng, Molecular complex-based dispersive liquid–liquid microextraction: Analysis of polar compounds in aqueous solution. Journal of Chromatography A, 2010. 1217(45): p. 7010-7016.

104. Trujillo-Rodríguez, M.J., et al., Ionic liquids in dispersive liquid-liquid microextraction. TrAC Trends in Analytical Chemistry, 2013. 51: p. 87-106.

105. Sereshti, H., P. Khorram, and N. Nouri, Recent trends in replacement of disperser solvent in dispersive liquid-liquid microextraction methods. Separation & Purification Reviews, 2019. 48(2): p. 159-178.

106. Campone, L., et al., pH-controlled dispersive liquid–liquid microextraction for the analysis of ionisable compounds in complex matrices: Case study of ochratoxin A in cereals. Analytica Chimica Acta, 2012. 754: p. 61-66.

107. Du, D., et al., Salting-out induced liquid–liquid microextraction based on the system of acetonitrile/magnesium sulfate for trace-level quantitative analysis of fluoroquinolones in water, food and biological matrices by high-performance liquid chromatography with a fluorescence detector. Analytical Methods, 2014. 6(17): p. 6973-6980.

108. Rezaee, M., Y. Yamini, and M. Faraji, Evolution of dispersive liquid–liquid microextraction method. Journal of Chromatography A, 2010. 1217(16): p. 2342-2357.

109. Mansour, F. and M. Khairy, Pharmaceutical and biomedical applications of dispersive liquid–liquid microextraction. Vol. 1061-1062. 2017.

110. Mousavi, L., Z. Tamiji, and M.R. Khoshayand, Applications and opportunities of experimental design for the dispersive liquid–liquid microextraction method – A review. Talanta, 2018. 190: p. 335-356.

111. Mano, T., et al., Effects of Thyroid Hormone on Catecholamine and its Metabolite Concentrations in Rat Cardiac Muscle and Cerebral Cortex. Thyroid, 1998. 8(4): p. 353-358.

112. Eldrup, E., E.A. Richter, and N.J. Christensen, DOPA, norepinephrine, and dopamine in rat tissues: no effect of sympathectomy on muscle DOPA. Am J Physiol, 1989. 256(2 Pt 1): p. E284-7.

113. Adeghate, E., A.S. Ponery, and R. Sheen, Streptozotocin-Induced Diabetes Mellitus Is Associated with Increased Pancreatic Tissue Levels of Noradrenaline and Adrenaline in the Rat. Pancreas, 2001. 22(3): p. 311-316.

114. ÖStenson, C.-G., P. Hjemdahl, and S. Efendic, Release of Catecholamines Is Increased but Does Not Contribute to the Impaired Insulin Secretion in the Perfused Pancreata of Diabetic Rats. Pancreas, 1993. 8(1): p. 34-38.

115. Lundquist, I., et al., Monoamines in Pancreatic Islets of Guinea Pig, Hamster, Rat, and Mouse Determined by High Performance Liquid Chromatography. Pancreas, 1989. 4(6): p. 662-667.

116. <Eunyoung et al 2004 - Catecholamines and 5-Hydroxytryptamine in Tissues of the Rabbit Pancreas.pdf>.

117. Yi, E., et al., Catecholamines and 5-Hydroxytryptamine in Tissues of the Rabbit Exocrine Pancreas. Pancreas, 2004. 29(3): p. 218-224.

118. Garofalo, M.A., et al., Effect of acute cold exposure on norepinephrine turnover rates in rat white adipose tissue. J Auton Nerv Syst, 1996. 60(3): p. 206-8.

119. Yang, L. and M.F. Beal, Determination of Neurotransmitter Levels in Models of Parkinson's Disease by HPLC-ECD, in Neurodegeneration: Methods and Protocols, G. Manfredi and H. Kawamata, Editors. 2011, Humana Press: Totowa, NJ. p. 401-415.

120. Rothwell, N.J. and M.J. Stock, Neural regulation of thermogenesis. Trends in Neurosciences, 1982. 5: p. 124-126.

121. Nguyen, K.D., et al., Alternatively activated macrophages produce catecholamines to sustain adaptive thermogenesis. Nature, 2011. 480: p. 104.

122. Fischer, K., et al., Alternatively activated macrophages do not synthesize catecholamines or contribute to adipose tissue adaptive thermogenesis. Nature Medicine, 2017. 23: p. 623.

123. Al-Goblan, A.S., M.A. Al-Alfi, and M.Z. Khan, Mechanism linking diabetes mellitus and obesity. Diabetes, metabolic syndrome and obesity : targets and therapy, 2014. 7: p. 587-591.

124. Solinas, G. and B. Becattini, JNK at the crossroad of obesity, insulin resistance, and cell stress response. Molecular metabolism, 2016. 6(2): p. 174-184.

125. Hirosumi, J., et al., A central role for JNK in obesity and insulin resistance. Nature, 2002. 420(6913): p. 333-336.

126. Benzler, J., et al., Acute Inhibition of Central c-Jun N-terminal Kinase Restores Hypothalamic Insulin Signalling and Alleviates Glucose Intolerance in Diabetic Mice. Journal of Neuroendocrinology, 2013. 25(5): p. 446-454.

127. Manning, A.M. and R.J. Davis, Targeting JNK for therapeutic benefit: from junk to gold? Nature Reviews Drug Discovery, 2003. 2(7): p. 554-565.

128. Morris, A.P., et al., Large-scale association analysis provides insights into the genetic architecture and pathophysiology of type 2 diabetes. Nature genetics, 2012. 44(9): p. 981-990.

129. Brodie, B.B., et al., APPLICATION OF STEADY STATE KINETICS TO THE ESTIMATION OF SYNTHESIS RATE AND TURNOVER TIME OF TISSUE CATECHOLAMINES. Journal of Pharmacology and Experimental Therapeutics, 1966. 154(3): p. 493.

130. Dunn, A.J., Systematic interleukin-1 administration stimulates hypothalamic norepinephrine metabolism parallelling the increased plasma corticosterone. Life Sciences, 1988. 43(5): p. 429-435.

131. Stephens, M.A.C. and G. Wand, Stress and the HPA axis: role of glucocorticoids in alcohol dependence. Alcohol research : current reviews, 2012. 34(4): p. 468-483.

132. Kvetnanský, R., et al., Endogenous glucocorticoids restrain catecholamine synthesis and release at rest and during immobilization stress in rats. Endocrinology, 1993. 133(3): p. 1411-1419.

133. Golczynska, A., J.W.M. Lenders, and D.S. Goldstein, Glucocorticoid-induced sympathoinhibition in humans. Clinical Pharmacology & Therapeutics, 1995. 58(1): p. 90-98.

134. Kuo, T., et al., Regulation of Glucose Homeostasis by Glucocorticoids. Advances in experimental medicine and biology, 2015. 872: p. 99-126.

135. Buijs, R.M., et al., Parasympathetic and sympathetic control of the pancreas: A role for the suprachiasmatic nucleus and other hypothalamic centers that are involved in the regulation of food intake. Journal of Comparative Neurology, 2001. 431(4): p. 405-423.

136. Mizuno, K. and Y. Ueno, Autonomic Nervous System and the Liver. Hepatology Research, 2017. 47(2): p. 160-165.

137. Bartness, T.J., et al., Sensory and sympathetic nervous system control of white adipose tissue lipolysis. Molecular and cellular endocrinology, 2010. 318(1-2): p. 34-43.

138. Shiuchi, T., et al., Induction of glucose uptake in skeletal muscle by central leptin is mediated by muscle β2-adrenergic receptor but not by AMPK. Scientific Reports, 2017. 7(1): p. 15141.

139. Augusto, V., et al., Skeletal muscle fiber types in C57BL6J mice. J. morphol. Sci, 2004. 21: p. 89-94.

140. Peyronnard, J.M., et al., Motor, sympathetic and sensory innervation of rat skeletal muscles. Brain Research, 1986. 373(1): p. 288-302.

141. Grobe, N., et al., Urinary excretion of morphine and biosynthetic precursors in mice. Proceedings of the National Academy of Sciences, 2010. 107(18): p. 8147.

142. Poeaknapo, C., et al., Endogenous formation of morphine in human cells. Proceedings of the National Academy of Sciences of the United States of America, 2004. 101(39): p. 14091.

143. Surmeier, D.J., et al., Chapter 4 - What causes the death of dopaminergic neurons in Parkinson's disease?, in Progress in Brain Research, A. Björklund and M.A. Cenci, Editors. 2010, Elsevier. p. 59-77.

144. Stayte, S. and B. Vissel, Advances in non-dopaminergic treatments for Parkinson's disease. Frontiers in Neuroscience, 2014. 8(113).

145. Charron, G., et al., Endogenous morphine-like compound immunoreactivity increases in parkinsonism. Brain, 2011. 134(8): p. 2321-2338.

146. Neri, C., et al., Dopamine is necessary to endogenous morphine formation in mammalian brain in vivo. Journal of Neurochemistry, 2008. 106(6): p. 2337-2344.

147. Yan, T., et al., Acute Morphine Treatments Alleviate Tremor in 1-Methyl-4-Phenyl-1,2,3,6-Tetrahydropyridine-Treated Monkeys. PLOS ONE, 2014. 9(2): p. e88404.

148. Wang, B., et al., The Neuroprotection of Low-Dose Morphine in Cellular and Animal Models of Parkinson's Disease Through Ameliorating Endoplasmic Reticulum (ER) Stress and Activating Autophagy. Frontiers in Molecular Neuroscience, 2018. 11(120).

149. Atici, S., et al., OPIOID NEUROTOXICITY: COMPARISON OF MORPHINE AND TRAMADOL IN AN EXPERIMENTAL RAT MODEL. International Journal of Neuroscience, 2004. 114(8): p. 1001-1011.

150. Snyder, C. and K. Mantione, The effects of morphine on Parkinson's-related genes PINK1 and PARK2. Medical science monitor basic research, 2014. 20: p. 63-69.

151. Ford, B., Pain in Parkinson's disease. Movement Disorders, 2010. 25(S1): p. S98-S103.

152. Cooper, T.E., et al., Morphine for chronic neuropathic pain in adults. Cochrane Database of Systematic Reviews, 2017(5).

153. Shimizu, T., et al., Antinociceptive mechanism of l-DOPA. PAIN, 2004. 110(1): p. 246-249.

154. Cashaw, J.L., Tetrahydropapaveroline in brain regions of rats after acute ethanol administration. Alcohol, 1993. 10(2): p. 133-138.

155. McCoy, J., et al., A re-evaluation of the role of tetrahydropapaveroline in ethanol consumption in rats. Vol. 60. 2003. 59-65.

156. Kim, Y.M., et al., Inhibition of dopamine biosynthesis by tetrahydropapaveroline. Neuroscience Letters, 2005. 386(1): p. 1-4.

157. Okada, T., et al., Tetrahydropapaveroline and its derivatives inhibit dopamine uptake through dopamine transporter expressed in HEK293 cells. Neuroscience Research, 1998. 30(1): p. 87-90.

158. Surh, Y.-J. and H.-J. Kim, Neurotoxic effects of tetrahydroisoquinolines and underlying mechanisms. Experimental neurobiology, 2010. 19(2): p. 63-70.

159. Moore, R.A., et al., HPLC of Morphine with Electrochemical Detection: Analysis in Human Plasma. Annals of Clinical Biochemistry, 1984. 21(2): p. 125-130.

160. Fiedler, D., et al., HPLC-UV determination of morphine in human plasma and its application to the clinical study. Acta poloniae pharmaceutica, 2011. 68: p. 473-9.

161. Wallace, J.E., S.C. Harris, and M.W. Peek, Determination of morphine by liquid chromatography with electrochemical detection. Analytical Chemistry, 1980. 52(8): p. 1328-1330.

162. Fricchione, G., et al., Identification of endogenous morphine and a μ3-like opiate alkaloid receptor in human brain tissue taken from a patient with intractable complex partial epilepsy. Vol. 14. 2008. CS45-49.

163. Neri, C., et al., Endogenous morphine and codeine in the brain of non human primate. Vol. 10. 2004. MS1-5.

164. Goumon, Y. and G.B. Stefano, Identification of morphine in the rat adrenal gland. Molecular Brain Research, 2000. 77(2): p. 267-269.

165. Goumon, Y., et al., Lipopolysaccharide increases endogenous morphine levels in rat brain. Neuroscience Letters, 2000. 293(2): p. 135-138.

166. Zhu, W., et al., Presence of morphine in rat amygdala: Evidence for the μ3 opiate receptor subtype via nitric oxide release in limbic structures. Vol. 10. 2005. BR433-9.

167. Ishikawa, K., J.L. Martinez, and J.L. McCaugh, Simultaneous determination of morphine and monoamine transmitters in a single mouse brain. Journal of Chromatography B: Biomedical Sciences and Applications, 1982. 231(2): p. 255-264.

168. Ollikainen, E., et al., Rapid analysis of intraperitoneally administered morphine in mouse plasma and brain by microchip electrophoresis-electrochemical detection. Scientific Reports, 2019. 9(1): p. 3311.

169. Yang, Z., et al., Simultaneous analysis of gemfibrozil, morphine, and its two active metabolites in different mouse brain structures using solid-phase extraction with ultra-high performance liquid chromatography and tandem mass spectrometry with a deuterated internal standard. Journal of Separation Science, 2016. 39(11): p. 2087-2096.

170. Charlet, A., et al., Abnormal nociception and opiate sensitivity of STOP null mice exhibiting elevated levels of the endogenous alkaloid morphine. Molecular pain, 2010. 6: p. 96-96.

171. Cashaw, J.L., et al., A method for determination of subpicomole concentrations of tetrahydropapaveroline in rat brain by high-performance liquid chromatography with electrochemical detection. Analytical Biochemistry, 1987. 162(1): p. 274-282.

172. Cashaw, J.L., Determination of tetrahydropapaveroline in the urine of Parkinsonian patients receiving l-dopa—carbidopa (Sinemet) therapy by high-performance liquid chromatography. Journal of Chromatography B: Biomedical Sciences and Applications, 1993. 613(2): p. 267-273.

173. Turner, A.J., et al., Tetrahydropapaveroline : Formation in vivo and in vitro in rat brain. Life Sciences, 1974. 14(11): p. 2247-2257.

174. Sango, K., et al., Enantio-selective occurrence of (S)-tetrahydropapaveroline in human brain. Neuroscience Letters, 2000. 283(3): p. 224-226.

175. M. Riggin, R. and P. Kissinger, Determination of tetrhydroisoquinoline alkaloids in biological materials with high performance liquid chromatography. Analytical chemistry, 1977. 49: p. 530-3.

176. Pfister, G., et al., Detection of catecholamines in single specimens of groundwater amphipods. Analytical and Bioanalytical Chemistry, 2013. 405(16): p. 5571-5582.

177. Fernández, P., et al., Analysis of drugs of abuse in human plasma by dispersive liquid–liquid microextraction and high-performance liquid chromatography. Journal of Applied Toxicology, 2015. 35(4): p. 418-425.

178. Ahmadi-Jouibari, T., et al., Dispersive liquid–liquid microextraction followed by high-performance liquid chromatography–ultraviolet detection to determination of opium alkaloids in human plasma. Journal of Pharmaceutical and Biomedical Analysis, 2013. 85: p. 14-20.

179. Alahyari, E., et al., Analysis of opioids in postmortem urine samples by dispersive liquid-liquid microextraction and high performance liquid chromatography with photo diode array detection. Egyptian Journal of Forensic Sciences, 2018. 8(1): p. 13.

180. Shamsipur, M. and N. Fattahi, Extraction and determination of opium alkaloids in urine samples using dispersive liquid–liquid microextraction followed by high-performance liquid chromatography. Journal of Chromatography B, 2011. 879(28): p. 2978-2983.

181. Fisichella, M., S. Odoardi, and S. Strano-Rossi, High-throughput dispersive liquid/liquid microextraction (DLLME) method for the rapid determination of drugs of abuse, benzodiazepines and other psychotropic medications in blood samples by liquid chromatography–tandem mass spectrometry (LC-MS/MS) and application to forensic cases. Microchemical Journal, 2015. 123: p. 33-41.

182. Na, C., et al., Spent Nuclear Fuel Reprocessing Flowsheet A Report by the WPFC Expert Group on Chemical Partitioning of the NEA Nuclear Science Committee. 2012: Nuclear Energy Agency of the OECD (NEA). p. 122.

183. González, A., J. Avivar, and V. Cerdà, Determination of priority phenolic pollutants exploiting an in-syringe dispersive liquid–liquid microextraction–multisyringe chromatography system. Analytical and Bioanalytical Chemistry, 2015. 407(7): p. 2013-2022.

184. Hadjmohammadi, M.H., M, Inverted Dispersive Liquid–Liquid Micro Extraction of Nicotinic Acid from Human Plasma and its Determination by High-Performance Liquid Chromatography. Austin Chromatogr., 2016. 3(1): p. 1038.

185. Cuypers, R., Hydrogen bonding in the recovery of phenols and methyl-t-butyl ether : molecular modeling and calorimetry. Irrigation and Drainage - IRRIG DRAIN, 2010.

186. Parthasarathi, R., V. Subramanian, and N. Sathyamurthy, Hydrogen Bonding in Phenol, Water, and Phenol−Water Clusters. The Journal of Physical Chemistry A, 2005. 109(5): p. 843-850.

187. Bidari, A., et al., A novel methodology based on solvents less dense than water through dispersive liquid–liquid microextraction: application in quantitation of l-ascorbate in fruit juices and soft drinks by fiber optic-linear array detection spectrophotometry. Analytical Methods, 2011. 3(3): p. 724-730.

188. Hyde, A.M., et al., General Principles and Strategies for Salting-Out Informed by the Hofmeister Series. Organic Process Research & Development, 2017. 21(9): p. 1355-1370.

189. Hashemi, P., et al., Reversed-phase dispersive liquid–liquid microextraction with central composite design optimization for preconcentration and HPLC determination of oleuropein. Talanta, 2010. 80(5): p. 1926-1931.

190. Hashemi, P., F. Nazari Serenjeh, and A.R. Ghiasvand, Reversed-Phase Dispersive Liquid–Liquid Microextraction with Multivariate Optimization for Sensitive HPLC Determination of Tyrosol and Hydroxytyrosol in Olive Oil. Analytical Sciences, 2011. 27(9): p. 943-943.

191. Chisvert, A., et al., Determination of N-nitrosodiethanolamine in cosmetic products by reversed-phase dispersive liquid-liquid microextraction followed by liquid chromatography. Talanta, 2017. 166: p. 81-86.

192. Lourenço, E.C., et al., A simple, rapid and low cost reversed-phase dispersive liquid-liquid microextraction for the determination of Na, K, Ca and Mg in biodiesel. Talanta, 2019. 199: p. 1-7.

193. Muller, A., et al., Endogenous morphine in SH-SY5Y cells and the mouse cerebellum. PloS one, 2008. 3(2): p. e1641-e1641.

194. Laux, A., et al., Mapping of endogenous morphine-like compounds in the adult mouse brain: Evidence of their localization in astrocytes and GABAergic cells. Journal of Comparative Neurology, 2011. 519(12): p. 2390-2416.

195. Björklund, A. and S.B. Dunnett, Dopamine neuron systems in the brain: an update. Trends in Neurosciences, 2007. 30(5): p. 194-202.